Synergizing angiogenesis and osteogenesis in a smart bone substitute

Alfayez, Eman Saud

Awarding institution:
King's College London

Synergizing angiogenesis and osteogenesis in a smart bone substitute

Thesis submitted for the degree of Doctor of Philosophy

Eman Alfayez

Tissue Engineering and Biophotonics Division

Dental Institute

King's College London

2016

Abstract

The major aim of this project was to develop a biologically active bone scaffold that could induce vascularization in critical-size defects (CSD) and hence bone formation. In this study, functionalization of three-dimensional (3D) printed biphasic calcium phosphate (BCP) scaffolds was investigated. The first functionalization approach involved printing scaffolds with two different pore geometries and sizes; square (400µ) and round (800µ). The second was by coating scaffolds with DAR16-II; a self-assembly peptide that forms a hydrogel nanostructure mimicking extracellular matrix (ECM). A rabbit model was used to study these functionalization methods; square and round pore scaffolds with and without DAR16-II coating were implanted into experimental rabbit calvaria bone CSD defects. After 8 weeks, animals were killed and tissue was processed for histomorphometric analysis. Histological evaluation showed that bone formation was pore size and geometry independent while DAR16-II was successful in inducing bone formation compared to non-coated scaffolds. The following *in vitro* studies aimed towards understanding the basic cell response that enhanced bone formation *in vivo*. Human mesenchymal stem cells (MSCs) were used to identify the osteogenic potential of DAR16-II. Molecular analysis and mineralization staining showed that DAR16-II lacks osteoinductive properties. However, DAR16-II preserved cell viability when used as a BCP coating *in vitro*. In addition, DAR16-II exhibited angiogenic potential upon culturing with human umbilical vein endothelial cells (HUVECs) *in vitro*. DAR16-II induced the spreading of endothelial cells, activation and tubular-structure formation. Angiogenesis Real time-2 (RT^2) polymerase chain reaction (PCR) array was used for gene expression analysis and showed that DAR16-II angiogenic effect was regulated by overexpression of endoglin (ENG or CD105), a clade E member of the serine protease inhibitor-1 (SERPIN-1) and β-Actin (ACTB) and down-regulation of VEGF receptor I (Flt1) and VEGF receptor II (KDR) Flt1. Furthermore, DAR16-II enhanced attachment of monocyte THP-1 cells. Results have demonstrated that DAR16-II add a proactive factor to BCP scaffolds. The proposed functionalization methodology increases the potential of enhancing vascularization and bone formation within ceramic scaffolds.

Acknowledgments

This thesis is dedicated to my mother

I would like to acknowledge the Oral Biology department at King Abdulaziz University and the Saudi Ministry of Higher Education for providing me with this opportunity. I would like to express my deepest appreciation to my supervisor Prof. Lucy Di Silvio for her continuous support throughout my PhD study, for her patience, motivation, dedication and immense knowledge. This thesis would not have come to be without her invaluable input. I could not have imagined having a better advisor and mentor for my PhD study. In addition, I would like to thank Dr. Trevor Coward for his insightful comments, encouragement and persistent supervision, who gave me access to the 3D printing laboratory and research facilities. Without his precious support it would not be possible to conduct this research. My sincerest gratitude to Dr. Lorenzo Veschini for his insightful knowledge, stimulating discussion, help in laboratory techniques and data analysis, his continuous encouragement which inspired me to widen my research from various perspectives. I was lucky to have him on board before the completion of my research; his contribution was substantial to this research and in pushing me to be more inquisitive and to reach my goals. I also recognize Prof. Monica Dettin in providing the peptide material for this study and for her patience in answering my many questions. In addition, I would like to thank Dr. James Smay and his students for their help in 3D printing. I wish to express my appreciation to Dr. Shahram Ghanaati for his instrumental help in the animal study. I would like to thank Dr. Bernadine Idowu for her help at the beginning of my PhD, her time and support in the lab. I would like to give my thanks to my colleagues in the department for their help providing valuable lab support, these include; Paula Coward and Hassan Farah. I would like thank my dear friend Galila Alkhateeb for her exceptional help with the images. A special thank you must go to my friends Sarah Alshareef and Shara Sajeni who started this journey with me and helped me to keep things in perspective.

My greatest Acknowledgment goes to my mother, I am forever grateful for your faith in me and for setting the bar so high. A special thank you to my beloved brothers Faisal, Amr, Motasem and Abdullah for their immeasurable support and encouragement, in particular my brother Amr for being my ‘rock’ when all I have known was rock bottom, without them none of this would have been possible.

Table of Contents

List of Tables

List of Figures

List of Awards and Publications

- Best presentation in the post graduate research day (PGR) at King's College London 2014
- Poster presentation at the UK society for Biomaterials meeting (UKSB), Birmingham, UK 2013
- Oral presentation at the 4th China-Europe Symposium on Biomaterials in regenerative medicine (CESB), Sorrento, Italy 2013
- Poster at the 7th Saudi Student Conference in UK (SSC7), Edinburgh, UK 2014
- Oral presentation at the 5th China-Europe Symposium on Biomaterials in regenerative medicine (CESB), Hangzhou, China 2015
- Poster at the 4th International Conference on Tissue Science and Regenerative Medicine, Rome, Italy 2015
- Poster at the 9th Saudi Student Conference in UK (SSC9), Birmingham, UK 2016
- Oral presentation at the 10th World Biomaterials Congress (WBC), Montréal, Canada 2016
- Manuscript 'Surface functionalization of 3D printed scaffold for bone regeneration with a novel self-assembly polypeptide' (In preparation)

List of Abbreviations

3D	Three dimensional
ACTB	beta-Actin, β-Actin
ALK	Activin-receptor like kinase
ALP	Alkaline phosphatase
ANOVA	Analysis of variance
AsAP	Ascorbic acid-2-phosphate
ASC	Adipose stem cells
AV	Arteriovenous
BCP	Biphasic calcium phosphate
b-FGF	basic fibroblast growth factor
BMGC	Biomaterial-associated multinucleated giant cell
BMP	Bone morphogenetic protein
BSP	Bone sialoprotein
Ca2+	Calcium ion
CaM	Calcium/calmodulin
CaMK2α	Calcium/calmodulin-dependent protein kinase
CaP	Calcium phosphate
CaPp	Calcium phosphate precipitate
cDNA	Complementary DNA
CESP	Cell-sheet-engineered periosteum
CG	Collagen glycosaminoglycan
CO_2	Carbon dioxide
Col1	Collagen type I
CREB	cAMP response element-binding protein
CSD	Critical size defect

CT	Computed tomography
DAR16-II	ADADARARADADARAR
DCM	Dichloromethane
Dex	Dexamethasone
DIEA	N,N-diisopropylethylamine
DMEM	Dulbecco's modified Eagle's medium
DMF	N,N-dimethylformamide
DNA	Deoxyribonucleic acid
DW	Direct Write
EAK16-II	n-AEAEAKAKAEAEAKAK-c
EC	Endothelial cell
ECM	Extracellular matrix
EDTA	Ethylene diamine tetra-acetic acid
EGM	Endothelial cell growth medium-1
ENG	Endoglin
EPC	Endothelial progenitor cell
ERK1/2	Extracellular signal-regulated kinase 1/2
ESC	Embryonic stem cell
EtOH	Ethanol
FBS	Foetal bovine serum
FGF	Fibroblast growth factor
Flt1	VEGF receptor I
Fmoc	Fluorenylmethyloxycarbonyl
GAGs	Glycosasmino glycans
GAPDH	Glyceraldehyde-3-Phosphate-Dehydrogenase
GF	Growth factor

H&E	Haematoxylin and Eosin
HA	Hydroxyapatite
Hap	Porous hydroxyapatite
HBTU	2-(1H-Benzotriazole-1-yl)-1,1,3,3-tetramethyluronium hexafluorophosphate
HDMEC	Human dermal microvasculature
HDMEC	Human dermal microvasculature
HHT	Hereditary hemorrhagic telangiectasia
HOP	Osteoprogenitor cell
hPDC	Human periosteum-derived cell
HUVEC	Human umbilical vascular endothelial cell
IL	Interleukin
iPS	Induced pluripotent stem cell
KDR	VEGF Receptor 2, VEGFR2
MBHA	4-Methylbenzhydrylamine hydrochloride
MC3T3-E1	Mouse pre-osteoblast
MEM	Minimal essential medium
Mf	Macrophages
Mo/Mf	Monocytes/Macrophages
MSC	Mesenchymal stem cell
NICD	Notch intracellular domain
NMP	N-methyl-2-pyrrolidone
OB	Osteoblast
OC	Osteoclast
OCN	Osteocalcin
OEC	Outgrowth endothelial cell

OM	Original magnification
OPG	Osteoprotegerin
OPN	Osteopontin
Osx	Osterix
PBS	Phosphate-buffered saline
PCL	Poly-ε-caprolactone
PCR	Polymerase Chain Reaction
PDGF	Platelet-derived growth factor
PDGF-BB	Platelet-derived growth factor subunit B
PDR	Proliferative diabetic retinopathy
PECAM1	Platelet endothelial cell adhesion molecule
PEG	Polyethylene glycol
PHP	PolyHIPE polymer
Pi	Inorganic phosphate ions
PIB	p(N-isopropylacrylamide-co-butyl methylacrylate)
PKC	Protein kinase C
PLGA	Polyacetic-co-glycolic acid
PMA	Phorbol 12-myristate 13-acetate
qPCR	Quantitative real-time reverse transcription– polymerase chain reaction
RADA16-I	AcN-RADARADARADARADA-CNH2
RADA16-II	AcN-RARADADARARADADA-CNH2
RANK	Receptor activator for nuclear factor κ B
RANKL	NF-κB ligand
RANKL	RANK ligand
RGD	Arginine-glycine-aspartic acid
RP	Rapid prototyping

RPL	Ribosomal protein L
RT	Room temperature
RT-PCR	Reverse Transcriptase-Polymerase Chain Reaction
Rux2	Runt-related transcription factor 2
SAP	Self-assembly peptides
SEM	Scanning electron microscopy
SERPIN1	Clade E member of the serine protease inhibitor 1
SFF	Solid free form fabrication
Smad	Small mothers against decapentaplegic
SMC	Smooth Muscle Cells
SP1	Sphingosine-1-1phosphate
SuSCs	Suture stem cells
TCP	Tricalcium phosphate
TE	Tissue engineering
TEM	Tie2 Expressing Monocytes/Macrophages
TES	Triethoxysilane
TFA	Trifluoroacetic acid
TGF-β	Transforming growth factor-β
Tie2	Tyrosine-protein kinase receptor
TNF	Tumour necrosis factor
VEGF	Vascular endothelial growth factor
vWF	Von Willebrand factor

1. Chapter 1: Literature review: Bone vascularization and current limitations

1.1 Introduction

Bone is the major structural supportive connective tissue of the body. It is a rigid organ that constitutes the skeleton. It provides support and protection to internal organs, allows movement and harbours the haematopoietic compartment, which produces blood cells. Bone is composed of collagen fibres and inorganic bone mineral in the form of small spicules. It has different shapes and sizes with variable internal and external structures. Bone is metabolically active and remodels constantly throughout the whole lifetime of an individual. Turnover warrant adaptation of the skeleton, preserves its function, and allows healing of bone upon damage. In this process, bone forming cells (osteoblasts, OB) of mesenchymal origin and bone resorbing cells (osteoclasts, OC) of myeloid origin resorb and appose new bone in a tightly regulated way. During bone repair upon injury these mechanisms are activated to restore lost bone. These mechanisms are also active during the repair of small bone defects. This involves the formation of a primary callus providing a provisional matrix for bone repair. Invasion of this matrix by neo-formed blood vessels guide and drive the migration and differentiation of osteogenic precursors. As these cells fully differentiate into osteoblasts they lay down new bone matrix to restore the lost hard tissue. With the increase in aging population, prevalence of sport related traumas, accidents, tumours and pathological conditions such as osteoporosis all increase the demand of bone related interventions to repair or replace damaged bone. Indeed, when the size of the defect extends beyond the intrinsic regenerative capacity of bone, reconstruction is required.

Autologous bone grafts are the gold standard method for reconstructing bone tissue. Autologous bone comprise cells, signalling molecules, extracellular matrix (ECM), cytokines and growth factors (GFs) which overall contribute to defect repair upon transplantation (Dimitriou et al., 2011). In the case of large defects, the additional step of harvesting bone from the donor site prior implantation is a major drawback for this type of graft as it increases the patient's pain, discomfort, risk of infection and time of the procedure. In addition, the limited availability of bone tissue that can be grafted has led to the use of exogenous grafts including xenografts, allografts and synthetic grafts (De Long et al., 2007). Still the absence of cells and biological cues in these grafts limit their healing potential to osteoconduction only by supporting cells migrating from the boundaries of the defect site to form new bone. One major drawback of the current grafting materials is the insufficient ingrowth of blood vasculature from the host, which in turn is necessary to promote new bone formation and the healing of the defect.

To promote vascularization and subsequent osteogenesis upon graft implantation, different types of cells and biological active agents have been used to functionalize scaffolds. Various co-culture models of endothelial, osteogenic and stem cells were used to pre-vascularize scaffolds before implantation. Although enhanced vascularization and bone formation were achieved, the use of cells to functionalize scaffolds is far from the clinical application. As the size of the defect increases, more cells are needed to seed the scaffold and more time is required. Biological agents were added to scaffolds as an alternative to cells prior implantation in order to induce specific cell response and enhance bone healing. Two types of biological agents have been used including morphogens and growth factors (GFs). Morphogens (e.g. Bone morphogenic proteins (BMPs)) act by altering the cellular phenotype while growth factors have mitogenic and chemotactic properties such as vascular endothelial growth factor (VEGF) (Cochran and Wozney, 1999, Smith et al., 2008). However, the major drawback of using these agents in a clinical application is the challenge in maintaining their potency after implantation.

These agents are subjected to enzymatic degradation, dilution and rapid absorption at the defect site (Curry et al., 2016).

Hence there is a growing need to develop a practical and sustainable method to functionalize scaffolds. The main aim of adding these factors is to incorporate a chemotactic element that attract the host undifferentiated cells at the healing site and induce their osteogenic differentiation. Since angiogenesis temporally precedes osteogenesis, it is pivotal to incorporate factors that can induce vascularization within implanted scaffolds (Carano and Filvaroff, 2003). Vascularization is essential for successful bone regeneration as angiogenesis and osteogenesis are coupled throughout the natural bone healing process. In early stages of bone healing, angiogenic growth factors induce sprouting microvessels which recruit osteoblasts and osteoprogenitor cells to the healing site (Gerber and Ferrara, 2000). In the late phase of bone healing, vascularization and mineralization are synchronized and disruption of vascularization result in defective bone formation (Ivkovic et al., 2003, Kanczler and Oreffo, 2008). Therefore, developing a biocompatible scaffold with customized properties such as internal geometry and porosity can be a key factor in cell infiltration and blood vessels formation. In addition to scaffold geometry, adding a proactive factor that can enhance endothelial cells recruitment and differentiation is essential to form fast growing and stable vasculature to promote bone formation.

1.2 Bone biology

1.2.1 Bone structure

A typical mature bone is composed of two types of structures; cancellous and cortical. The cortical/compact bone forms the outer shielding layer comprising 80% of the total bone mass and its strength protects the inner cancellous/spongy bone. Cancellous bone has a honeycomb structure and accounts for the remaining 20% of the bone mass and contains bone marrow, which is rich in stem cells (e.g. mesenchymal, haematopoietic and pluripotent stem cells), hence this explains the high metabolic activity in comparison to the cortical bone (Parfitt, 2001). Both types are composed of the same matrices, however their physiological properties differ because of the different density, metabolic activity and bone structure (Mellon and Tanner, 2012).

Microscopically, bone is composed of two types; primary (woven) bone and secondary (lamellar) bone. Woven bone is the first stage of bone development during embryonic life and early stages of bone healing. This type is composed of weak disordered collagen fibril, which is replaced during growth and late stages of bone healing with lamellar bone (Figure 1.1). On the other hand, lamellar bone is strong and highly organized as it is made of compact collagen fibrils running parallel in sheets containing osteocytes and bone matrix. Lamellar bone is presented differently in the cortical and cancellous portions of bone.

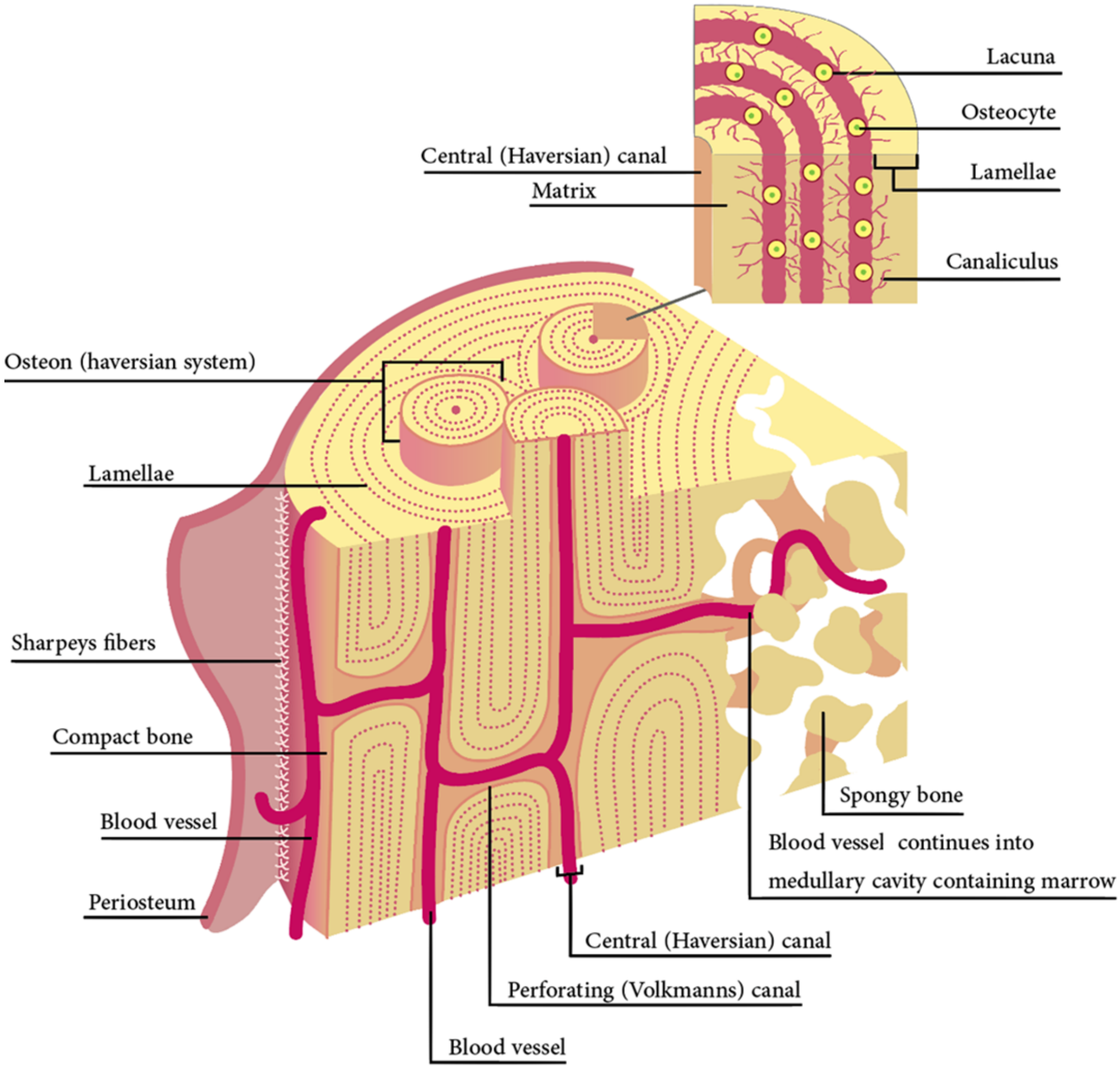

Figure 1.1 Bone anatomy. The outer compact bone is composed of osteons (Haversian system). This Haversian system is made of concentric lamellae and central (Haversian canal) contains blood vessels, lymphatic and nerves. Cancellous (spongy) bone is trabecular in structure and is highly vascularized (Adapted from www.liebertpub.com/teb, 2004 Pearson Education,Inc., publishing as Benjamin Cummings).

In the cortical layer, this lamellar bone is presented in the form of osteons consisting of 4-20 concentric sheets of lamellae with a central duct called the Haversian canal. This canal is running through the centre of the osteon and contains blood vessels, lymphatics and nerves (Safadi et al., 2009).

Whereas in the cancellous portion, lamellar bone is trabecular and arranged in semicircular shapes known as "packets". Its trabecular structure, richness of cells and vascularity is translated through its high metabolic activity in comparison to cortical bone (Jepsen, 2009).

The outer bone surface is covered with periosteum, which consists of two layers: an external layer devoid of cells that attach to joints or bones and inner cambium, which contains osteoprogenitor cells and a vascular plexus. The latter is connected to the endosteum and marrow space with small channels called Volkman's canals which transport blood and nutrients to the osteons (Buckwalter et al., 1995).

1.2.2 Bone matrix

Bone is a remarkable dynamic and hierarchical tissue. Its extracellular matrix (ECM) is composed of inorganic and organic components. This matrix has a major impact in determining bone properties. The inorganic component provides bone with strength and stiffness while the organic part provides toughness due its spongy nature (Burr, 2002). 60-70% of this matrix is composed of inorganic hydroxyapatite (HA) mineral [Ca10(PO4)6(OH)2], remaining matrix is composed of organic proteins, where collagen type I (Col1) is the main constituent, and water (Sommerfeldt and Rubin, 2001, Bilezikian et al., 2008) (Table 1.1). Previously, the mineral phase was considered the main component that affect the bone mechanical behaviour with its high elastic modulus (~100 GPa) providing bone with its rigidity and anisotropic behaviour (Hasegawa et al., 1994). However, currently the collagen phase is considered a significant factor in bone biomechanics. Leng *et al.* have reported in his research that as the Young's modulus of demineralized bone samples decreased with aging, the stiffness and strength of the collagen phase in cortical bone decreased respectively (Leng et al., 2013). Also, water was found to play a crucial role in maintaining bone's mechanical properties. This was demonstrated by drying bone at different temperatures, loss of water resulted in increased stiffness while strength and toughness were decreased respectively (Nyman et al., 2006).

Organic matrix proteins	Function
Collagen I	Matrix calcification
Osteonectin	Bone mineralization
Fibronectin	Osteoblast attachment
Osteopontin	Bone remodelling
Osteocalcin	Bone remodelling

Table 1.1 Some of the bone organic matrix proteins and functions.

1.2.3 Bone cells

Osteoprogenitor cells that differentiate into osteoblasts and osteocytes originate from mesenchymal cell lineage while osteoclasts originate from hematopoietic lineage (Boyle et al., 2003, Pittenger et al., 1999). The interaction of these three cells results in bone development and homeostasis. Table 1.2 summarize the morphological characteristics and function of each cell type (Iñiguez-Ariza and Clarke, 2015, Shapiro, 2016).

Cell type	Origin	Morphology	Function
Osteoblast (OB)	Mesenchymal stem cells (MSCs)	Cuboidal polarized cells	- Synthesis of collagenous organic matrix - Regulation of matrix mineralization by releasing membrane-bound vesicles that: a) Transfer calcium and phosphate b) Destroy mineralization inhibitors
Osteocyte	OB	Stellate shaped	- Mechanical stimulation - Blood-calcium homeostasis - Osteoid matrix calcification
Osteoclast (OC)	Hematopoietic stem cell	Multinucleated polarized cells	- Bone resorption

Table 1.2 Bone cell types, origin, morphology and respective functions.

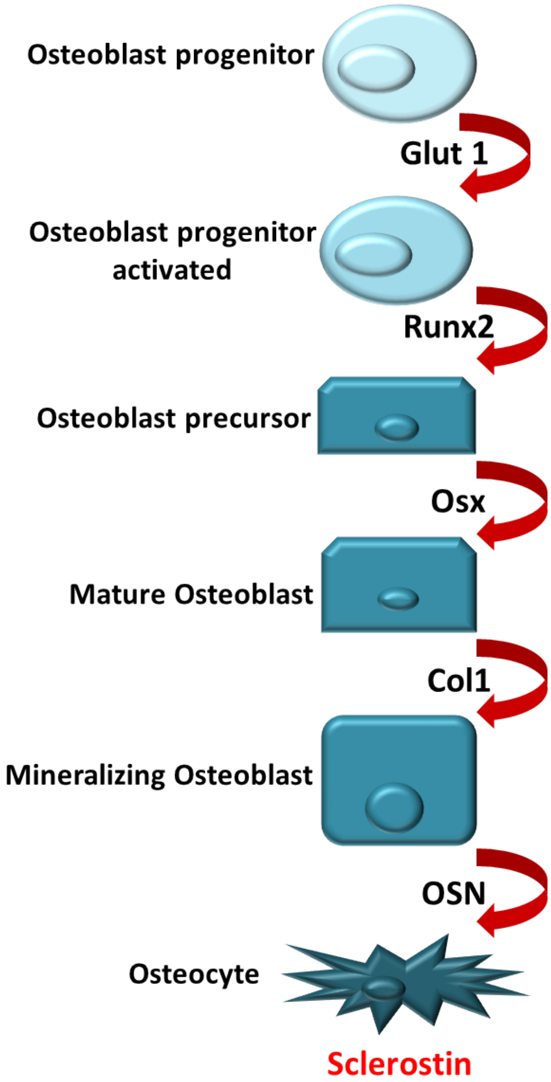

Figure 1.2 Osteoblasts differentiation progression and corresponding transcription factors. Glucose initiates osteogenic differentiation via Glut1 glucose transporter. A cascade of gene expressions follow Glut1 including: runt-related transcription factor 2 (Runx2), osterix (Osx), collagen type I (Col1) and osteocalcin (OCN). Each gene expression corresponds to a specific osteoblast maturation stage until osteoblasts become osteocytes and secrete sclerostin protein (Adapted from Maes et al., 2010b, Wei et al., 2015).

OB differentiation (Figure 1.2) is initiated by glucose uptake through an insulin-independent mechanism facilitated by Glut1glucose transporter. Glut1 expression is required for OBs to express Runt-related transcription factors 2 (Runx2) (Wei et al., 2015). Runx2 is considered the principle transcription factor in OBs differentiation followed by Osterix (Osx) gene expression during skeletogenesis (Nakashima et al., 2002). Following this, differentiated OBs produce matrix proteins including the main

ECM protein Col1 (Marie, 2008). Next, OBs mineralize ECM and express osteocalcin (OCN). Finally, OBs become embedded in the mineralized ECM and differentiate into osteocytes (Karsenty and Wagner, 2002).

When OB progenitor cells express Runx2 and Col1 they enter a proliferation phase in which cells display alkaline phosphatase (ALP) activity and become preosteoblasts (Capulli et al., 2014). Once these cells express Osx and secrete bone matrix proteins such as OCN and bone sialoproteins I/II (BSP I/II) they are considered mature OBs (Nakashima et al., 2002, Florencio-Silva et al., 2015).

1.2.4 Matrix formation

OBs deposit woven organic matrix (osteoid) by secreting three main constituents; collagen proteins (mainly type I), non-collagen protiens (OCN, osteopontin and BSP II) and proteoglycans (decorin and biglycans). Mineralization of this organic matrix starts with a vesicular phase when the apical domain of OBs secretes approximately 100 nm matrix vesicles into the organic matrix (Anderson, 2003). These vesicles bind to organic components, negatively charged sulphated proteoglycans immobilize positively charged calcium ions within the matrix vesicles. Once OBs secrete degrading enzymes and calcium ions are freed from proteoglycans, they cross the calcium channels of the matrix vesicle membrane (Arana-Chavez et al., 1995). When OBs secrete ALP which degrade phosphate containing compounds and release phosphate within the vesicle, calcium and phosphate ions nucleate within the matrix vesicles forming HA crystals (Glimcher, 1998). The second phase of mineralization which is known as fibrillar phase takes place when excess calcium and phosphate ions rupture the matrix vesicles and HA crystals diffuse into the matrix (Boivin et al., 2008). These crystals mineralize this woven matrix to develop new bone. On the other hand, osteoclasts remodel bone by resorbing woven matrix to form a highly organized structure with fibres running parallel to applied forces (Gaston and Simpson, 2007).

1.3 Types of bone growth

Two types of ossification lead to bone development; intramembranous and endochondral ossification. Endochondral bone formation starts with MSCs condensations that differentiate into chondrocytes. These primary cartilage cells form a cartilaginous matrix by secreting type II collagen, aggrecan and express SOX9 along with other transcription factors (Kronenberg, 2003). The cartilage enlarges in response to chondrocyte proliferation and matrix formation. Chondrocytes located in the centre of the cartilage enlarge and hypertrophy and start to secrete collagen type X. Hypertrophic chondrocytes start the mineralization phase by secreting angiogenic factors such as VEGF to attract blood vessels. Hypertrophic chondrocytes recruit chondroclasts (cells from macrophage lineage) to digest the matrix and induce perichondral cells to differentiate into osteoblasts. These hypertrophic chondrocytes undergo apoptosis and osteoblasts use the cartilage matrix as a scaffold to lay bone matrix. This type of bone growth is restricted to skeletal bone development and bone healing while development of skull flat bones is achieved through intramembranous ossification. In intramembranous ossification, MSCs condensations differentiate directly into osteoblasts and produce bone matrix rich in Col1.

It was found that MSCs isolated from craniofacial sutures (SuSCs) were superior to MSCs isolated from the bone skeleton in terms of self-renewing, differentiation potential and clonal expansion (Maruyama et al., 2016). SuSCs exclusively express Gli1+ and Axin2 and induce bone formation by intramembranous ossification (Zhao et al., 2015, Maruyama et al., 2016). This can explain the preferable results when craniofacial defects were reconstructed with craniofacial skeletal grafts compared to grafts harvested from endochondral bones in both volumetric maintenance and survival rate (Phillips et al., 1992).

1.4 Angiogenic/Osteogenic coupling

In both types of bone ossification, vascularization maintain skeletal homeostasis by acting as a communication and transportation system for all essential factors and circulating cells, therefore impairment of blood supply results in skeletal pathological conditions such as osteonecrosis (Childs, 2005). In addition, the vascular system acts as an angiocrine organ during healing by generating tissue specific-angiocrine factors and initiate the repair process to maintain homeostasis (Rafii et al., 2016). It was found that in postnatal long bone, specialized bone vessels; types H and L, regulate osteoblasts and chondrocytes differentiation (Kusumbe et al., 2014, Ramasamy et al., 2014). Type H vessels include columnar tubes and arches located in the bone metaphysis and endosteum. While type L is the extension of type H vessels in the diaphysis and forms sinusoidal vessels within the haematopoietic bone cavity. Osteoprogenitors expressing Osx, Col1 and Runx2 selectively arrange themselves around type H vessels. Blind-ends of type H vessels are closely positioned to the growth plate chondrocytes in the metaphysis (Figure 1.3). As chondrocytes produce VEGF-A; the main specific mitogen for endothelial growth, the Noggin expression is stimulated by endothelial Notch signalling. Noggin promotes osteogenesis and angiogenesis by monitoring osteoprogenitors differentiation and chondrocytes hypertrophy (VEGF-A source). This angiocrine pathway couples angiogenesis and osteogenesis.

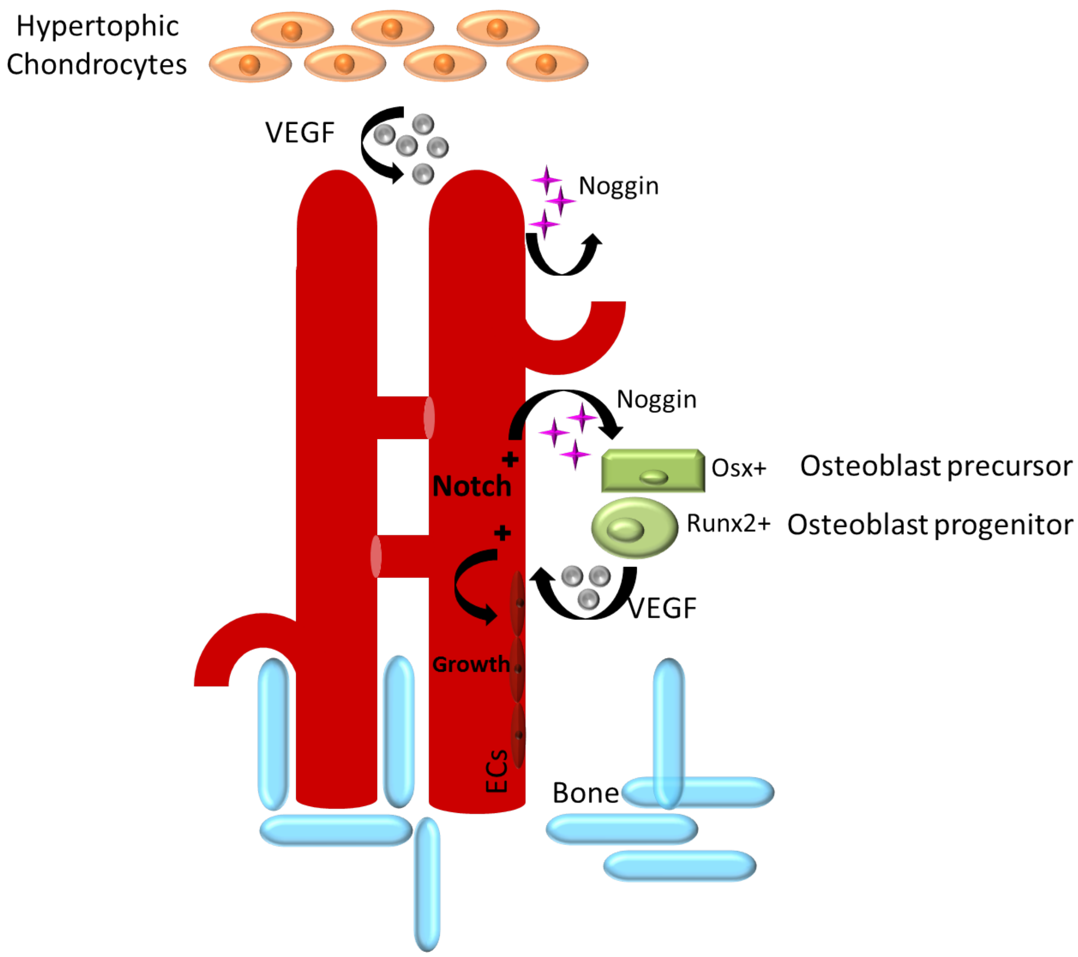

Figure 1.3 Osteogenesis and angiogenesis coupling in postnatal long bone by signalling interaction between chondrocytes, ECs and osteoprogenitor cells. Type H vessels which are embedded in the metaphyseal bone trabeculae are connected via arches at the distal end. These arches extend into the growth plate chondrocytes and receive VEGF-A which is an essential factor for angiogenesis. Notch signalling promotes the expression of endothelial Noggin which is required for perivascular osteoprogenitors differentiation and hence osteogenesis. Also, endothelial Notch and Noggin expression modulate chondrocyte maturation and hypertrophy which regulate VEGF-A expression and thereby angiogenesis (Adapted from Ramasamy et al., 2014).

1.5 Vascularization in bone healing

In small size defect, bone can self-repair and heal through three phases (Figure 1.4); the inflammatory phase, the repair phase and the remodelling phase (Jin et al., 2015). Vascularization plays a crucial role in the healing process by forming a haematoma within the fracture site. This haematoma infiltrates inflammatory cells such as macrophages into the bone in the inflammatory phase. This results in granulation tissue development, vascular tissue ingrowth and migration of MSCs and Endothelial cells (ECs) to healing site. This granulation tissue is replaced by fibrous tissue during repair phase and supports the vasculature ingrowth. Next, external callus is formed by direct bone formation while internal callus is formed by MSCs chondrogenic differentiation. During the healing process, the periosteum is recognized as a key element in the bone repair process. Its internal layer is highly vascularized and predominantly composed of progenitor cells. These cells include osteoblasts that deposit new bone matrix and pluripotent cells that migrate to the healing site and differentiate to regenerate bone (Ozaki et al., 2000, Colnot, 2009). Osteoblasts recruited to the fracture site calcify the cartilage matrix of the internal callus and form mineralized woven bone matrix. During remodelling phase, woven bone is remodelled into stronger lamellar bone by osteoclastic resorption of the callus. Finally, the healing bone restores the original bone shape, structure and function (Jin et al., 2015).

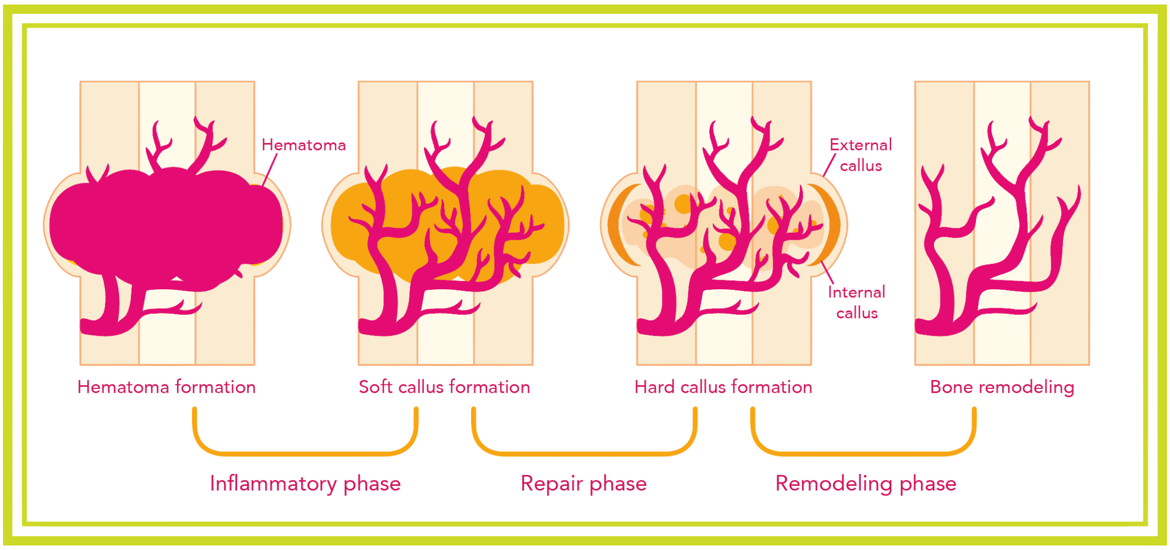

Figure 1.4 Schematic of the fracture healing. The three distinct but overlapping healing stages: the inflammatory, the repair and the remodelling phases. Haematoma is developed to start the healing process in the inflammatory phase. Followed by soft callus/unmineralized cartilage formation. After that, fibrous tissue is formed and followed by hard callus formation/secondary bone. Finally this hard callus is remodelled and lost bone is regenerated (Adapted from Jin et al., 2015).

1.7 Bone scaffolds

Critically sized bone defects going beyond the endogenous regenerative potential require the utilisation of grafting scaffolds to promote healing. Autografts are still considered the gold standard scaffolds for bone replacement. However, shortcomings included 50% failure rate in non-union treatments, limited tissue available for grafting and the second surgical site morbidity involvement (Brighton et al., 1995, Clavero and Lundgren, 2003). As an alternative, allografts (grafts transplanted from a donor from the same species) were used for bone replacement. Still, two main drawbacks were associated with this type including significant loss of strength with 30-60% failure rate over 10 years of implantation and late rejection tendency (Wheeler and Enneking, 2005, Finkemeier, 2002). On the other hand, the use of Xenografts (grafts transplanted from a donor of different species) for bone replacement is far from ideal candidate due to the difference in physiological structures and function from human bone (Goldstein, 2002).

Taking into account the limitations of available bone grafts, there is an increase need for developing tailored engineered bone scaffolds that mimic the lost bone structure and facilitates the healing process. An ideal scaffold for bone tissue engineering should mimic natural bone, promote endogenous repair mechanisms and eventually degrade over time leaving space for natural neo-formed bone. Scaffold structure and composition can play a major role in this crucial process since one of the primary functions of a scaffold is providing mechanical stability upon implantation. Furthermore, scaffold structure must be osteoconductive, promoting the recruitment of host cells. Bone engineering is mainly dependant on four basic elements presented in Figure 1.5; 1) a scaffold which act as the backbone in which new tissue will develop, 2) cellular component to initiate bone formation, 3) signalling molecules such as growth factors to induce cellular differentiation and 4) vascularization in order to drive formation of new bone and then to maintain cellular homeostasis.

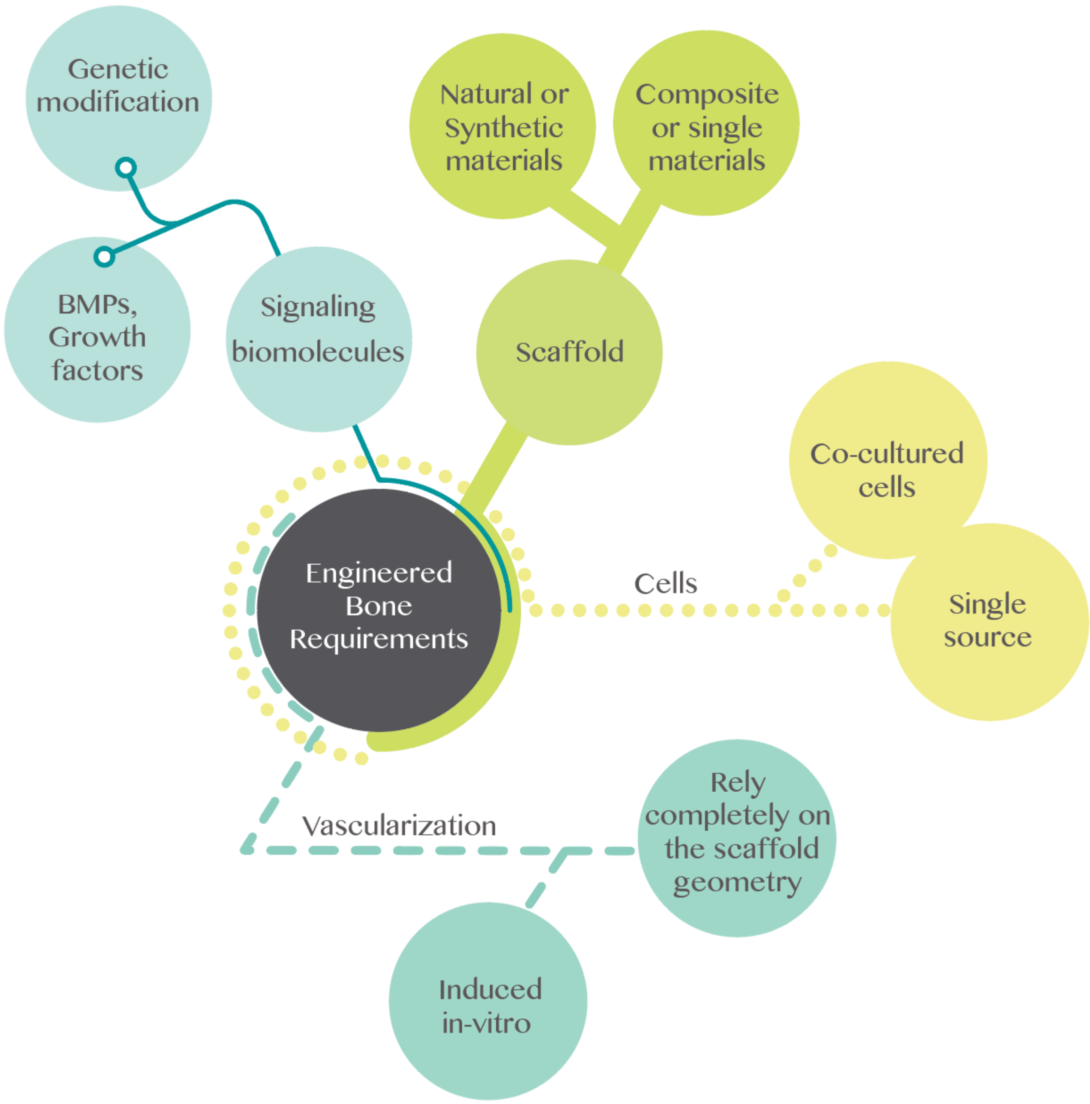

Figure 1.5 Basic factors of engineering tissues; potential combinations and their interaction. 1) Scaffold is the key player in the regeneration process as it acts as a template for new tissue formation. It can be fabricated from a single natural (e.g. Collagen) or synthetic (ceramic) material or a composite of different materials in order to enhance mechanical and biological functions. 2) Cellular component from a single cell source or a co-culture of different types of cells to induce bone formation. 3) Signalling biomolecules to activate the cellular response to the implanted scaffold during bone regeneration. 4) Vascularization which is essential for initiating and maintaining the bone regeneration process.

1.7.1 Scaffold material

1.7.1.1 Natural

Polymers purified from plants and animals including collagen, chitosan and glycosasmino glycans (GAGs) have been extensively used in the vast body of bone engineering research as a natural scaffold material (Harley and Gibson, 2008, Minuth et al., 2010). These materials are composed of natural components of ECM and they contain specific molecules that enhance osteoblast adhesion and function (Harley and Gibson, 2008).

a. Collagen

As collagen is the most abundant protein in bone matrix and a biocompatible material, it has been widely used in bone engineering (Glowacki and Mizuno, 2008). It induces differentiation of osteoprogenitor cells into osteoblasts and osteoblast maturation into osteocytes via transmembrane alpha (2) beta (1) integrin receptor interaction (Chen et al., 2007, Mullen et al., 2013). Also, it was found that the addition of GAGs to collagen structure augments its osteogenic capacity (Farrell et al., 2006, Keogh et al., 2010). However, its use in bone engineering is limited by its inadequate mechanical properties. Chemical crosslinking is the commonly used method to improve its mechanical strength (Charulatha and Rajaram, 2003). For example, augmenting the use of photochemical crosslinking via riboflavin (a non-toxic photoinitiator) with plastic compression method enhanced Young's modulus of collagen by 2.5 fold compared to non-crosslinked collagen controls (Rich et al., 2014).

b. Gelatine

Gelatine is a modified form of collagen; it has a denatured structure and has been used in bone engineering studies (Jones and Cartmell, 2005). Gelatine scaffolds induced osteogenic differentiation of bone marrow-derived MSCs in cranial defects of athymic nude mice models (Ben-David et al., 2011). However, collagen-based scaffolds lack the required mechanical properties for bone replacement (O'brien, 2011). Modifying collagen cross-linking in order to improve mechanical stiffness has been investigated (Tierney et al., 2009, Haugh et al., 2009, Bailey et al., 2011, Haugh et al., 2011). Still scaffolds lack the required mechanical stiffness to replace bone in load bearing areas. Furthermore, the core degradation at the centre of collagen glycosaminoglycan (CG) scaffolds in *in vitro* culture raised the concern of the long term sustainability of collagen-based scaffolds (Keogh et al., 2010).

c. Alginate

Alginate is a polysaccharide extract from brown algea and has been studied for its application in bone engineering (Alsberg et al., 2001, Sun and Tan, 2013). Its porosity and the feasibility in changing its chemical structure permit cellular interaction and controlled release of cells and growth factors (Quinlan et al., 2015). It has been used as a carrier for BMP-2 and angiogenic factors to enhance bone regeneration and vascularization (Boerckel et al., 2011, Freeman and Cohen, 2009). In order to use it for bone replacement it has to be combined with a supporting material such as chitosan and hydroxyapatite (HA) to enhance its strength and improve osteogenic differentiation in the healing site (Li et al., 2005, Turco et al., 2009, He et al., 2012).

d. Chitosan

Chitosan is also a polysaccharide that is derived from chitin found in crustaceans and coral (Di Martino et al., 2005). It is a biocompatible, biodegradable and porous antimicrobial material (Venkatesan and Kim, 2010). Similar to previously mentioned natural materials; it has to be combined with strong materials to enhance its mechanical properties. Recently, fresh water fish scales have been studied as a source of biological porous hydroxyapatite (Hap) and a possible bone replacement material (Panda et al., 2014). However, it was demonstrated that they carry the risk of infection in addition to the common disadvantage of all natural derived scaffolds represented in the poor mechanical strength (Vuola et al., 2000, Ivankovic et al., 2010, Battistella et al., 2012).

1.7.1.2 Synthetic

1.7.1.2.1 Polymers

Poly-ε-caprolactone (PCL) has been used in bone engineering for its mechanical properties, porosity and biodegradability (Ekaputra et al., 2011, Cipitria et al., 2013). Its porosity allows cellular cross-talk and integration thus supports osteogenic and angiogenic mechanisms across its structure (Kyriakidou et al., 2008, Mitsak et al., 2011). One of the main drawbacks of PCL is hydrophobicity and subsequent low surface energy which affect its use in tissue regeneration. In order to enhance PCL cellular interaction, surface functionalization was investigated by using different materials such as plasma treatment and double protein coating of gelatine B and fibronectin which effectively induced cell adhesion, proliferation and tissue formation (Jacobs et al., 2013, Declercq et al., 2013).

Polyethylene glycol (PEG), another type of synthetic polymer, also can be functionalized to induce bone regeneration with integrin-specific peptides, growth factors and polysaccharides (Shekaran et al., 2014, Pratt et al., 2004, Rizzi et al., 2006). However, the poor mechanical properties and the need for a supportive material limit the use of these polymers for bone replacement.

.

1.7.1.2.2 Bioactive glasses and ceramics

A .Bioactive glasses

Bioactive glasses are calcium- and possibly- phosphate containing silica glasses that produce a bioactive hydroxycarbonate apatite layer once immersed in a biological fluid. It can be engineered to control ion release and stimulate specific gene transduction pathways to enhance osteogenic differentiation (Hench and Polak, 2002, Jell and Stevens, 2006). It is a porous and biocompatible material which facilitates cellular integration and maintain cells viability (Jones and Hench, 2004). Its brittleness is the main drawback for its use as a bone replacement material. However, Chen *et al*. in a recent study incorporated a novel p(N-isopropylacrylamide-co-butyl methylacrylate) (PIB) nanogels with bioactive glass scaffolds and improved scaffolds mechanical properties and promoted bone formation in critical-size femur defect of mature osteoporotic female Wistar rats *in vivo* (Chen et al., 2015b). In addition, coating with polylactic-co-glycolic acid (PLGA) induced human mesenchymal stem cells (hMSCs) proliferation and osteogenic differentiation *in vitro* (Chen et al., 2015a).

B. Ceramics

In addition to bioactive glasses, ceramics are considered attractive materials in bone engineering because of the resemblance of their chemical composition to the bone mineral phase. Ceramics contain calcium and phosphate as basic structures; HA and tricalcium phosphate (TCP) are the commonly used types as bone scaffolds (LeGeros, 2002, LeGeros, 2008). Ceramics are biocompatible; osteoconductive materials which osteointegrate via chemical bonds in the healing site to encourage new bone formation (Kim et al., 2014a, Cambra-Moo et al., 2014). The major disadvantage of ceramic is its inherent brittleness hence rendering its use to non-load bearing areas (Cardoso et al., 2015). Improving mechanical properties of ceramics is one of the important areas of research in addition to bone engineering. Although different materials were used in conjunction to ceramics in order to enhance mechanical properties of fabricated scaffolds, compressive strength and toughness were far below the normal bone values of fracture toughness of 2–12 MPa · $m^{1/2}$ and compressive strength of 130–180 MPa (Wang and Shaw, 2009, Fielding et al., 2012, Gao et al., 2014). Developing an effective method to overcome this limitation is essential as ceramics are becoming the material of interest in 3D printing and have showed promising results in cell proliferation and osteogenic differentiation by controlling pore sizes, surface topography and grain size (Alenezi et al., 2013). For example, calcium phosphate (CaP) scaffolds composed of TCP, polyethylene glycol and trisodium citrate were 3D printed at room temperature and implanted in a sheep model *in vivo* (Bergmann et al., 2014). Superior mineral density was detected with 3D printed scaffolds compared to control autografts. The significance of using such techniques in addition to the above-mentioned advantages is the possibility of using ceramics as viable carriers of bioactive molecules like BMP's, growth factors and drugs without undergoing denaturation because of the heat needed in sintering ceramics.

1.7.2 Scaffold design

1.7.2.1 Scaffold architecture

Bone scaffolds act as a transient skeleton or template for cells to infiltrate and attach during the healing process. Scaffold architecture can facilitate the bone formation and vascular growth by adjusting the pores size, porosity and interconnectivity. The pores network is essential for metabolites exchange and cellular cross-talk (Lee et al., 2010). In addition, in bone engineering, porosity is essential for osteoblast infiltration and osteogenic differentiation (Kasten et al., 2008). Kuboki *et al*. showed that HA porous scaffolds induced bone formation in a rat ectopic model whereas no bone formation was detected with non-porous scaffolds (Kuboki et al., 1998). The scaffold porosity can be adjusted in order to enhance specific cellular responses. Bone formation is linked to the degree of scaffold porosity with favourable results associated with 70-93% porosity (Kruyt et al., 2003, Roy et al., 2003, Takahashi and Tabata, 2004).

A. Pore size

The pioneering work of Hulbert *et al.* demonstrated the effect of pore size on bone regeneration by using calcium aluminate cylindrical pellets with 10-200 µm pore sizes in dog femoral defects (Hulbert et al., 1970). Pores with smallest sizes <75 µm, resulted in fibrous tissue formation while medium sized pores 75-100 µm resulted in unmineralized osteoid tissue formation. Large pores >200 µm enhanced both bone ingrowth and vascular formation. Kuboki *et al.* showed that larger pores ranging from 300 to 400 µm induced more bone formation in HA scaffolds implanted subcutaneously in rats (Kuboki et al., 2001). The enhanced bone formation was explained by the rapid vascular ingrowth. Bai *et al*. confirmed the importance of pore size on blood vessels formation by implanting beta-tricalcium phosphate (β-TCP) scaffolds with different pore sizes in a rabbit model (Bai et al., 2010). Scaffolds with pore sizes smaller than 400 µm restricted blood vessels growth while increasing the pore size beyond this value had no significant difference on scaffold vascularization. They proposed that the optimal pore size for blood vessels formation is 400 µm.

B. Pores interconnectivity

Pore interconnectivity has a crucial role during healing as it facilitates nutrient and oxygen delivery as well as waste removal (Kim et al., 2010). In addition, increasing pore interconnectivity can promote scaffold vascularization by increasing the size and number of developed blood vessels during healing (Bai et al., 2010). Moreover, bone formation was found to be affected by pore interconnectivity. Uebersax *et al.* studied the effect of pores interconnectivity on MSCs seeded in silk fibroin scaffolds (Uebersax et al., 2006). They found that higher interconnectivity resulted in a homogenous mineralization and bone formation.

1.7.2.2 Scaffold fabrication techniques

Conventional approaches of fabricating 3 dimensional (3D) scaffolds include salt leaching, gas foaming, emulsion/freeze drying and expansion in supercritical fluid (Chung and Park, 2007). It is difficult to control scaffold external and internal geometry by using these conventional methods. They require manual handling and result in inconsistent reproducibility (Miranda et al., 2006). Rapid prototyping (RP) however, also known as solid free form fabrication (SFF) is an advanced fabrication technique used to print custom-made 3D scaffolds. By using this technique, both external and internal architecture of printed scaffolds can be controlled and reproduced including the pore size, shape and orientation (Hollister, 2005). The main concept is to build the scaffold by automated extrusion of biomaterials in tomographic layer sequence based on a pre-designed structure. This pre-design is constructed from scanning the defect site and transfer scanned images to a computer program (Chang and Chiang, 2003, Soo and Yu, 2003). Different methods currently used in fabricating 3D scaffolds depend on the RP technology include; stereolithography, selective laser sintering, shape deposition manufacturing, fused deposition modelling and robocasting (Yang et al., 2002, Yeong et al., 2004, Manjubala et al., 2005, Hollister, 2005). However, these methods showed limited control over printed scaffolds resolution and interconnectivity excluding robocasting. Robocasting (also known as Direct Write (DW) technology) is a filament based direct assembly method in which ink is continuously extruded using a cylindrical nozzle (Lewis et al., 2006). The rheology of extruded inks allows them to flow steadily and once they are deposited, they gel and their viscosity and elastic modulus rise (Ricci et al., 2012). This flow behaviour allows development of scaffolds with controlled pore size and interconnectivity (Smay et al., 2002, Michna et al., 2005). In addition to the design control, different materials can be mixed and deposited by a multi-reservoir ink chamber or they can be deposited in gradient mode. The robocasting resolution is very high and limited only by the nozzle diameter and very reproducible (Ricci et al., 2012). Moreover, different types of inks can be used that may or may not need firing. In the case of using non-firing colloidal inks such as chitosan, biological cues like growth factors can be added during fabrication. While in the case of using firing colloidal inks such as biphasic calcium phosphate (BCP), any biological agent has to be added post-firing and adsorbed into the printed scaffold (Ricci et al., 2012).

1.8 Vascularization as a key challenge in bone engineering

A prerequisite for successful bone engineering is adequate vascularization to allow successful integration with host tissue. In critical size defect (CSD), which defined as the smallest size defect that cannot heal spontaneously, nutrient and oxygen transport occurs mainly through diffusion. This diffusion is limited to 100 to 200 μm only from the surrounding vasculature into the implanted scaffold (Carmeliet and Jain, 2000). In addition, several scaffolds used for bone regeneration demonstrated poor angiogenic induction upon implantation. This lead to the formation of insufficient vasculature to sustain the formation of healthy new bone and to eliminate the byproducts of the degrading scaffold (Mikos et al., 1993, Nomi et al., 2002). Therefore, the accumulation of these byproducts interferes with the healing process and elicits inflammatory responses (Taylor et al., 1994). The subsequent challenge after the development of neovascularization within the graft is the anastomosis with the host's vasculature

(Scheufler et al., 2008). This process can take up to one week which might result in ischaemia and rejection of the graft (Lokmic and Mitchell, 2008). In order to develop a strategy to overcome these problems, different methods were proposed including cell seeding and the addition of bioactive factors.

1.9 Vascularization strategies in bone engineering

1.9.1 Scaffolds prevascularization

The concept of *in vivo* prevascularization of grafts was applied for the first time in bone engineering when axial vascularization was established in solid porous constructs through arteriovenous (AV) loop (Figure 1.6-middle section) (Kneser et al., 2006). In this two-step procedure, the graft is first implanted ectopically in a vascularized mesh until a vascular network is developed within the graft from the surrounding vasculature. After that the graft is transferred to defect site as a free flap where immediate vascularization can be achieved due to surgical anastomosis with the main feeding vessels in site. However, the two surgical procedures involved in this method and the time consuming factor are the main drawbacks.

Another approach of current interest is *in vitro* prevascularization, which counteracts the aforementioned drawbacks, where single surgical procedure is needed and shorter time is required (Rouwkema et al., 2008). Its principle is based on seeding the scaffold with a single source of vasculogenic cells or a co-culture of vasculogenic and bone forming cells in a supportive environment to form *in vitro* blood vessels before implanting the graft (Figure 1.6, Top) (Hutton and Grayson, 2014). This technique was used in engineering different types of tissues including skin, cardiac muscle, skeletal muscle and bone (Shepherd et al., 2006, Caspi et al., 2007, Levenberg et al., 2005, Rouwkema et al., 2006, Choong et al., 2006). Another *in vitro* technique is to seed the graft prior implantation with specialized cells, signalling molecules and factors that can induce blood vessels formation (Figure 1.6, bottom). In this procedure, cell cross-talk with cells *in situ* can facilitate the cellular interaction and aggregation to form a functioning vascular network. Also, controlled release of specific growth factors can be achieved which enhance both bone and blood vessels development.

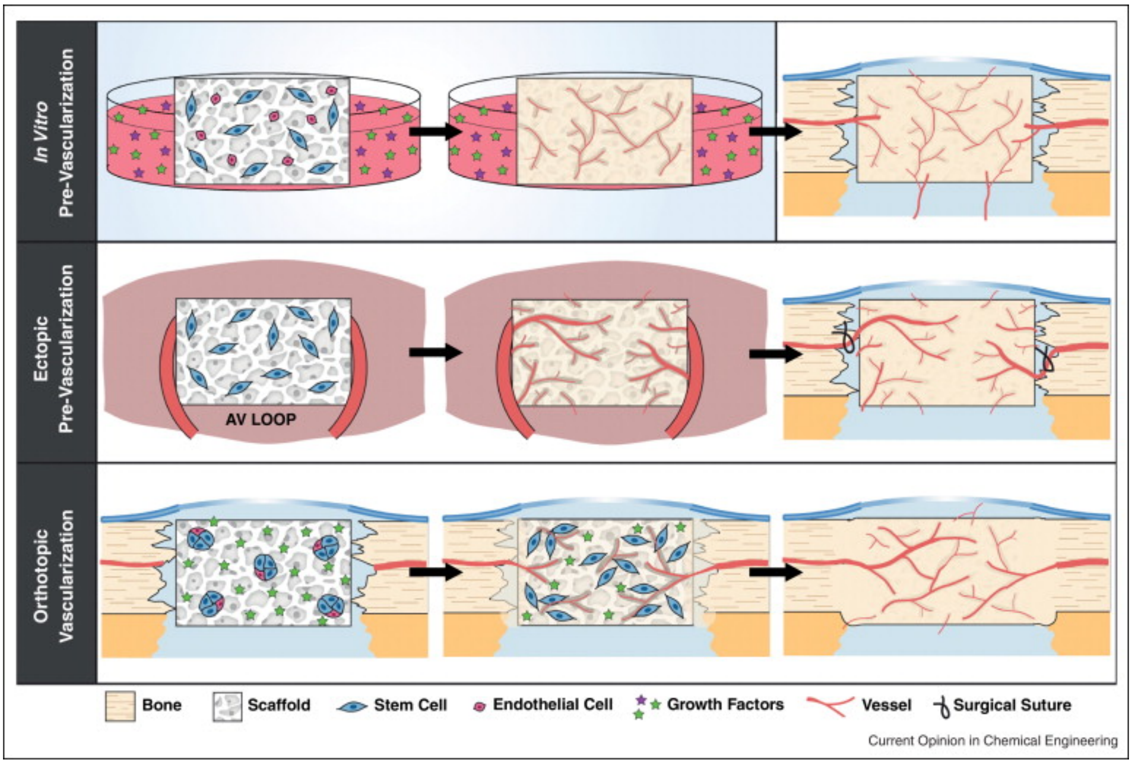

Figure 1.6 Vascularization techniques for bone tissue engineering. 1) <u>Top</u>: *In vitro* pre-vascularization of scaffolds by seeding cells and induce blood vessels formation by growth factors. The concept is based on implanting scaffolds with engineered capillaries to anastomose with host vasculature and perfuse the entire scaffold. 2) <u>Middle</u>: *In vivo* ectopic pre-vascularization involves an extra step to the previous method. After seeding the scaffold with cells, scaffold is implanted into a highly vascularized bed, such as muscle or arteriovenous (AV) loop, to allow extensive vascular ingrowth. After that, the vascularized scaffold is transplanted as a free flap to the bone defect and surgically anastomosed with surrounding vessels to allow immediate perfusion. 3) <u>Bottom</u> *In vivo* orthotopic vascularization involves direct implantation of cell seeded scaffolds loaded with growth factors into the bone defect for in situ tissue development. In this type, the vascularization development is mainly dependent on cell survival, endogenous cell signaling and controlled release of growth factors (Adapted from Hutton and Grayson, 2014).

In an attempt to mimic the vascularized periosteum and to use it in enhancing bone graft survival and regenerative capacity, Kang *et al*. fabricated a vascularized cell-sheet-engineered periosteum (CESP) (Kang et al., 2014). Two cell sheets were prepared in which the first was composed of human umbilical vascular endothelial cells (HUVECs) cultured on top of hMSCs layer mimicking the fibrous layer of the periosteum. The second sheet composed of mineralized hMSCs to mimic the cambium layer of the periosteum. The mineralized cell layer was wrapped around β-TCP scaffold followed by the vascularized layer. The engineered periosteum *in vitro* enhanced vascularization and anastomosis with the host vasculature and induced bone matrix formation *in vivo* (Kang et al., 2014).

Different co-culture models were studied *in vitro* and *in vivo* in order to understand the order of growth factors released and how these chemicals can affect the cell-to-cell interactions and contribute to capillary-like structure formation. As a general rule in vascularized bone engineering, cells from an endothelial source were co-cultured with cells from an osteogenic origin.

1.9.1.1. Cell sources

A. Endothelial cell source

ECs are considered the building blocks of newly formed blood vessels during development and healing process. These cells release pro-inflammatory factors and express cell adhesion molecules, which are necessary for the angiogenesis process and long-term stability by forming the inner surface of these vessels. Primary endothelial cells isolated from HUVECs and human dermal microvasculature (HDMECs) are commonly used because of their accessibility and ease of isolation (Jaffe et al., 1973, Peters et al., 2002). Angiogenic factors including collagen type I, VEGF and basic fibroblast growth factor (bFGF) are required as supplements when endothelial cells are cultured *in vitro* in order to form capillary-like structures (Peters et al., 2002). Another potential cell source is endothelial progenitor cells (EPCs) (Urbich and Dimmeler, 2004). EPCs are stem cells that have the potential to differentiate into endothelial-like cells in response to specific factors. These progenitors include MSCs, adipose stem cells (ASCs), embryonic stem cells (ESCs) and induced pluripotent stem cells (iPS) (Oswald et al., 2004, Vittet et al., 1996, Choi et al., 2009, Shah et al., 2014). EPCs are isolated and characterized from circulating blood and originate from haematopoietic and endothelial lineages. These cells express angiogenic markers CD31+ (also known as Platelet endothelial cell adhesion molecule (PECAM1)) and, CD34+ or CD133+ on their surfaces and can develop capillary-like structures *in vitro* (Fuchs et al., 2010a). The main advantage of EPCs over primary cells is their unlimited passaging capacity in *in vitro* culture prior differentiation into mature endothelial-like cells (Bianco et al., 2001).

Primary cells in general share a limiting factor of insufficient number of isolated cells from the body in addition to the limited passaging potential *in vitro* before cells exhibit changes in their phenotype and start to de-differentiate.

B. Osteogenic cell source

Primary bone cells are OBs isolated from different bone tissues in the body and they were used mainly in biomaterials characterization studies (Coelho et al., 2000, Coelho and Fernandes, 2000). Osteogenic progenitor cells are stem cells that differentiate into mature osteoblasts when cultured in osteogenic differentiation medium. The same cell sources are shared between endothelial and osteogenic progenitor cells including MSCs, ASCs, ESCs and iPSCs (Shrivats et al., 2014). Therefore the same advantage of unlimited passaging prior differentiation is shared and favoured their use in tissue regeneration over primary cells (Bianco et al., 2001, Kassem et al., 1997).

1.9.1.2 Co-cultured cells models

a. Endothelial cells and osteoblast cells

HDMECs and OBs co-culture successfully formed capillary-like structures on cell culture plastic *in vitro* (Unger et al., 2007). When the same co-culture model was used with porous 3D materials including; HA and CaP, nickel titanium and silk fibroin sheets, the same capillary-like structures were developed (Unger et al., 2007, Unger et al., 2010). It was found that cellular-talk in this model formed microcapillary-like structures with lumens and stained for type IV collagen reflecting the progression of development (Santos et al., 2009). In addition, significant amount of Col1 and VEGF was secreted and angiogenic markers such as VEGFR-2, angiopoietin-2 (ANG-2) and its receptor Tie-2 were upregulated (Stahl et al., 2004, Santos et al., 2009).

The second model of co-culturing primary cells involved HUVECs and OBs. Capillary-like structures were also developed on a macroporous CaP cement with Col1 and VEGF upregulation and CD31 and von Willebrand factor (vWF) positive staining (Thein-Han and Xu, 2013, Chen et al., 2014a). Applying the same cellular model on poly lactide/LLA- material upregulated Insulin-like growth factor 1 (IGF-1) gene expression in addition to VEGF (Xing et al., 2013). Reciprocal effect was also detected by enhancing osteodifferentiation in this model by upregulating the gene expression of ALP, OCN and Runx2 (Stahl et al., 2004, Thein-Han and Xu, 2013). In addition, *in vivo* studies supported the validity of capillary-like structures developed *in vitro* by using primary endothelial and bone cells through anastomosis of these structures with host vasculature (Unger et al., 2007, Walser et al., 2013).

b. Endothelial cells and mesenchymal stem cells differentiated to osteoblasts

When mesenchymal stem cells are isolated from bone marrow and undergo osteogenic differentiation they become human osteoprogenitor cells (HOPs). HOPs were co-cultured instead of primary osteoblasts with primary endothelial cells in order to investigate the advantages of this model on angiogenesis and osteogenesis mechanisms (Kaigler et al., 2003, Guillotin et al., 2008). Comparable findings were associated with this cellular model as capillary-like structures were developed and angiogenic factors were detected such as VEGF and Ang-1,2 (Grellier et al., 2009, Pedersen et al., 2012, Li et al., 2013a, Li et al., 2011). Furthermore, applying this co-culture model with 3D scaffolds fabricated from β-TCP, HA/β-TCP and silk/HA biomaterials enhanced osteodifferentiation (Kang et al., 2013, Kim et al., 2014b, Sun et al., 2012). Also, supporting *in vivo* studies displayed the functionality of capillary-like structures developed *in vitro* by anastomosing with host blood vessels post implantation (Rivron et al., 2012, McFadden et al., 2013, Ma et al., 2014).

c. Endothelial progenitor cells and osteoblast cells

Early and late outgrowth endothelial cells (OECs) are endothelial-like cells isolated from EPCs. These cells were the cells of interest as an endothelial cell source in co-culture models composed of primary osteoblasts and endothelial progenitors (Fuchs et al., 2007). Capillary-like structures were formed by co-cultured OECs and OBs on cell culture plastic, starch-poly (caprolactone) and Ca-deficient HA-polylactone scaffolds (Dohle et al., 2010, Fuchs et al., 2009, Fuchs et al., 2010b). Various angiogenic factors were upregulated including Ang-1and 2, VEGF and Platelet-derived growth factor subunit B (PDGF-BB) (Dohle et al., 2011, Li et al., 2013b). Also, co-cultured cells promoted osteogenic differentiation and calcification in comparison to mono-cultured cells by upregulating ALP, BMP-2 and BMP-4 gene expressions (Herzog et al., 2014). Like previously mentioned models, anastomosis with blood vessels surrounding implanted scaffolds were also confirmed (Fuchs et al., 2009, Ghanaati et al., 2011).

d. Endothelial and osteoblast differentiated cells from progenitor stem cells

Following previous models, OEC and HOPs were considered interesting cell sources in bone regeneration studies (Fu et al., 2014). Promising outcomes were represented in capillary-like structures formation *in vitro* and anastomosis with the host vasculature post implantation *in vivo* (Liu et al., 2012, Shi et al., 2014). Increased production of VEGF, PDGF, Ang-1, 2 and ALP reflected the enhanced angiogenesis and osteogenesis processes (Kolbe et al., 2011, Thébaud et al., 2012).

1.9.1.3 Single cell source

Co-culturing cells that originate from the same cell source can take bone regeneration one-step closer to clinical application. In order to investigate this possibility, MSCs were differentiated into bone-like and endothelial-like cells and co-cultured *in vitro* on cell culture plastic and on β-TCP for an *in vivo* study (Tao et al., 2009). However, only osteogenic differentiation was evaluated *in vitro* in which ALP and OCN productions were significantly higher in co-cultured group. In addition, histological analysis showed more bone and vessels formation in implanted scaffold *in vivo* with co-cultured cells. ASCs were also used as a single cell source promoting both osteogenesis and angiogenesis synergistically (Shah et al., 2014). Cells were co-cultured on polylactic scaffolds in 1:1 ratio. Although angiogenesis and osteogenesis were significantly induced in endothelial-like cells and osteoblast-like cells monocultures respectively *in vivo*, there was no significant increase in the co-cultured group.

More studies are still required to optimise the ratios of cells used in co-culture models and long-term studies are also needed to assess the validity of the blood vessels developed. In addition, in order to regenerate critical size defects, the number of cells, the required time for cell culturing as well as the necessary amount of differentiating agents are still raising questions if this method is clinically suitable in inducing angiogenesis within bone scaffolds.

1.9.2 Growth factors, drugs and gene delivery.

Functionalizing scaffolds in order to induce in situ vascularization is of great interest in bone engineering. Incorporating GFs in bone scaffolds can facilitate bone regeneration by activating specific cell receptors and induce a ligand-receptor interaction. For example, BCP scaffolds loaded with VEGF and implanted into critical size cranial defects in Balb/c mice promoted biomaterial vascularization, osseointegration, and bone formation (Wernike et al., 2010). In addition, co-loading of BMP-2 and VEGF was found to enhance both vascularization and bone formation (Patel et al., 2008, Young et al., 2009, Kempen et al., 2009). Adding laminin, basement membrane protein, to collagen scaffolds promoted vascularization by increasing VEGF uptake (Stamati et al., 2014). Using CaP scaffolds as drug delivery systems was also explored by using drugs like gentamicin, vancomycin and ibuprofen which enhanced the bone healing process (Verron et al., 2010, Bose and Tarafder, 2012). GFs and drugs can be added to scaffolds by absorption when scaffold immersed in GFs and drugs containing solutions for fast release. For controlled and prolonged release, GFs and drugs can be encapsulated within scaffold material or integrated by covalent immobilization. However, controlled release is quite important to achieve optimal regeneration. More organized blood vessels formation was achieved via controlled release of VEGF in comparison to uncontrolled

VEGF release (Ehrbar et al., 2004). Combining different GFs to be released in a controlled manner would complement their functions temporally and spatially (Jain, 2005).

Another approach is biological delivery of GFs from seeded cells by genetic modification (Krebsbach et al., 2000). Using gene-delivery technique in providing BMP-9 to a non-union radius bone defect in mice resulted in bridging the gap and improved bone regeneration (Kimelman-Bleich et al., 2011). To promote angiogenesis, and hence bone formation, Keeney *et al*. explored the delivery of a plasmid encoding vascular endothelial growth factor$_{165}$ (pVEGF$_{165}$) in a mouse intra-femoral model (Keeney et al., 2010). They found that a collagen/calcium phosphate scaffold can mediate transfection and can promote bone formation via the delivery of pVEGF165.

1.10 Peptides in bone engineering

There has been a growing interest in developing biomaterials with improved functionality for tissue engineering applications (Bokhari et al., 2005). The main concept is based on mimicking the ECM to organize cells into 3D architecture and induce specific cellular response in order to regenerate specific tissue type (Yang et al., 2001). Peptides constructed from synthetic amino acids were used to fabricate biological materials that can self-assemble via ionic interactions with physiologic solutions (Zhang et al., 1992, Zhang et al., 1993). Different structures were fabricated by self-assembly peptides (SAPs) including synthetic membranes, tubules and fibrillar networks (Zhang, 2003). SAPs are attractive candidates in tissue engineering as they are biomimetic and provide spatial and temporal regulation (Shastri, 2009). In addition, mechanical and physiochemical properties of SAPs 3D structures can be manipulated and optimized to regenerate the tissue of interest (Loo et al., 2012). Hartgerink *et al*. used a pH-induced self-assembly of a peptide-amphiphile to induce mineralization (Hartgerink et al., 2001). They designed the peptides to be reversibly cross-linked and to direct mineralization of HA along the axes of the fibres. In addition, it has been shown that the same SAP scaffold can support regenerating different types of tissues. For example, RADA 16-I is a self-assembly peptide developed by Zhang *et al*. and available commercially as PuraMatrix^{TM} was found to support the neurite growth and differentiation, neural stem cell differentiation, brain regeneration, osteoblast differentiation and bone regeneration (Zhang et al., 1995, Holmes et al., 2000, Gelain et al., 2006, Ellis-Behnke et al., 2006, Bokhari et al., 2005, Misawa et al., 2006). P11-4 is another SAP that was extensively studied and was used to treat bone defects, dental hypersensitivity and dental caries (Firth et al., 2006, Kirkham et al., 2007). It was hypothesized that mineralization was achieved through de novo nucleation of HA by attracting calcium via the anionic groups of the side-chains of the self-assembly peptide. However, the lack of specific signalling motifs in these scaffolds suggested that the 3D nanostructure played a crucial role in regeneration. Gelain *et al*. showed that RADA16-I has a comparable ultra-structure to extracellular matrix (Matrigel) in the nanofibers structure and porosity (Gelain et al., 2006).

1.10.1 Designer peptides

SAPs can be functionalized to induce specific cellular interaction by incorporating active peptide motifs. For example, coupling of RADA16-I with 2-unit integrin receptor-binding site of Arginine-glycine-aspartic acid (RGD) binding sequence PRG and laminin cell adhesion motif stimulated fibroblasts proliferation, migration and collagen production (Kumada et al., 2010, Kumada and Zhang, 2010). Specific peptides motifs were designed for osteogenesis including ALK (ALKRQGRTLYGF) bone-cell secreted-signal peptide and osteopontin motif DGR (DGRGDSVAYG) (Horii et al., 2007). It was demonstrated that ALP activity and OCN secretion were significantly increased in murine pre-osteoblast (MC3T3-E1). Self-assembly peptides are nanofibrous 3D scaffolds that resemble ECM architecture and enhance regeneration by promoting cell attachment, proliferation and differentiation. In addition, the ease in coupling the peptides structure with bioactive motifs makes self-assembly peptides promising candidate biomaterials for tissue regeneration.

1.11 Limitations of current systems

For centuries, bone grafting was the treatment of choice in patients suffering from loss of bone tissue. Different materials are still being tested to provide the optimal bone regeneration. To date, engineering a biomaterial *in vitro* that can replace missing bone and induce osteoinduction, osteoconduction, osteointegration and promote angiogenesis *in vivo* has not yet been achieved. Because bone structure is complex, advanced fabrication techniques are replacing the conventional methods in order to mimic the complex structure and facilitate the bone regeneration process. 3D printing techniques especially robocasting fabricate precise, consistent and customized scaffolds to each defect. 3D printed BCP scaffolds showed promising results in inducing bone regeneration in both *in vitro* and *in vivo* studies (Ricci et al., 2012). However, vascularization is the key factor in regenerating bone in critical sized defects. Although various cells were studied to prevascularize bone scaffolds prior implantation, their clinical use is still debatable. Also, growth factors gained a significant amount of interest in functionalizing scaffolds as they play an important role in differentiating and guiding cells migration. However, more research is required to determine the best delivery system for a controlled release in order to facilitate bone formation. The use of SAPs in tissue engineering is promising as they form biomimetic hydrogels that enhance the local environment of cells, induce tissue regeneration and drug delivery (Gelain et al., 2010, Miller et al., 2010). Moreover, SAPs can modify surface properties of materials and facilitate cell attachment and proliferation (Yang et al., 2007, Gelain et al., 2007). However, further studies are required to identify the biochemical and environmental factors that can induce bone graft vascularization and the optimal factors that can be used to functionalize bone grafts to enhance the bone formation process.

1.12 Aims of the Study

This study was designed to develop a bone scaffold that can promote cellular interaction at the implanted site in order to enhance vascularization and therefore bone formation. 3D printed BCP scaffolds that showed promising results in bone regeneration were used in this study (Ricci et al., 2012). Two factors were evaluated as methods of enhancing osteogenesis in these scaffolds including: 1) pore geometry and 2) novel SAPs; DAR16-II fabricated with a reverse sequence of RAD16-II, a free N-terminus and an amide group at the C-terminus. DAR16-II was investigated as a proactive coating material to BCP scaffolds.

These aims were intended to add a smart design and matrix that mimics ECM to the surface of CaP scaffolds to augment its osteoinductive properties employed by calcium and phosphate ions release during scaffolds resorption.

1.12.1 Main aim of the study

1. To investigate the effect of pore size and geometry in functionalizing 3D printed BCP scaffolds.
2. To determine if DAR16-II can be used as a proactive coating matrix for BCP scaffolds.
3. To investigate the biological effect of DAR16-II at the cell level on osteogenesis and angiogenesis.

1.12.2 Specific aims of the study

- **Chapter 2 (*in vivo*)**

1) To evaluate the effect of two different pore-geometries; square and round in the bone formation process.

2) To assess the biological compatibility of BCP scaffolds and DAR16-II.
3) To evaluate DAR16-II as a BCP coating in enhancing osteogenesis.

- **Chapter 3 (*in vitro*)**

1) To investigate the effect of DAR16-II coating BCP scaffolds on MSCs proliferation and osteogenic differentiation.
2) To explore the effect of DAR16-II on MSCs (fibroblast-like and mesenspheres) differentiation without BCP scaffolds.

- **Chapter 4 (*in vitro*)**

1) To evaluate the DAR16-II effect on endothelial cells proliferation, adhesion and activation.
2) To assess to effect of DAR16-II on inflammatory cells attachment and polarization.

2. Chapter 2: Functionalization of 3D printed scaffolds: In-Vivo study

2.1 Introduction

Tissue engineering aims to regenerate damaged tissue by restoring structure and function of the lost tissue. In small bone defect, this can be achieved by using a biocompatible scaffold that acts as a template on which the surrounding (endogenous) cells migrate, proliferate and differentiate. In CSD, employment of materials with improved characteristics such as osteo-inductivity (i.e. the ability to directly promote stem cell differentiation into osteoprogenitor cells) is required. It has been clearly demonstrated that during endochondral ossification, angiogenesis and osteogenesis are coupled via specialised endothelial cells acting through Notch signalling (Kusumbe et al., 2014, Ramasamy et al., 2014). Endothelial Notch signalling promotes endothelial cell proliferation and vessel growth in bone and is required for endothelial Noggin expression. This controls the differentiation of perivascular osteoprogenitor cells thereby controlling osteogenesis. Consequently, the development of a scaffold that is able to provide a bio-active niche that enhances endothelial cell attachment and differentiation would have the potential to promote better angiogenic and osteogenic responses in these large defects.

Bioactive BCP is a biocompatible and partially biodegradable material. It has been previously used in treating various maxillofacial defects (Mercier et al., 1996, Hirano et al., 1997, OKII et al., 2001). BCP is composed of amorphous β-TCP [Ca3 (PO4)2] and fine crystalline HA [Ca10(PO4)6(OH)2]) in proportions similar to those of natural bone (Greenwald et al., 2001). The HA biomaterial is semi-permanent and ideally, scaffolds should entirely remodel/resorb to allow complete bone regeneration. Therefore, the BCP scaffolds developed in this project were fabricated from 15%HA/85%β-TCP colloidal ink that result in 99% β-TCP resorbable scaffolds after processing and firing (Ricci et al., 2012). β-TCP is an osteoconductive and resorbable biomaterial that allows osteoclastic resorption and complete bone remodelling (Lu et al., 2002). In the present study, scaffolds were three-dimensionally fabricated by robocasting (three-dimensional ink writing or direct write [DW] technology) (Figure 2.1).

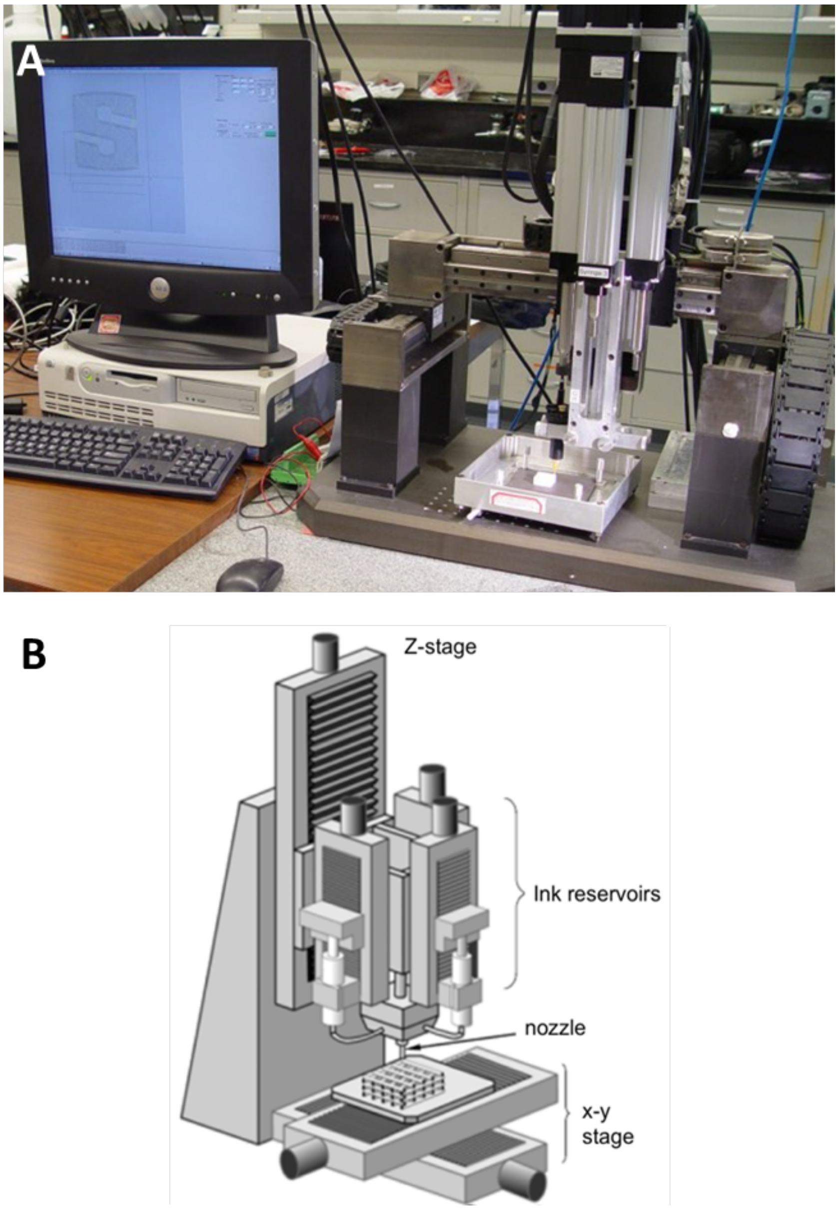

Figure 2.1 BCP 3D printing technique. A) Robocasting apparatus (Dr.James Smay's laboratory, Oklahoma State University (OSU), Aerotech Inc., Pittsburg, PA) connected to a computer aided program RoboCAD (Robocad 3.1, 3D Inks, Stillwater, OK) to customize the BCP scaffold design and control the printing process. B) Schematic drawing (adapted from Smay et al., 2002) of the robocasting apparatus: colloidal gel-based inks were housed in individual syringes mounted on the z-axis motion stage. A cylindrical nozzle disperses the ink onto a moving x-y stage. The first layer is printed on a platform in the x-y plane, after that, the gantry (vertical platform supports equipment) ascends in the z direction above the platform and writes the next layer.

In robocasting, concentrated colloidal ink is extruded from a cylindrical nozzle and builds a computer-designed scaffold layer-by-layer. BCP (15%HA/85%β-TCP) scaffolds fabricated by robocasting have shown controlled and reproducible architecture and rapid bone healing in CSD in a rabbit trephine model *in vivo* at 6 and 18 weeks (Ricci et al., 2012). They described scaffolds printed in the shape of a continuous lattice with two pore sizes: 250x250 μm and 400x400 μm. The larger pore size, part of the printed scaffold, was similar to cancellous bone comprising 70% bone and scaffold while 30% was marrow and soft tissue. After 16 weeks, scaffolds showed 30% remodelling through osteoclastic activity with consistent bone growth across the defects (Ricci et al., 2012). In addition to the consistent printing of pores shape, size and strut size (the thickness of the printed ink) can also be customized by firing temperature and colloidal particle size. Moreover, scaffold struts are nanoporous structures that can allow material adsorption.

BCP scaffolds are highly osteogenic, safe and efficient bone replacement material that showed comparable regeneration capacity to autologous bone grafts (Fellah et al., 2008). This was demonstrated by comparing osteogenicity of BCP fillers to autografts in ectopic and orthotopic sites in adult white milk goats. BCP showed superior stability and osteogenic properties compared to autologous bone grafts in CSD defects (Fellah et al., 2008). Hence, developing new strategies to induce vascularization in BCP scaffolds can improve its regeneration potential and enhance bone formation. Several strategies have been proposed to enhance vascularization including: cell loading, growth factors delivery and the design of 3D scaffolds (Crisan et al., 2008, Ferrara et al., 2003, Mannsfeld et al., 2010). However, to date, these methods have achieved limited success in increasing vascularization in new bone. On the basis of these facts, we proposed to study the effect of the scaffold internal structure including pore size and geometry in enhancing vascularization of 3D printed BCP scaffolds.

2.1.1 Pore geometry

Pore shape has a significant influence on tissue regeneration as demonstrated in various *in vitro* and *in vivo* studies (Table 2.1). It has been established that the rate of tissue formation is proportional to the surface curvature (Rumpler et al., 2008, Bidan et al., 2012, Bidan et al., 2013). Particularly, curvatures in the shape of concavities have been shown to enhance tissue growth in comparison to convex or flat surfaces (Ripamonti et al., 2012, Bidan et al., 2012, Bidan et al., 2013). Furthermore, concave surfaces showed a higher actin and myosin fibre formation suggesting a higher state of cell stress (Gamsjäger et al., 2013). Moreover, surface concavities of calcium phosphate scaffolds enhanced mineralization *in vitro* (Bianchi et al., 2014). Sacarano *et al*. showed that the number of blood vessels formed with TCP/HA coated titanium scaffolds in rabbit's tibia were significantly higher in concavities compared to convex surfaces (Scarano et al., 2014). Besides mineralization and vascularization, pore geometry was found to influence inflammation by producing pro-inflammatory cytokines: tumor necrosis factor (TNF)-α and interleukin (IL)-12/23 *in vitro* with larger and wider angle pores (Almeida et al., 2014). It has been established that a moderate level of inflammation is required during the tissue regeneration process (Mountziaris et al., 2011, Brown et al., 2012).

(Author, year)	Study type	Material	Cells or Animal model	Pore geometry	Outcome
(Rumpler et al., 2008)	In-vitro	HA	MC3T3-E1	Triangular, square, hexagonal and circular	Tissue amplification was greater in hexagonal than the square, followed by the triangular pores
(Bidan et al., 2012)	In-vitro	HA	MC3T3-E1	Semicircular and circular	More tissue growth with circular pores
(Ripamonti et al., 2012)	In-vitro	CaP/CaCO3	MC3T3-E1	Surface concavities	Induced cell orientation and alignment
(Van Bael et al., 2012)	In-vitro	Titanium	Human periosteum-derived cells (hPDC)	Triangular, hexagonal and rectangular	Significant increase in ALP activity with triangular pores
(Bidan et al., 2013)	In-vitro	HA	MC3T3-E1	Square and cross-shaped	Faster tissue deposition with cross-shaped pores
(Bianchi et al., 2014)	In-vitro	HA and b-TCP	Simulated body fluid	Surface concavities	Higher mineralization inside cavities
(Xu et al., 2014)	In-vitro	Nagelschmidtite ceramic	MC3T3-E1	Square, triangular and parallelogram	Highest ALP activity with parallelogram pores
(Almeida et al., 2014)	In-vitro	PLA, PLA/CaP or Chitosan	Human Monocytes/ Macrophages	Orthogonal and orthogonal double layer	Larger pores and wider angles induced TNF-α and IL-12/23 production
(Ripamonti et al., 2012)	In-vivo	HA coated titanium	Chacma baboons *P. ursinus* (mandible, tibia and rectus abdominis muscle)	Surface concavities	More bone in contact (BIC) was found with surface concavities compared to plain constructs
(Scarano et al., 2014)	In-vivo	TCP/HA coated titanium	New Zealand white mature male rabbits tibia	Surface concavities and convexities	Significant difference in blood vessels numbers with concavities

Table 2.1 In-vitro and in-vivo studies of the effect of pore geometry on tissue regeneration.

2.1.2 Pore size

It was demonstrated that the 400 μm is the ideal pore size for blood vessels formation (Bai et al., 2010). Scaffolds with larger pore size showed no significant difference on scaffold vascularization.

Kommareddy *et al*. studied the kinetics of preosteoblasts MC3T3-E1 tissue growth in 3D channels in different polymeric scaffolds. They demonstrated that growth follows two stages (Kommareddy et al., 2010); the first stage is material dependent, cell attachment and differentiation is affected by material composition and stiffness. After a few weeks, the second stage of tissue growth becomes dependent on pore geometry rather than scaffold material as the cells begin to grow within their own matrix. A following study by Tamjid *et al*. supported the same findings in which they described tissue growth into 3D channels and showed that pore geometry was the main factor in the final stage of tissue growth within the channels (Tamjid et al., 2013). However, to date no long *in vitro* or *in vivo* studies have been reported that assess the effect of pore geometry on bone regeneration. In the present study, two different pore geometries were compared: square and round. The smallest pore size achieved by 3D printing to form round-shaped pores was 800 μm, while square pores were printed at 400 μm. This square pores were used as controls in this study as they were previously described and successfully induced bone formation across CSDs in rabbit skull (Ricci et al., 2012).

However, the biological process of angiogenesis should be considered in order to induce cell adhesion, growth and angiogenesis in the designed scaffold. Cell adhesion is critical for blood vessels formation and integrines, cell adhesion molecules, were found to play an essential role during vascular regeneration (Brooks et al., 1994, Eliceiri and Cheresh, 2001). Six types of integrins including αvβ3, αvβ5, α5β1, αvβ1, α2β1 and α1β1were found to be involved in blood vessels formation (Camenisch et al., 2002). Type αv integrin in particular was highly expressed in activated ECs during wound healing (Eliceiri and Cheresh, 1999). These integrins specifically recognize Arg-Gly-Asp (RGD) peptide in ECM to regulate the EC migration and adhesion (Reynolds et al., 2009). Hence, the use of a smart matrix that can mimic the RGD peptides in conjunction to BCP scaffold can recruit activated EC required for angiogenesis and enhance bone regeneration. In order to develop this matrix, we proposed to use self-assembly peptides (SAPs), synthetic peptides, which have a peptide sequence similar to RGD to enhance the biological cell response of 3D printed scaffolds.

2.1.3 Self-assembly peptide

SAPs consist of alternating ionic hydrophilic and hydrophobic amino acids. These peptides interact with salt-containing solutions and form hydrogels composed of 99.5–99.9% water (Hauser and Zhang, 2010). They form stable beta sheets (β-sheets) and have been shown to be useful as nanofiber scaffolds (Gelain et al., 2006, Horii et al., 2007, Wang et al., 2008). SAPs interact through: 1) non-covalent hydrogen bonds along the backbones, 2) the arrays of ionic + and charge interactions, 3) alanine hydrophobic interactions and van der Waals interactions, and 4) water-mediated hydrogen bond formations (Yokoi et al., 2005). The developed β-sheet has been reported to be stable at challenging conditions such as high temperatures, wide pH range and concentrated denaturing chemicals as urea and guanidium hydrochloride (Zhang et al., 1994). The nanopores developed within SAPs scaffolds range from 5-200 nanometres (Zhang et al., 2005, Wang et al., 2008). It was shown that these nanoporous scaffolds significantly facilitated cell infiltration, oxygen and signalling molecules' delivery, as well as waste product removal (Koutsopoulos et al., 2009, Luo et al., 2011). These nanostructured materials have shown the ability to promote cell attachment, tissue regeneration and to be useful in drug delivery (Zhang et al., 2005). The original SAPs sequence was inspired by a yeast protein called Zuotin (Zhang et al., 1992). Zuotin has a repetitive 16-reside sequence motif, n-AEAEAKAKAEAEAKAK-c (EAK16-II), of alternating Lysine-Alanine-Glutamate segments. Modified SAPs with Arginine–Alanine–Aspartate amino acids were developed in the following sequences: RADA16-I (AcN-RADARADARADARADA-CNH2) and RADA16-II (AcN-RARADADARARADADA-CNH2) in which arginine and aspartic acid residues substitute lysine and glutamate in EAK peptides (Zhang et al., 2005). This RAD motif is similar to the RGD that is found in ECM proteins. As a result, RADA16-I and RADA16-II nanofiber scaffolds showed enhanced neural cells attachment, neurite outgrowth and active synapse formation in rats (Holmes et al., 2000). In addition, RADA16-I was found to be a homeostatic scaffold as it stopped bleeding in different tissue types in less than 15 seconds (Ellis-Behnke et al., 2006). Furthermore, injecting RADA16-II in mouse myocardium, led to the development of a favourable nanofiber microenvironment for vascularization by recruiting endothelial progenitor cells that form functional vascular structures (Davis et al., 2005). Moreover, it was demonstrated that RADA16-II scaffolds *in vitro* promoted human microvascular endothelial cell survival and capillary-like network formation in the absence of angiogenic factors as well as upregulating angiogenic factor VEGF expression (Narmoneva et al., 2005). The alanines in the SAPs sequence develop overlapping hydrophobic interactions in water which is similar to silk fibroin produced by the silkworm and to spider silk (Zhang et al., 2005). Due to this distinctive ability in forming this silk-like structure, we proposed to use SAPs as a coating material to functionalize BCP scaffolds.

The SAPs developed in the present study was DAR16-II (ADADARARADADARAR), the reverse sequence of RADA16-II with a free N-terminus (amino group: NH2) and with an amide group (CONH2) at the C-terminal. Since the struts of BCP scaffolds are nanoporous and the main composition of the ceramic is β-TCP, DAR16-II has the ability to form a hydrogel coating by interacting with the ceramic salts. Both BCP scaffolds and the (RADA) motif used in this study were tested in different studies for immunogenicity, mechanical properties, degradation and cellular interactions, both were found biocompatible and enhanced cellular interactions in *in vitro* and *in vivo* models (Zhang et al., 1995, Holmes et al., 2000, Ricci et al., 2012, Witek et al., 2013).

In the present study, an *in vivo* rabbit model was chosen to assess the pore geometry and DAR16-II effects on bone regeneration. Rabbit models are the most commonly used animal models in musculoskeletal research (Neyt et al., 1998). Rabbits have a fast skeletal turnover and it was found that their bone mineral density and fracture toughness of mid-diaphyseal bone is similar to that of humans (Wang et al., 1998, Castaneda et al., 2006). Hence, due to these features, in addition to their availability and ease of housing and handling, rabbits are considered the first animal model choice to test bone scaffolds *in vivo* (Li et al., 2015).

Using the rabbit model, the objective of the study was to investigate the osteoinductive potential of DAR16-II; a modified self-assembling peptide (developed by Prof/Dettin at Padova University) adsorbed into the surface of a 3-dimensional (3D) printed BCP scaffold together with pore geometry.

The main aims of the present study were to:

1. Optimize and to develop a 3D BCP scaffolds (produced in Dr.James Smay's laboratory (Oklahoma State University (OSU)) providing an off-the-shelf custom-fabricated bone scaffolds.
2. Enhance the biological response by supplementing the scaffolds with factors to induce vascularization and bone formation, thus taking the 3D BCP scaffolds one step closer to the original aim.
3. Two factors were evaluated as a mode of enhancing osteogenesis in the 3D printed scaffolds: 1) pore geometry and 2) self-assembly peptides (SAPs) functionalization.

2.2 Materials and Methods

2.2.1 Scaffold fabrication

2.2.1.1 Calcination and attrition milling

Commercially available powders of HA (product 10185602, lot 43640; Honeywell, Seelze, Germany) [$Ca_{10}(PO_4)_6(OH)_2$] and β-TCP (product 21218, lot 1305078; Sigma-Aldrich, St Louis, MO) [$Ca_3(PO_4)_2$] were calcined in an alumina crucible at 800°C (for β-TCP) and 1100°C (for HA) for 11 hours (Figure 2.2). The powder was attrition milled (0.9-1.1 mm zirconia milling media; Union Process, Akron, OH) in ethanol (EtOH, analytic purity, product 241000200; Fisher Scientific, Hampton, NH) for 3 hours (model L001, Szegvary Attritor System; Union Process). After that, the suspension was separated from milling media and the ethanol-ceramic slurry was centrifuged in an angled rotor at 8000 revolutions/min for 4 minutes in polycarbonate centrifuge tubes (Eppendorf 5804 centrifuge, Eppendorf AG, Hamburg, Germany). Following centrifugation, the ethanol was decanted and the solid deposit was dried in an Oakton low-temperature oven at 80°C for 4 to 6 hours. Next, the solid material was dry milled for 5 minutes on a paint shaker with zirconia milling media (10-20 pieces of 10-mm-diameter milling media in a 500-mL polyethylene bottle per batch).

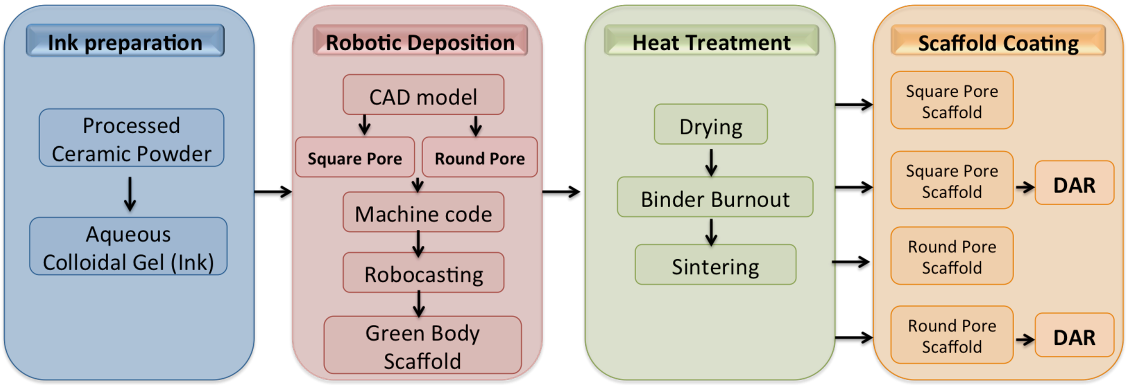

Figure 2.2 HA and β-TCP ceramic powders were converted into stable, small particles by calcination and attrition milling and then converted into colloidal gel formulations. Tool path calculation was designed with a CAD code for the two pore geometries: square and round. The robocasting direct-write machine executed the code (x, y, z linear interpolation) extruding the HA and β -TCP filaments through a fine nozzle (330μm) in the desired pattern and dimensions. The green body ceramic obtained at the end of the robocasting process was dried at room temperature and then heated to burn out the polymer binder and sinter the ceramic particles to achieve the final scaffold dimensions, strength, and density. At the end, scaffolds were either coated with DAR16-II or used as controls without coating.

2.2.1.2 Ink formation

The calcined and milled ceramic powder was used for the ink formulation. Concentrated HA and β-TCP suspensions, where volume fraction of ceramic φceramic = 0.45 to 0.5, were produced by mixing an appropriate amount of ceramic powder and ammonium polyacrylate (Darvan 821A; RT Vanderbilt, Norwalk, CT) solution to disperse particles into water (Table 2.2). The optimal dispersant proportion per gram of ceramics was 14.5 mg as determined by trial and error. The qualitative metric was determined so that the suspension would become very fluid after a short (60 seconds) mixing period upon addition of the powder to the dispersant solution. The powders were added to the mixture in 2 parts: first β-TCP and then HA according to the calculated weight, maintaining the 85:15 ratio. After each addition of powder, the suspension was mixed in the conditioning mixer (Thinky AR-250; Thinky, Tokyo, Japan) for 3 minutes after the addition of β-TCP, and then for a minute once HA was added, at 2000 rpm. Next, hydroxypropylmethylcellulose (Methocel F4M, Dow Chemical Company, Midland, MI) 5% weight aqueous solution, was added as a thickening agent and was mixed for 1 minute, and de-foamed for 30 seconds the conditioning mixer. As a final step, the suspension was gelled by adding poly-ethyleneimine (PEI, Product 195444, INC Biomedicals Inc, Aurora, OH) 10% weight solution, and mixed and de-foamed for 1 min and 30 seconds respectively. This resulted in the final ink that was used for printing. The ink needed to be stiff enough to maintain the shape after deposition but also needed to be able to flow through the syringe nozzle easily when a minimum amount of pressure was applied. The desired consistency was achieved by adding further PEI drop by drop and mixed and de-foamed after each drop was added.

Material	Quantity in grams
DI water	17.89
Darvan 821A	1.02
β-TCP	54.55
HA	9.44
F4M (5%)	3.89
Polyethyleneimine (10%)	1.10
Total Volume= 45mL **Liquid Volume= 24.30mL** **Solid Volume= 20.70mL** **Density of β-TCP= 3.1 g/cm^3** **Density of HA= 3.04 g/cm^3**	

Table 2.2 φ ceramic = 0.46 HA: β-TCP = 15:85 Ink Formulation.

2.2.1.3 Scaffolds robocasting

Robocasting uses a gantry robotic control (Aerotech Inc., Pittsburg, PA) to extrude colloidal ink through fine nozzles. The printing operation is both motion and flow rate controlled. The ink syringe containing the colloidal ink is attached to a z-axis mounted controlled stage for printing on a moving x-y stage. The 3-axis motion is independently controlled by a custom-designed, computer aided program RoboCAD (Robocad 3.1, 3D Inks, Stillwater, OK). Square-shaped scaffolds (10x10-mm, 3-mm thickness with 400µm-square or 800µm-round pores) were designed on the CAD program (Fig 2.3).

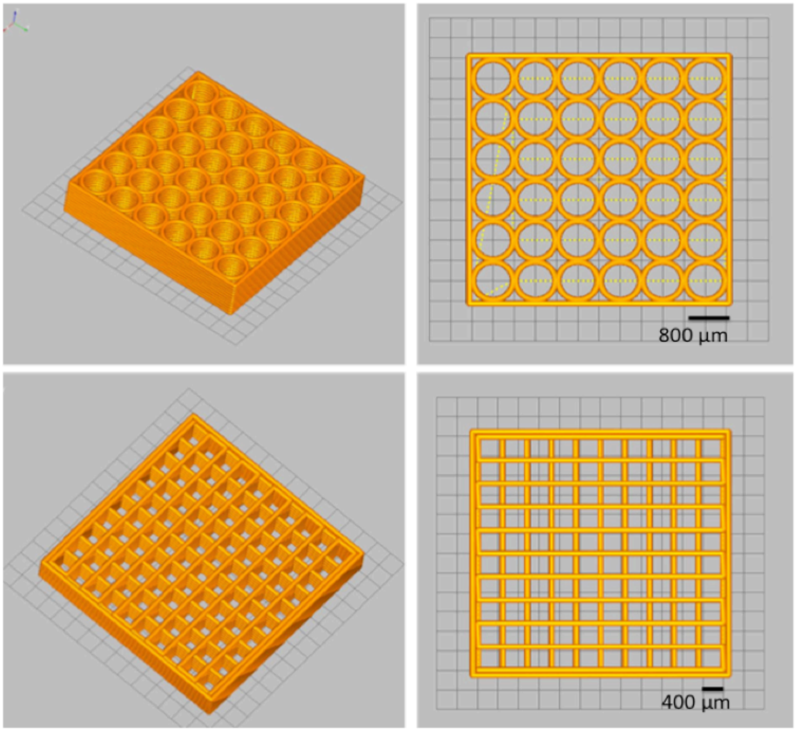

Figure 2.3 The CAD design developed by RoboCAD 3.1 software for the BCP scaffolds. Two patterns were designed: square and round pores with 400 µm and 800 µm pore size respectively. The designs were saved as "dot g" files and once the design was ready, a syringe was filled with the colloidal ink and loaded onto the robocasting apparatus and a ceramic printing surface was placed below the syringe in the oil medium to ensure a levelled surface for printing.

The CAD design was transferred to machine code to drive the x-y plane robotic deposition of the ink contained in a syringe. The round shaped pores could not be printed in a size smaller than 800 µm as the ink collapsed with the cylindrical nozzle used. Once a layer was printed, the nozzle was translated up (Δz) in the z-axis and another layer was printed. This process was repeated until entire scaffold was printed. This Δz distance is a function of the deposition nozzle diameter (D) and for all structures fabricated in this project, a Δz of 0.79D was used. The ink was housed in a syringe of 150-500 µm internal diameters (EFD Inc, Nordson, Ohio) and deposited through a cylindrical nozzle of 330µm internal diameter to produce the required scaffolds. After sintering the diameter of bone struts was designed to be 250µm. The ink exits the nozzle as a continuous, rod- like filament. The layers were printed at 6 to 10 µm/s deposition velocity in low viscosity paraffin oil (Ultra-Pure lamp oil, Lamplight Farms Inc., Menomonee Falls, WI). An alumina ceramic plate was used as the substrate (on which the scaffolds are printed) in the oil medium. This oil bath was used to prevent drying of printed scaffolds and to allow fine features to be patterned without clogging the nozzle.

2.2.1.4 Heat Treating the Scaffolds

Heat treatment was carried out for scaffold material to sinter and to enhance mechanical strength. It is a slow process that takes almost 7 hours with a gradual increase in temperature. The firing schedule started by heating at 4°C/min until 400°C, a hold at 400°C for 1 hour, then heated rapidly by 5°C/min until 1100°C and a hold of 4 hours and finally cooled by 9°C/ min until the samples reach room temperature and the desired scaffolds were achieved (Figure 2.4).

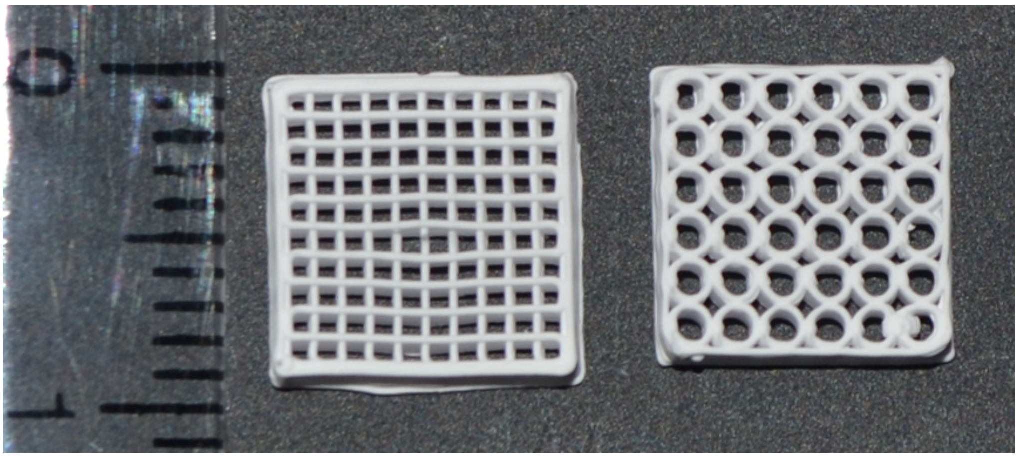

Figure 2.4 BCP scaffolds with square and round pore geometries after sintering. 10x10 mm and 2mm height. 400x400 µm the square pore size and 800x800 µm the round pore size.

2.2.2 Peptide synthesis

2.2.2.1 Materials

The solid support resins Rink-Amide 4-Methylbenzhydrylamine hydrochloride (MBHA) and the Fluorenylmethyloxycarbonyl (Fmoc) protected amino acids were from Novabiochem (Merck KGaA, Darmstadt, Germany). The coupling reagents 2-(1H-Benzotriazole-1-yl)-1,1,3,3-tetramethyluronium hexafluorophosphate (HBTU) and 1-Hydroxybenzotriazole (HOBt) were from Advanced Biotech (Seveso, MI, Italy). N,N-diisopropylethylamine (DIEA) and piperidine were from Biosolve (Leenderweg, Valkenswaard, Netherlands). Triethoxysilane (TES) was from Sigma-Aldrich (Steinheim, Germany). Solvents including N,N-dimethylformamide (DMF), trifluoroacetic acid (TFA), N-methyl-2-pyrrolidone (NMP) and dichloromethane (DCM) were from Biosolve.

2.2.2.2 SAPs fabrication

The peptide was synthesized on Rink-Amide MBHA resin (0.59 mmol/g) with Fmoc chemistry using a synthesizer Model 431 A (Applied Biosystem, Forster City, CA, USA) with 0.25 mmol scale. The following side-chain protections were used: *tert*-butyl ester (OtBu) for Asp; 2,2,5,7,8-pentamethylchroman-6-sulfonyl (Pmc) for Arg. The loading of the first amino acid was performed with a double coupling. The following four insertions were carried out with single couplings (4 equivalents of Fmoc-amino acid, 4 eq. HBTU, 4 eq. HOBt, 8 eq. DIEA, for 25 min) and the remaining with double couplings. The coupling solvent was NMP. Fmoc removal was carried out with 20% piperidine in NMP for 3 min. The peptide was unblocked from the resin and unprotected from side chain protecting groups using 95% TFA, 2.5% TES, 2.5% water mixture (v:v:v), for 2 h and 30 min at room temperature under magnetic stirring. Purification of the crude product was performed through reverse phase high performance liquid chromatography (RP-HPLC). The homogeneity (>98%) of the purified product was obtained by integration of the analytical HPLC peaks, whereas the identity of each product was determined by electrospray ionization time of flight (ESI-TOF) mass spectrometry (exp. mass = 1670.9 Da; theor. mass = 1670.8 Da). SAPs were synthesized as C-terminal amides with the following sequence: ADADARARADADARAR, named DAR16-II.

2.2.2.3 DAR16-II solution

The solution was prepared in 0.15% w/w concentration in distilled water. 300µl was required for each BCP scaffold. 22.5 mg of DAR16-II was dissolved in 15 ml distilled water. Solution was sterilized by filtration with 0.22 um filters (diameter 4 mm, Millex Cod. Z227501 by Millipore). Unused solution can be stored in -20°C.

2.2.3 In-vivo study

2.2.3.1 Bone substitute scaffolds

The BCP scaffolds were divided into the following groups (Table 2.3):

Group	Pore shape	Pore size	DAR16-II
1	Round	800 µm	–
2	Round	800 µm	+
3	Square	400 µm	–
4	Square	400 µm	+

Table 2.3 The four groups of BCP scaffolds that were implanted in calvaria rabbit model to assess osteogenesis.

2.2.3.2 Animals

The study was performed in collaboration with the Faculty of Medicine, University of Niš, Serbia, with the approval of the Local Ethical Committee (ref.–no.: 01–9337-25). The animals were previously obtained from the Military Medical Academy (Belgrade, Serbia). Eight male New Zealand white rabbits where used for this study. Prior to implantation the animals were maintained for one week to allow for acclimatization, under standard conditions with regular animal pellets, access to water ad libitum and an artificial light–dark cycle of 12 h each.

2.2.3.3 Experimental design and implantation

The rabbits were randomly distributed into the study groups as shown in table 2.4. In each rabbit, three defects were made in which two were filled with BCP scaffolds and one was left empty as a control. The animals were anesthetized by an intraperitoneal injection of ketamine hydrochloride (10mg/kg) potentiated with infiltrative local anaesthesia of operation site with 1.6 ml Xylocaine Xilazine [2%] and the implantation region was shaved and disinfected with iodine solution. Subsequently, the calvaria was exposed by medio-sagital skin incision approaching bone, lateral mobilisation reflection of the skin, galea and periosteum. Three critical size bone defects (10 mm in diameter) were performed in each animal (one central defect in the midline of frontal squama of frontale and one defect in each parietal bone: two defects in both sides of parietal bone) (Figure 2.5) (SkyScan 1272 μ X-ray CT imager, Bruker, Germany). Drilling was made using round diamond burs under water irrigation avoiding dura mater lesion. To coat BCP scaffolds with DAR16-II; each scaffold was immersed in 300μl DAR16-II solution for 1 hour at 37°C prior implantation.

8 Rabbits	1-4 Rabbits	In each rabbit: 1.Round +DAR 2.Round –DAR 3.Control defect
	5-8 Rabbits	In each rabbit: 1.Square +DAR 2.Square –DAR 3.Control defect

Table 2.4 Showing the experimental design and the animal distribution over the BCP scaffolds used to fill prepared defects.

After placement of BCP scaffolds into the two parietal bones defects, the incision was sutured in layers using interrupted stiches of resorbable polyglycolic-acid (PGA) 5/0 for periosteum and running polypropylene 4/0 stitch for peri-cranium and skin closure.

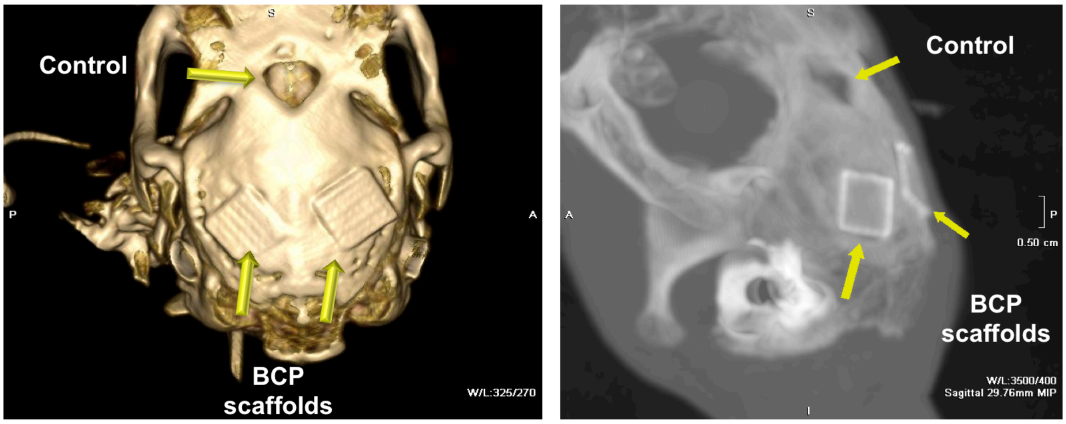

Figure 2.5 CT scans show the rabbit calvaria defects and BCP scaffolds implanted. Three defects were prepared (10x10 mm) in which two parietal defects were filled with BCP scaffolds (with and without DAR16-II coating) and one frontal defect was used as a control defect without biomaterial insertion. After 8 weeks, experiment was terminated and defects were analysed.

2.2.3.4 Processing procedure

At 8 weeks postoperatively, the rabbits were euthanized by one overdose of the ketamine and the calvarial bones were harvested for radiographic and histological examination.

Fresh calvarial specimens were cut ensuring 0.5 cm bone was present around the implant and control. Immediately after the euthanasia, the implanted bone substitute scaffolds were cut out together with the peri-implant tissue surgical scissor. Following excision, the explants were fixed in 10% neutral-buffered formalin for 48 hours and decalcified in 10% ethylene-diamine-tetraacetic (EDTA) acid (Fluka, Germany) at room temperature for 7-10 days. Histological preparation was performed at the FORM-Lab of the Clinic of Oro-Maxillofacial and Plastic Surgery of the Goethe University Frankfurt. Specimens were dehydrated in a series of increasing alcohol concentrations followed by Xylol treatment and embedding in paraffin. Then sections with a thickness of 3-5 μm were made using a rotation microtome (Leica RM2255, Wetzlar, Germany). Slides were stained using the following histochemical staining: Haematoxylin and Eosin (H&E), and Azan as previously described (Ghanaati et al., 2010).

2.2.3.5 Histology analysis

Histological analysis was performed using a Zeiss light microscope (Zeiss PrimoStar HD, Carl Zeiss Microscopy GmbH, Jena, Germany). Histological images were photographed using a microscopic camera integrated into the above-mentioned microscope connected to a computer running the ZEN 2 lite software (Carl Zeiss Microscopy GmbH, Jena, Germany).

2.2.3.6 Histomorphometrical measurements

Histo-morphometrical analysis was performed following established protocol quantifying the different tissue fractions within the implantation beds of bone substitutes and, thus, the comparison of the bone regeneration mediated by different materials (Ghanaati et al., 2010). Large images of the implantation areas montaged from 20-40 single images at

100x orginal magnification (OM) were acquired by a light microscope (Nikon® Eclipse 80i, Tokyo, Japan) equipped with an automatic scanning table (Prior, USA), a digital DS-Fi1 camera and a Digital sight DS-L2 unit (both: Nikon, Tokyo, Japan) connected to a computer running the NIS-Elements software version 4.0 (Nikon, Tokyo, Japan) and used for histomorphometrical analysis. The histomorphometrical analysis was performed with the scientific image-analysis program ImageJ (Schneider et al., 2012). After measurement of the total area of the implants, the areas of new-built bone tissue, of the remaining bone substitute scaffolds and of connective tissue within the implantation beds were measured on four slides from different animals per group. Based on this data the percent area of the three tissue fractions was determined and statistically analysed.

2.2.3.7 Statistical analyses

Results are expressed as mean ± standard deviation (SD). Data were analysed using GraphPad Prism 6.0c software (GraphPad Software Inc., La Jolla, USA) statistical software. Significance was predetermined at $\alpha = 0.05$. One-way analysis of variance (ANOVA) with post hoc Tukey's Multiple Comparison Test was used to compare the means among groups.

2.3 Results

2.3.1 Results of the histological analysis

The histological analysis showed bone growth along the braces of all four-bone substitute scaffolds (Figure 2.6 A–D). Bone growth of a uniform pattern was observed along the material surfaces coated with DAR16-II up to the centres compared to non-coated scaffolds. Square/small pore scaffolds coated with DAR16-II showed more newly formed bone compared to round/large pore scaffolds coated with DAR16-II (Figure 2.6 A–D).

In the control group, growth of new bone outgoing from the defect borders was visible which did not extend to the defect centres (Figure 2.6 E). In the central defect region, a membrane-like structure composed of a fibre-rich connective tissue was found that seemed to bridge the open spaces that were not covered by newly formed bone (Figure 2.6 E).

Furthermore, the histological analysis revealed that most of the surface areas of all scaffolds were covered by newly formed bone (Figure 2.6 A1–D1). Within the neighbouring connective tissue, moderate numbers of inflammatory cells, i.e., mostly macrophages and some lymphocytes and fibroblasts, were observed together with moderate numbers of blood vessels (Figure 2.7). At the material surfaces of all four-bone substitute scaffolds that were not covered by bone tissue, mononuclear cells of the macrophage line were detectable beside a few biomaterial-associated multinucleated giant cells (BMGCs) (Figure 2.7 A2 – D2).

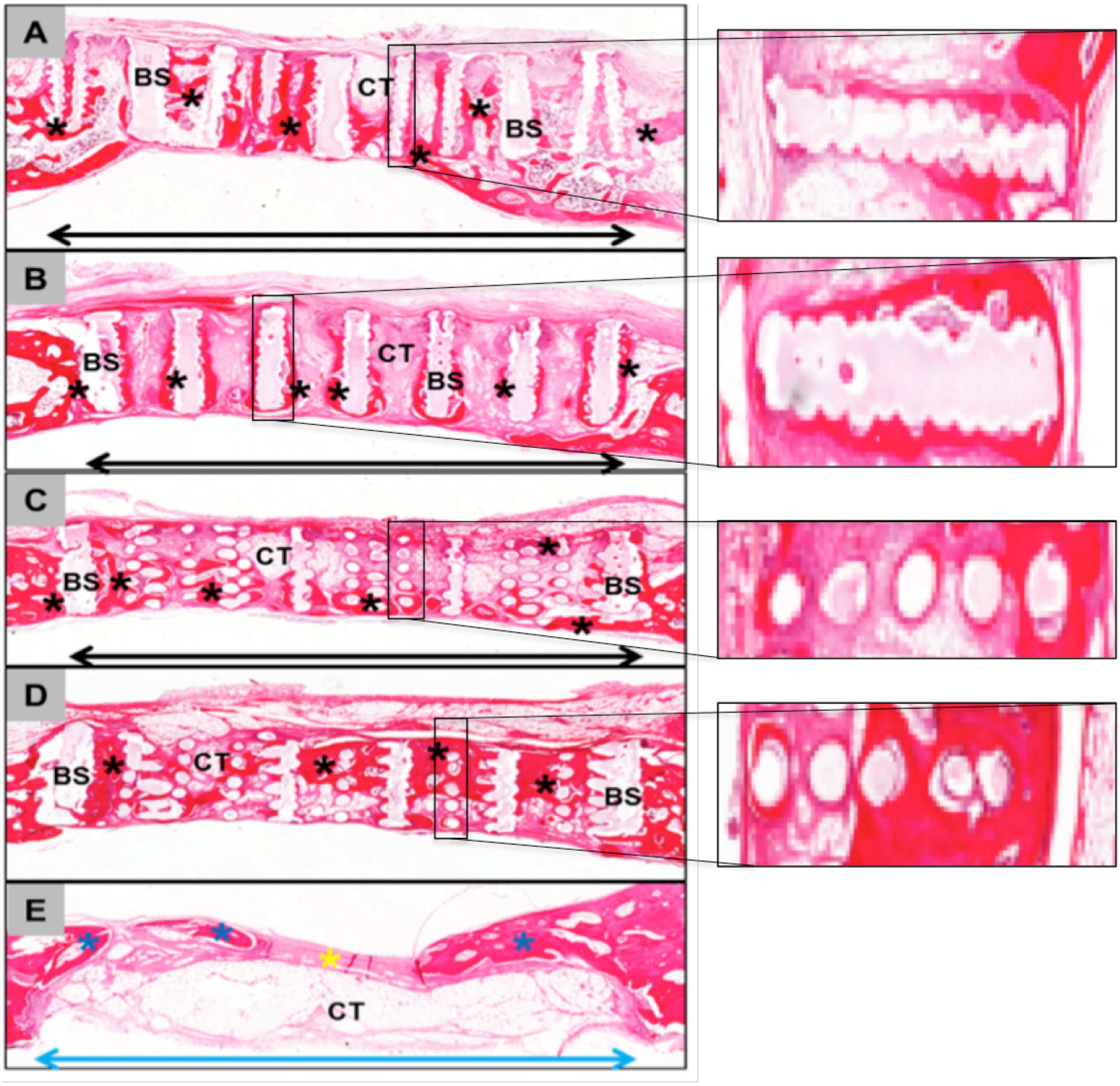

Figure 2.6 Overviews over the implantation areas of the four BCP bone substitute scaffolds (A: round (800µm), B: round (800µm) + DAR16-II, C: square (400µm); D: square (400µm) + DAR16-II) and the defect area of the control group (E). (A-D) In case of the four different bone substitute scaffolds (BS, black arrows) new-built bone (black asterisks) along the material surfaces up to the centres of the implantation sides was found (CT= connective tissue). (E) In case of the control defects (blue arrow) without material insertion bone growth (blue asterisks) outgoing from the defect borders towards the centre was observed. In the central defect area a membrane-like structure (yellow asterisks) composed of a fibre-rich connective tissue was found that appeared to cover the underlying brain tissue (NBT = neighbouring bone tissue, CT = connective tissue) (Hematoxylin and eosin (H&E) staining, total scans, 100x magnification).

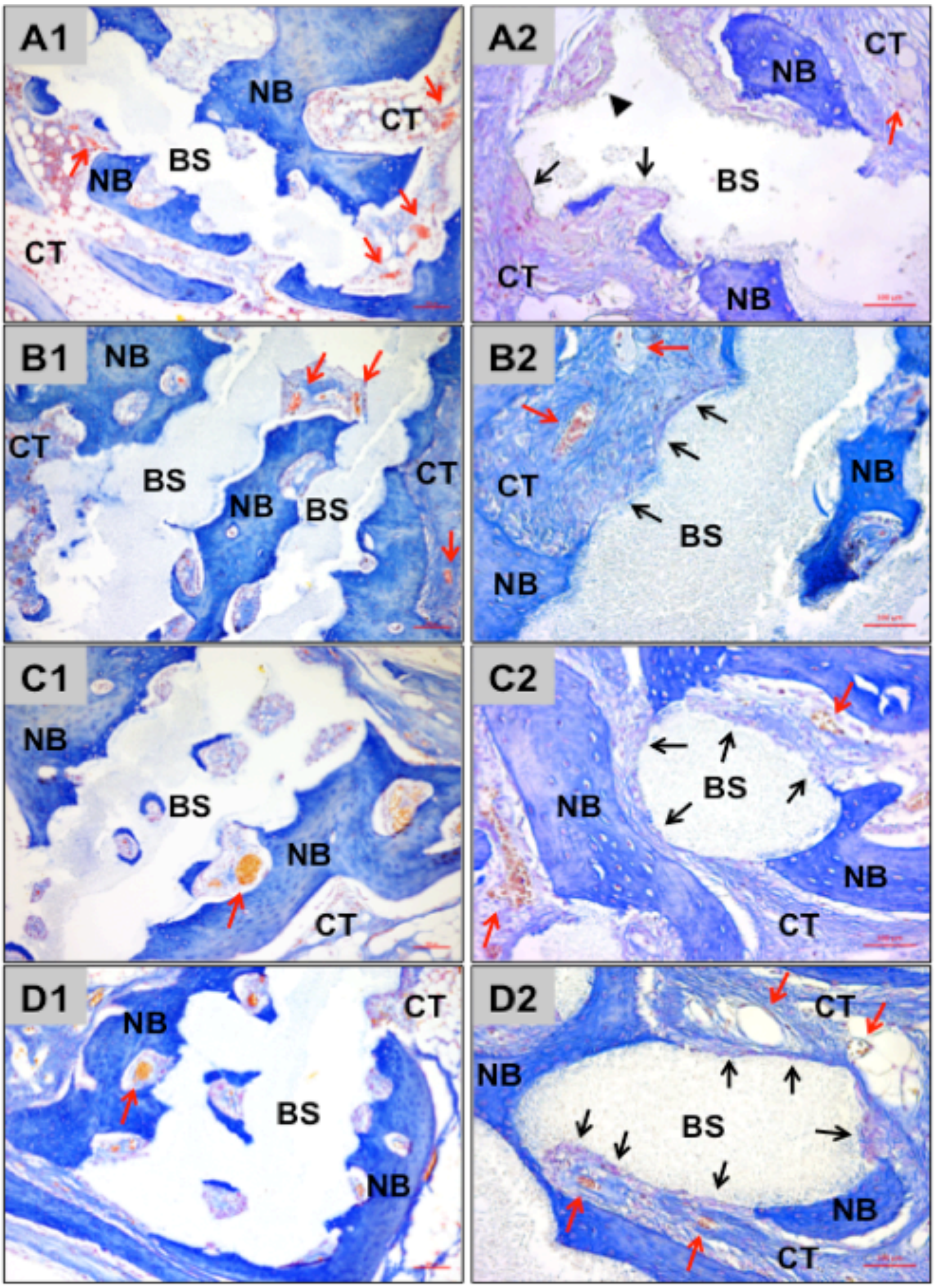

Figure 2.7 Integration and cellular response of the four BCP bone substitute scaffolds (A1 and A2: round (800µm), B1 and B2: round (800µm) + DAR16-II, C1 and C2: square (400µm); D1 and D2: square (400µm) + DAR16-II). A1 – D4 show that the surfaces of all bone substitute scaffolds (BS) were mainly covered by new-built bone tissue (NB). The surrounding connective tissue (CT) contained only low amounts of inflammatory cells and moderate vessel numbers (red arrows) (Azan-staining, 100x magnification, scale bars = 100 µm). A2 – D2 show the tissue reactions to the bone substitute scaffolds (BS) at the material-tissue interfaces. Mainly mononuclear cells (black arrows) were found at the surface areas that were not covered by new-built bone tissue (NB). Only low numbers of biomaterial-associated multinucleated giant cells (BMGCs, arrowhead in A2) were detected involved in the tissue reactions to all four scaffolds (BS) (CT = connective tissue, read arrows = vessels) (Azan-staining, 200x magnification, scale bars = 100 µm).

2.3.2 Results of total bone and histomorphometric analyses

Total bone analysis (Figure.2.8) showed that more bone was formed with DAR16-II coating in both pore geometries. Also, more bone was formed in the presence of square pores compared to round pore geometry. The histomorphometric analysis showed that the amount of bone in both pores; round and square pores was higher in the presence DAR16-II (Figure 2.9). In scaffolds with square pores, the amount of newly formed bone was significantly higher with the DAR16-II coating compared to non-coated square pores scaffold (* $p \leq 0.05$) (Figure 2.9).

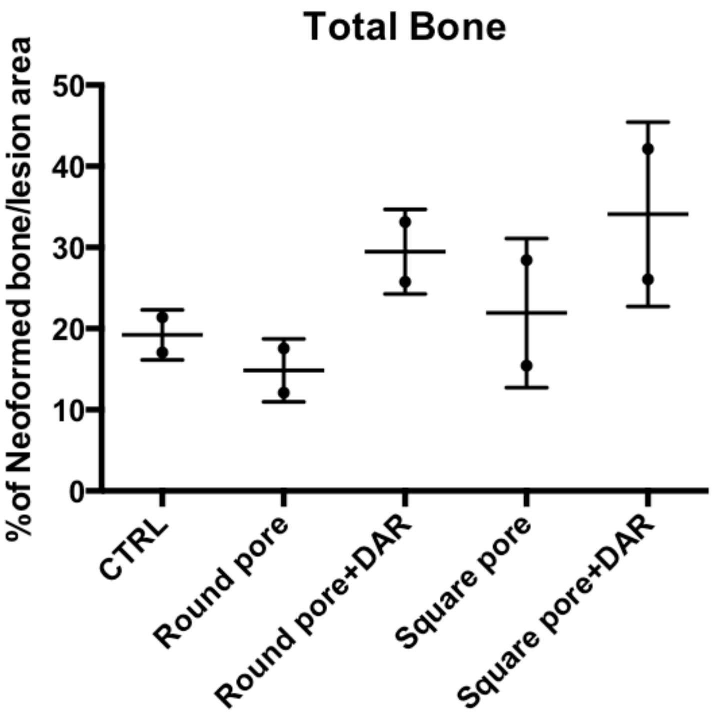

Figure 2.8 Total-bone developed in the four BCP scaffolds normalized by the lesion area. Scaffolds with round and square pore geometry induced more bone formation when coated with DAR16-II. More total-bone was found in square pore scaffolds compared to round pore scaffolds. Data represented as mean±SD, (n=2).

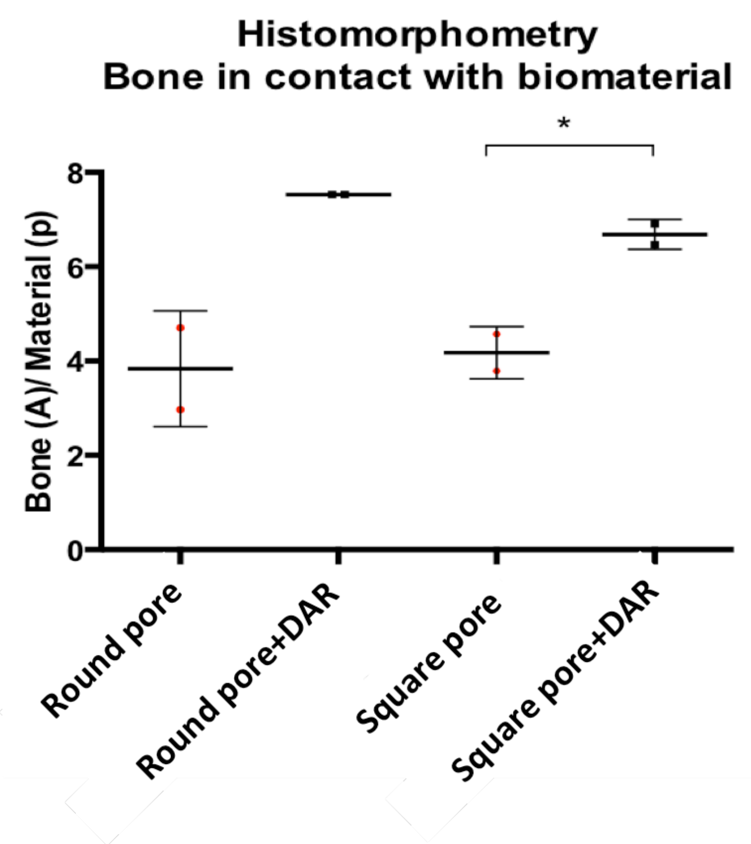

Figure 2.9 Newly formed bone in contact with the four BCP bone substitute scaffolds; (round pores with and without DAR16-II coating, square pores with and without DAR16-II coating). More bone in contact was detected with DAR16-II coating in both pore geometries. Coated scaffolds with round pores showed the highest amount of bone in contact development. Coated scaffolds with square pores showed a significant difference in forming bone in contact compared to non-coated square pore scaffolds ($p<0.05$). Data represented as mean±SD, (n=2).

2.4 Discussion

It is well established that angiogenesis and osteogenesis are coupled during bone formation and remodelling (Ramasamy et al., 2014, Kusumbe et al., 2014, Lafage-Proust et al., 2015). Consequently, bone scaffolds should acquire particular characteristics in order to induce vascularization to initiate and maintain new bone formation. Successful bone regeneration is dependent on scaffold chemical composition, continuous porosity, surface topography and 3D structural design (Zadpoor, 2015). It has been shown that pore size has a direct effect on bone regeneration and neo-tissue formation; however the optimal pore size remains debatable. For example, it was claimed that the optimal pore size for bone ingrowth was 100-400 µm (Itälä et al., 2001). Kuboki *et al*. precisely showed that HA scaffolds with pore size ranges from 300-400 µm were optimal for bone formation by showing higher ALP, OCN content and bone ingrowth (Kuboki et al., 2001). However, recently Taniguchi *et al*. have demonstrated that titanium scaffolds implanted in rabbit tibia significantly induced bone ingrowth with 600µm and 900µm pore sizes compared to 300 µm (Taniguchi et al., 2016). In contrast, work by Bai *et al*. showed that pore size of 400µm was found to be the upper limit for vascularization with no significant difference observed with larger pore size (Bai et al., 2010). Hence, in the *in vivo* study described in this chapter, 400 µm was the smallest pore size used in order to ensure adequate vascularization.

The pioneering work of Rumpler *et al*. in pore geometry established the theory of curvature-driven growth in which tissue formation follows the pore curvature (Table 2.1) (Rumpler et al., 2008). It was reported that tissue growth increased as the pore curvature increased. However, as the tissue filling the porous channels reached a circular geometry, this effect disappeared and growth followed a linear progression over the different pore geometries. In more recent work, Bidan *et al*. explored the effect of pore geometry on bone growth by applying the shape of osteons and hemi-osteons in HA plates (Table 2.1) (Bidan et al., 2012). They proposed a "cord" model in which circular pores resulted in more tissue growth compared to semi-circular pores. Circular pores were filled in a concentric way while semi-circular channels were filled layer by layer until the curvature surface was flat. It was demonstrated that cells anchored on curved surfaces, creating an actin ''chord'' by generating tension between the adhesion sites (Bidan et al., 2012). In their study, HA plates with a circular or semi-circular pore were used to assess the effect of pore geometry on tissue growth. In our study, the same concept was applied in designing scaffold pores (Figure 2.3). However, in our study, the optimized BCP colloidal ink used in printing scaffolds in low viscosity paraffin oil was only able to fabricate scaffolds with 800µm round pores as the smallest pore size achieved without pore closure during printing. On the other hand, square-pore scaffolds were printed with square 400µm pores as a control. Despite pore size differences, histomorphometric analysis showed that there was no significant difference between round and square pores in total bone and bone in contact (Figure 2.8, 2.9). In contrast, round pores with DAR16-II coating showed the highest and most consistent bone in contact formation compared to other groups (Figure 2.9). Furthermore, DAR16-II coating enhanced total bone formation and bone in contact in both pore geometries (Figure 2.8, 2.9). This finding demonstrates that DAR16-II coating was successful in functionalizing 3D printed BCP scaffolds. In addition, newly formed bone in coated scaffolds (Figure 2.6 B and D) was uniform around the pore surfaces all the way to the centre of the defect compared to non-coated scaffolds (Figure 2.6 A and C).

The main objective of this study was to functionalize 3D printed BCP scaffolds to enhance vascularization and bone formation using a practical and reproducible method. It demonstrated that soaking BCP scaffolds in 0.15% DAR16-II one-hour prior to implantation was able to functionalize scaffolds and induce further bone formation compared to non-coated scaffolds. Moreover, no foreign body reaction was detected and a favourable healing environment was demonstrated by the presence of blood vessels surrounding the four scaffolds (Figure 2.7). This agrees with previous studies demonstrating that (RADA) motif (the building block of the DAR16-II), is biologically compatible (Zhang et al., 1995, Holmes et al., 2000, Narmoneva et al., 2004). Although the reverse sequence; RADA16-II was found to promote vascularization in *in vivo* and *in vitro* studies, the mode of action was not identified at the cellular and molecular level (Davis et al., 2005, Narmoneva et al., 2005). Our results indicated that DAR16-II promoted better bone neo-formation around implanted biomaterials. This led us to further investigate the mechanism of action of DAR16-II at the cellular and molecular level.

2.5 Conclusion

Our results demonstrated that DAR16-II coating enhances bone formation without causing any adverse inflammatory reactions. In addition, pore geometries had no effect on bone formation. Overall, our results demonstrated a clear osteogenic effect of DAR16-II, which augments the osteoconductive properties of BCP. Therefore, in the following parts of this study we sought to define the cellular and molecular components mediating the observed effects.

3. Chapter 3: The role of DAR16-II in direct osteogenesis

3.1 Introduction

Bone has an inherent tendency to regenerate following traumatic injury. Residential stem cells, circulating blood cells, proinflammatory and anti-inflammatory macrophages orchestrate in order to regenerate the damaged tissue (Raggatt et al., 2014, Das et al., 2013, Kuroda et al., 2014). During healing, undifferentiated MSCs are recruited via signalling molecules to proliferate and differentiate into chondrocytes and osteoblasts to initiate the repairing process (Planell et al., 2009).

3.1.1 MSC-BCP in bone engineering

MSCs have been used with biomaterials for osteogenic studies since the first attempt of combining bone marrow-derived MSCs with ceramic scaffolds in an ectopic implantation in immune-deficient mice resulted in successful bone formation (Haynesworth et al., 1992). Mankani *et al*. showed that specifically BCP scaffolds and MSC combination was successful in regenerating critical-size dogs calvarial defects in a long-term study (Mankani et al., 2006a). The same findings were demonstrated by the same group in a similar long-term study using MSCs-BCP combination in regenerating calvarial and mandible defects in mouse model (Mankani et al., 2006b).

In humans, MSC-BCP was used as a bone graft in patients with unstable dorsal and lumbar spinal injuries (Bansal et al., 2009). MSC-BCP grafts were implanted on one side of the spine and on the other side autologous iliac crest bone grafts were implanted. Graft incorporation and fusion occurred in all patients on the MSC-BCP graft side showing analogous healing properties to autografts. In addition, HA, TCP or their combination have been employed in various human clinical studies, to treat long bone defects, maxillary sinus augmentation, femoral defect and maxillary reconstruction, and showed successful bone formation and good clinical recovery (Quarto et al., 2001, Shayesteh et al., 2008, Krečič Stres et al., 2007, Mesimäki et al., 2009). In order to decide the optimal HA:TCP ratio, Arinzeh *et al*. loaded implants of different ratios of HA and TCP with MSCs and implanted them subcutaneously in the back of severe combined immune-deficient (SCID) mice (Arinzeh et al., 2005). It was found that 20:80 HA:TCP showed the best bone formation *iv vitro* and *in vivo*. The release of calcium and phosphate ions as a result of BCP degradation can induce osteogenic differentiation through mechanisms that involve extracellular signal-regulated kinase 1/2 (ERK1/2) and cAMP response element-binding protein (CREB) signalling pathways in stem cells (Figure 3.1). Ca^{2+} ions infiltrate the cell membrane through ion channels and activate calcium/calmodulin (CaM) mediated calcium/calmodulin-dependent protein kinase (CaMK2α) (CaMK2α/CAM) pathway (Jung et al., 2010). CaMK2α/CAM pathway activates CREB-CRE (CRE is the cAMP response element) and ERK1/2 pathways (Zayzafoon et al., 2005). These pathways result in signal transduction of CRE and c-FOS (a proto-oncogene) pathways and promote osteogenic differentiation via production of BMP-2, osteopontin (OPN) and BSP. In addition, Ca^{2+} ions can activate the protein kinase C (PKC) pathway which modulate osteoblastic differentiation via ERK1/2 pathway (Barradas et al., 2012). Inorganic phosphate (Pi) ions also play a pivotal role in inducing osteogenesis by activating PKC and ERK1/2 pathways (Beck and Knecht, 2003). However, Ca^{2+} ions are required for phosphate in order to activate the ERK1/2 pathway via the formation of a calcium phosphate precipitate (CaPp) outside the cell (Khoshniat et al., 2011).

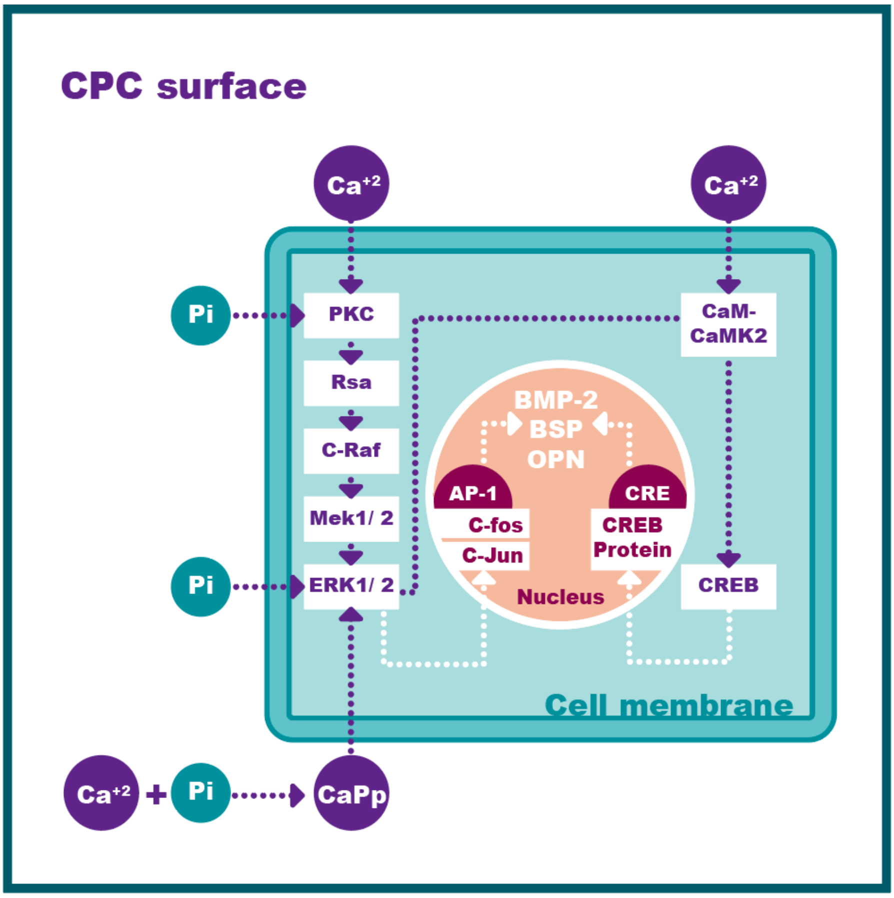

Figure 3.1 Diagram describes the role of calcium ions (Ca^{2+}) and phosphate (Pi) ions in osteoblastic differentiation. Ca^{2+} and Pi activates two pathways: extracellular signal-regulated kinase 1/2 (ERK1/2) and cAMP response element-binding protein (CREB). This activates the signal transduction of CRE and c-FOS pathways and promotes osteogenic differentiation via BMP-2, OPN and BSP production. This diagram demonstrates the collection findings of Jung et al., 2010, Zayzafoon et al., 2005, Barradas et al., 2012, Beck and Knecht., 2003 and Khoshniat el al., 2011.

As the MSC-BCP model is well established in osteogenic studies, it was used in the present study to investigate the mechanism of DAR16-II coating in direct osteogenesis *in vitro*.

3.1.2 MSCs for *in vitro* studies

MSCs are defined as "long-term self-renewing cell capable of generating the different mesenchymal lineages (osteolineage cells, chondrocytes, adipocytes, and muscle cells)" (Méndez□Ferrer et al., 2015). MSCs and fibroblasts share the properties of plastic adherence and proliferation capacity up to 50 passages before reaching senescence (Hayflick and Moorhead, 1961). As fibroblasts are abundant in bone marrow stroma, confusion in the properties or phenotype can lead to impure MSC isolation (Méndez□Ferrer et al., 2015). Human bone marrow MSC derived from CD45− CD71− CD31− CD105+ CD146+ nestin^{+} cell population was able to self-renew and spontaneously differentiate into mesenchymal lineage both *in vitro* and *in vivo* with potent hematopoiesis-supporting capacity (Isern et al., 2013). These cells were cultured as clonal mesenchymal spheres (mesenspheres) and it has been shown that they have the highest purity reported by expressing low-affinity nerve growth factor receptor CD271 in the absence of CD140a (PDGFRα) expression (Li et al., 2014). These mesenspheres were used in part of this study due to their promising applications in biomaterials research.

The objective of the following study was to explore the osteogenic effect of DAR16-II coating by seeding MSCs on coated and non-coated 3D printed BCP scaffolds *in vitro* without osteogenic conditioned media in a long-term study. In addition, the distinct osteogenic effect of DAR16-II was investigated by seeding MSCs on coated and non-coated tissue culture plates in short term-study.

Aims of the study:

1. Determine if DAR16-II coating of 3D printed BCP can enhance osteogenic differentiation compared to non-coated BCP scaffolds.
2. Explore the effect of DAR16-II on MSCs (fibroblast-like and mesenspheres) differentiation without BCP scaffolds.

3.2 Materials and methods

3.2.1 Cell culturing

Primary human MSCs isolated from bone marrow were obtained from Lonza (Slough, U.K.). The cells were cultured in humidified atmosphere (37 ºC, 5% Carbon dioxide, CO_2) in standard growth medium consisting of minimal essential medium (MEM), penicillin (50 U/ml), streptomycin (50 mg/ml), 20% fetal bovine serum (FBS) (all from Sigma-Aldrich, Dorset, U.K.), 10 ng/ml of basic fibroblast growth factor (b-FGF) (Prepotech, London, U.K.) and Glutamax (2 mM) (Invitrogen, Paisley, U.K.). Cells of passage 3 were used in this study.

3.2.1 BCP scaffolds coating and cell seeding

BCP scaffolds with square-shaped pores (previously described in chapter 2) were immersed in DAR16-II (previously described in chapter 2) solution (0.15% w/w DAR16-II in water) for one hour at 37°C-5%CO_2 atmosphere. Scaffolds without DAR16-II coating were used as controls. MSCs were micro-seeded at a density of $2x10^5$ cells per scaffold. These were micro-seeded in a total volume of 200 µl. 100 µl was micro-seeded onto the top of one side of BCP scaffold and allowed to attach for 30 min at 37°C. The scaffold was then turned and the same number of cells was seeded on the other side and left undisturbed for a further 30 min for the cells to attach at 37°C-5%CO_2 atmosphere. Scaffolds containing cells were then flooded with growth medium. The scaffolds were cultured for two time points of 14 and 42 days, with media change every 3 days.

3.2.2 Alkaline phosphatase (ALP) assay

Cell differentiation of the osteoblastic phenotype was determined by measuring the ALP production of MSCs. For lysates preparation, BCP scaffolds from days 14 and 42 were transferred to 1 ml of sterile water and went through three cycles of freezing, thawing at -80°C and 37°C, respectively for 20 minutes. A standard curve was prepared from 200 µg/ml 4-nitrophenol stock solution to give a range from 0 to 100 µg/ml. 50 µl of cell lysate was transferred to a 96 well plate and 50 µl of substrate reagent (p-nitrophenol phosphate, magnesium chloride hexahydrate and triton X-100 in Glycine) was added. The plate was placed on a shaker for 2 minutes and incubated at 37ºC for 20 minutes and measured spectrophotometrically (Dynex Technologies reader, USA) at a test wavelength of 405 nm. Tests were run on nine samples.

3.2.3 DNA assay

Cell growth and turnover was assessed by measuring total Deoxyribonucleic acid (DNA) production using the Hoechst 33258 dye. 100 µl aliquots from the previously prepared lysates were transferred to a 96-well plate; 100 µl Hoechst 33258 (Sigma-Aldrich, Dorset, U.K.) fluorimetric dye was added to each well. Hoechst 33258 reacted with lysates and DNA standards concentrations were 0, 0.31, 0.62, 1.25, 2.5, 5, 10 and 20 ng/ml. Florescence was measured at an excitation of 355 nm and emission wavelength of 450 nm on a Fluorometric plate reader (ChameleonTM, Hidex, Finland). The DNA content was calculated from the standard curve.

3.2.4 Runx2 release

Runx2 is an early marker of osteogenic differentiation. Supernatants were collected at days 14 and 42 and used to measure the amount of release of RUNX2 from cells. Runx2 release was measured using Cloude-clone ELISA kit (USCN, China). Optical density was measured spectrophotometrically at a wavelength of 450nm ± 10nm using a DYNEX Opsys technologies reader (Dynex Technologies reader, USA).

3.2.5 Gelatine preparation

Gelatine from porcine skin, Type A was dissolved in PBS (all form Sigma-Aldrich, Dorset, U.K) in 0.5% concentration. The solution was autoclaved at 123°C for 28 min using a compact 40 bench autoclave (Prioclave, Tactrol 2, RSC/E, UK). Sterile gelatine solution was stored at 4°C.

3.2.6 Seeding MSCs on tissue culture plates for gene expression analysis

6-well plates were either coated with 0.5% gelatine solution (as controls wells) or with 1:1 15%DAR16-II: 5% Gelatine solution (test wells). MSCs were seeded at a density of $3x10^5$ cells in growth medium for 48 hrs.

3.2.7 Gene expression analysis with quantitative real-time reverse transcription–polymerase chain reaction (qPCR)

***RNA extraction*.** Seeded cells were lysed using 300 µl of TRI-reagent (Ambion® AM9738). Each sample was transferred to an eppendorf tube and 60µl of chloroform (Sigma-Aldrich, Dorset, U.K) was added and tubes vortexed for 15 sec and then centrifuged at 20,000 g for 15 min at 4ºC. The colourless layer (aqueous phase) on the top was transferred into a new tube and the same process was repeated twice. After that, 150 µl isopropanol (Sigma-Aldrich, Dorset, U.K) was added. This was placed at −20°C overnight to maximize the yield of RNA before being centrifuged at 20,000 g for 20 min at 4°C to give a pellet. Sample supernatants were removed and pellets were washed twice in 1 ml of 75% ethanol by vortexing and centrifuging at 7,500 g for 5 min at 4ºC. Pellets were air-dried and re-suspended in 20 µl of nuclease-free water (Life technologies, Paisley, UK). The RNA yields were determined by spectrophotometry using the Nanodrop1000 (ND-1000 spectrophotometer; Isogen Life Science, Ijsselstein, The Netherlands).

Complimentary DNA (cDNA) synthesis. Reverse transcription was performed using 500 ng of total RNA sample, which was mixed with 2 µl of RT buffer (500 mM KCL, 100 Mm Tris-HCI, Ph 8.3). 0.8µl of 25xdNTP mixture, 2µl of 10x random hexamers, 0.4µl of RNase inhibitor (20U/ml) and 1µl of MultiScribe Reverse Transcriptase (50U/µl) (all from high capacity cDNA reverse transcription kit, Applied Biosystems, Warrington, UK). Nuclease-free water was added to bring the final reaction volume to 20µl. The mixes in the tubes were then incubated at 25ºC for 10 mins, 37ºC for 120 mins and then 85ºC for 5 mins in a Thermal Cycler Veriti (Applied Biosystems, Warrington, UK). The resultant cDNA samples were then stored at -20ºC.

<u>Reverse Transcriptase-Polymerase Chain Reaction (qPCR).</u> Real-time quantitative PCR was performed with a reaction volume of 10 µl per qPCR tube (Alpha Laboratories Limited, Luton, UK). The reaction volume was comprised of 5µl Ready Mix 2x, 0.5µl Forward Primers, 0.5µl Reverse Primers (all from a KiCqStart ® SYBR® Green Primers Kit (Sigma-Aldrich, Dorset, U.K)) and 4µl cDNA (in a 5:1 dilution with water). The Forward and Reverse Primers used were for the following genes: Runx2, GLUT1, VEGFA, Tyrosine-protein kinase receptor (Tie2) and ribosomal protein L (RPL). RPL was used as endogenous standard as it was found to have the most consistent expression level, when compared to β-actin and Glyceraldehyde-3-Phosphate-Dehydrogenase (GAPDH) (data not shown). The expression for the gene of interest was normalized to RPL expression. Relative expression for each target gene was calculated using the $2^{-\Delta\Delta CT}$ method. The Ct values of each target gene were normalized by the Ct of the housekeeping gene RPL to obtain the ΔCT values. These values were subtracted by the Ct value of the calibrator which in this article is the MSCs seeded on DAR16-II free coated wells to obtain the ΔΔCT values. This was performed in triplicates with the following cycler program: 1 cycle of 95°C–3min, 40 cycles of 95°C–10s and 60°C–20s, 1 cycle of 95°C–1min, 55°C–30s, 95°C–30s using the VA703m Corbett (Corbett Life Science, Sydney, Australia).

3.2.8 Culturing MSCs into Mesenspheres

MSCs were cultured as floating spheres, mesenspheres, in a defined xeno-free MSC growth medium Mesenchymal Stem Cell Growth Medium DXF (PromoCell, Heidelberg, Germany). Cells were seeded at 4000 cells per cm2 in a 5% CO_2 incubator at 37°C for 1 week to allow for mesenspheres to form. Half media change was carried out twice a week after the first week to maintain the cells.

3.2.9 Osteogenic medium

DXF medium was supplemented with 0.1μM dexamethasone (Dex), 0.05 mM ascorbic acid 2-phosphate (AsAP), and 10 mM glycerophosphate (Sigma-Aldrich, Dorset, U.K) for osteogenic differentiation.

3.2.10 Mesenspheres differentiation

Four types of coating conditions were compared: 1.DAR16-II coating (1:1 DAR16-II: Gelatine) with osteogenic media, 2. DAR16-II coating (1:1 DAR16-II: Gelatine) with DXF media, 3. Gelatine coating with DXF media (control) and 4.Gelatine coating with osteogenic media. In 96 wells, 50 µl of each coating solution was added to its designated well and removed after covering the entire well. Well were left to dry before seeding mesenspheres in a density of 6 mesenspheres per well. 100 µl of media was added to it designated well and left untouched for 9 days.

3.2.10 Alizarin Red S Staining of Mesenspheres

Mineralized matrix was stained with alizarin red S (1:100 in distilled water, adjusted to pH 4.2, and filtered) (Sigma-Aldrich, Dorset, U.K). Mesenspheres were washed with PBS (Sigma-Aldrich, Dorset, U.K) and fixed in phosphate-buffered 4% paraformaldehyde (FD Neurotechnologies, INC, MD, USA) for 15 minutes. Mesenspheres were washed with distilled water and stained for 10 minutes followed by five washes in 50% ethanol (Sigma-Aldrich, Dorset, U.K), and air dried. Mesenspheres were imaged using Olympus microscope with positive cells staining a bright, deep red colour (Olympus Biosystems, Münster, Germany).

3.2.11 Statistical analyses

Results are expressed as mean ± standard deviation (SD). Data were analysed using either On-way or two-way ANOVA with post hoc Tukey's Multiple Comparison to compare the means among groups. GraphPad Prism 6.0c software (GraphPad Software Inc., La Jolla, USA) was used as the statistical software. Significance was predetermined at $\alpha = 0.05$. Statistical differences were designated as significant if p-values were less than 0.05 (* $p \leq 0.05$), and as highly significant if P-values were less than 0.01 (** $p \leq 0.01$) or less than 0.001 (*** $p \leq 0.001$).

3.3 Results

3.3.1 Cell proliferation by total DNA content

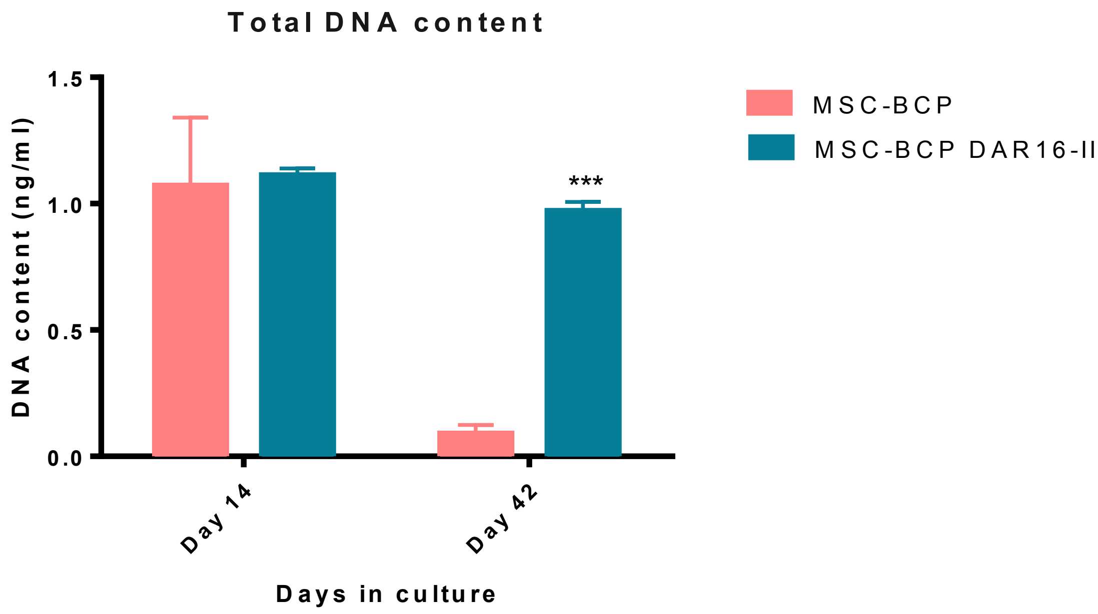

Figure 3.2 Total DNA content of MSCs seeded on DAR 16-II coated and non-coated BCP scaffolds at days 14 and 42. Significant reduction of cell proliferation was detected at day 42 in the non-coated scaffolds compared to DAR16-II coated scaffolds (p <0.001). Cell proliferation with DAR16-II coating at day 42 was comparable to cell proliferation at day 14 in coated scaffolds. Data represented as mean±SD, (n=9).

Total DNA content at day 14 showed that there was no significant difference in cell proliferation in the presence of DAR16-II coating. However, a significant difference in the cell proliferation rate was observed in the presence of DAR16-II coating at day 42 compared to non-coated scaffolds (p<0.001). Moreover, the level of cell proliferation with DAR16-II coating at both time points; days 14 and 42 was comparable. This suggests that DAR16-II preserves cell viability rather than induces cell proliferation (Figure 3.2).

3.3.2 Cell differentiation by ALP activity

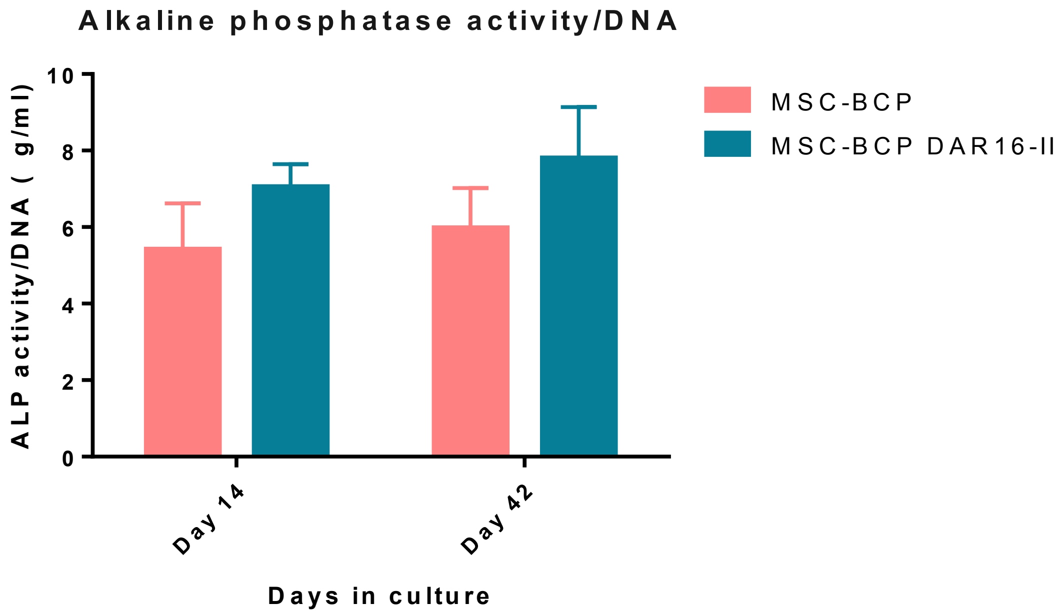

Figure 3.3 ALP activity of MSCs cultured on BCP scaffolds in the presence and absence of DAR16-II coating. No significant difference was observed between DAR16-II coated BCP scaffolds and non-coated scaffolds at days 14 and 42 of culture. Data represented as mean±SD, (n=9).

ALP production was used as an early indication of cell differentiation. Figure 3.3 shows the ALP activity of MSCs cultured on BCP scaffolds with and without DAR16-II coating. No significant difference of ALP activity was found in presence of DAR16-II coating on days 14 and 42. Thus osteogenic activity was not detected with or without DAR16-II coating.

3.3.3 RUNX2 release from MSCs

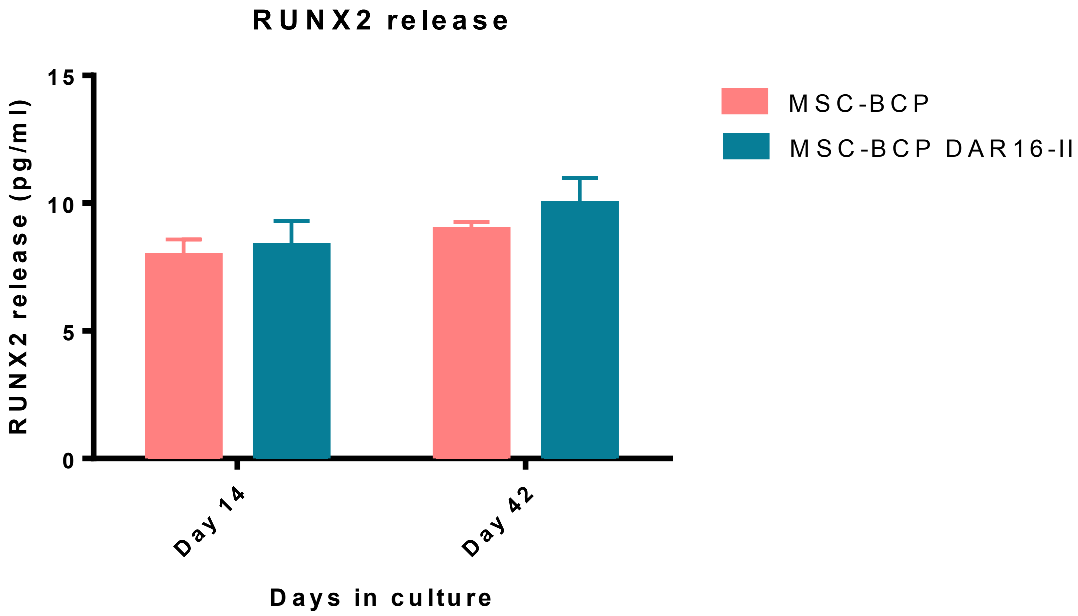

Figure 3.4 The amount of Runx2 released from MSCs cultured on BCP scaffolds with and without DAR16-II coating. No significant difference in Runx2 release was observed with or without DAR16-II coating at days 14 and 42 of culture. Data represented as mean±SD , (n=9).

Runx2 is an early transcription factor involved in osteogenic differentiation. Figure 3.4 shows that no difference was detected between DAR16-II coated and non-coated scaffolds in Runx2 protein expression at days 14 and 42. This suggests that DAR16-II did not have an early osteogenic effect on MSC differentiation.

3.3.4 q-RT-PCR

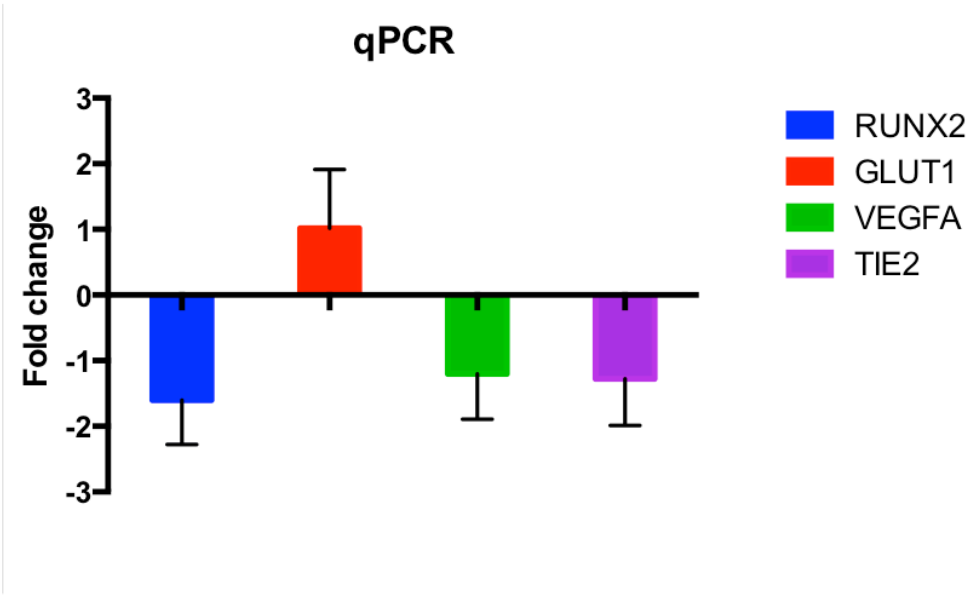

Figure 3.5 mRNA expression of Runx2, GlutI, VEGFA and Tie2 was analysed by quantitative-reverse transcription polymerase chain reaction (qRT-PCR). Down regulation of Runx2, VEGFA and Tie2 gene expression was detected from MSCs cultured for 48 hrs in DAR16-II coated wells with non-conditioned media. In addition, Glut1 gene was not expressed. Data represented as mean±SD (n=3).

qRT-PCR analysis showed that DAR16-II did not induce MSCs differentiations after 48 hrs of culture (Figure 3.5). Glut1 which is the earliest marker of osteogenic differentiation was not expressed. Runx2 expression which follows Glut1 during the osteogenic differentiation process was downregulated. Tie2, an early angiogenic marker, was downregulated as well as VEGFA gene expression; an endothelial-specific growth factor. These results indicate that DAR16-II lacks both an angiogenic and osteogenic differentiation effect on MSCs.

3.3.5 Alizarin red staining

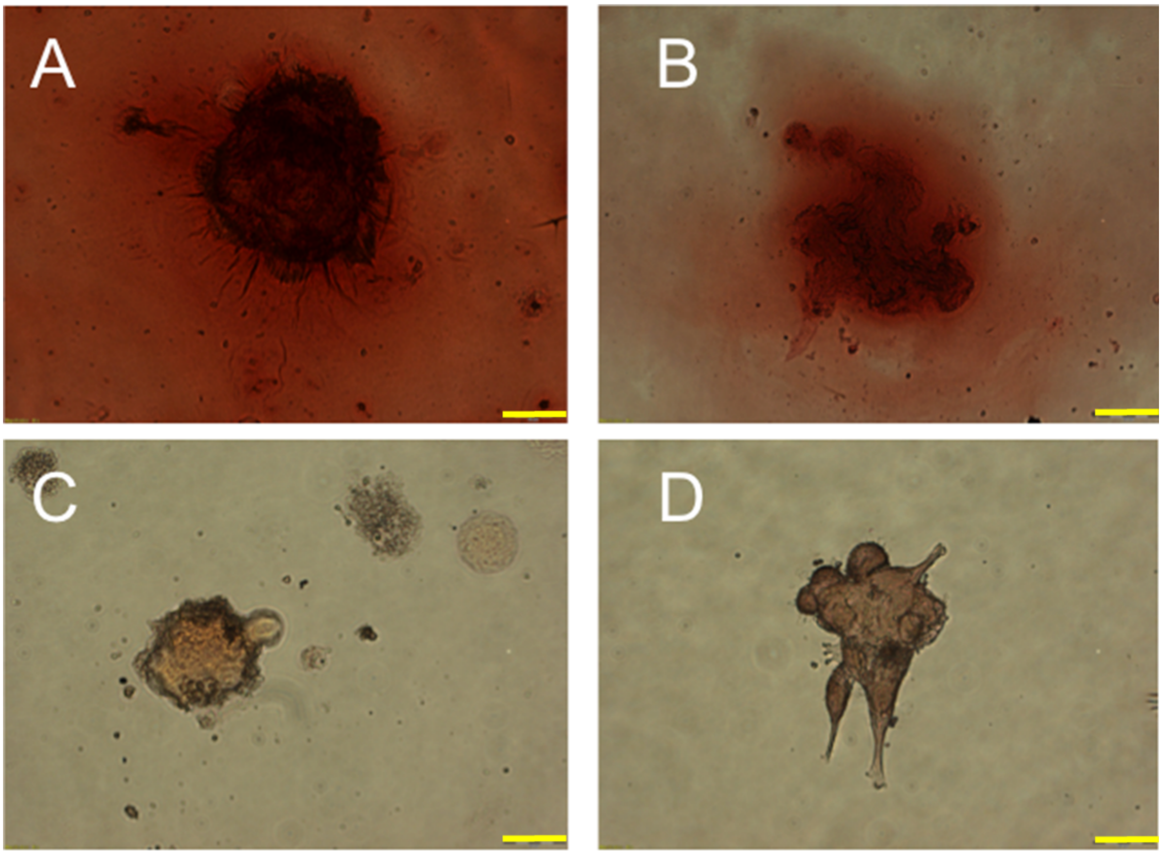

Figure 3.6 MSC mesenspheres cultured in A) Gelatine coating with osteogenic media, B) DAR16-II coating with osteogenic media, C) DAR16-II coating with DXF media and D) Gelatine coating with DXF media. Mineralized matrix was stained in red colour. (x40 magnification and bar= 20µm).

Mineralization was detected using Alizarin red stain and it was observed only in the presence of osteogenic media (Figure 3.6 A and B). However, the stain was more intense in the absence of the DAR16-II coating (Figure 3.6 A). The DAR16-II coating was forming gelatinous islands in culture, and they were attached to floating mesenspheres. This might explain the less mineralization detected with the DAR16-II as they might have interrupted the spheroidal structure of the mesenspheres and affected their stemness. In addition, no mineralization was detected in mesenspheres cultured in DAR16-II and gelatine coated wells without osteogenic media (Figure 3.6 C and D) further demonstrating that DAR16-II is unable to induce osteogenic differentiation in MSCs.

3.4 Discussion

Biomaterials that can be used in bone engineering applications should have osteoconductive and osteoinductive properties. Designer peptides in which SAPs were coupled to short osteogenic peptide motifs were used to induce osteoblasts proliferation, differentiation and cell migration (Horii et al., 2007, Kumada et al., 2010). However, the use of pure SAPs in osteogenic differentiation applications has not yet been explored. In this study, the direct osteogenic potential of pure DAR16-II was examined as a coating material *in vitro* for 3D printed BCP scaffolds. MSCs cultured in non-osteogenic differentiating medium on DAR16-II coated scaffolds significantly preserved cell viability compared to non-coated scaffolds for 42 days of *in vitro* culture (Figure 3.2). This improved cellular response can be related to the DAR16-II hydrogel structure that mimics ECM structure. Our results corresponded with Bokhari *et al*. findings in which the SAPs hydrogel structure enhanced osteoblasts proliferation suggesting that SAPs provide a 3D biomimetic environment that enhances cellular growth (Bokhari et al., 2005). However, neither osteogenic nor angiogenic markers were upregulated in MSCs cultured with DAR16-II coated BCP scaffolds or tissue culture plates in non-osteogenic media (Figures 3.3,3.4 and 3.5). Moreover, mineralization was not observed with DAR16-II coated plates in non-osteogenic media without the presence of BCP scaffolds (Figure 3.6). These data demonstrate that DAR16-II lack an osteogenic differentiating affect. The SAPs 3D ultra-structure was compared to ECM in nanofiber dimension and porosity (Matrigel) (Gelain et al., 2006, Kirkham et al., 2007). This might explain the enhanced cell viability when DAR16-II was used as a coating to BCP scaffolds.

3.5 Conclusion

The DAR16-II coating of BCP scaffolds preserved cell viability, demonstrating that DAR16-II can be used as a biomimetic hydrogel coating for BCP scaffolds. It provides a smart matrix that can enhance cell biological responses over a long time point *in vitro*. The peptides hydrogel structure provides a 3D environment that maintains cells viability and support cell adhesion. As more cells are embedded within the 3D matrix, more cells can be involved in the regeneration process. Also, the additional advantage of using this method is the ease of preparation of the peptide solution and the short time needed for scaffolds to be coated. In addition, designed osteogenic motifs can be incorporated in the DAR16-II peptide sequence to induce specific cellular interaction. Hence, DAR16-II coating can be used as a functionalizing coating material for all CaP scaffolds to enhance their osteoinductive potential.

4. Chapter 4: Effect of DAR16-II on angiogenesis

4.1 Introduction

Angiogenesis is the process of growing new blood vessels out of pre-existing capillaries. Angiogenesis involves several steps 1) EC activation (tip cell selection) which leads the way of vessel branching upon pro angiogenic stimuli, 2) tip cell migration and stalk cells (ECs trail behind the tip cell) proliferation to elongate the sprout, 3) anastomosis of neo-formed sprouts to form a functional network and 4) network pruning and remodelling (Potente et al., 2011). First step in angiogenesis is the activation of EC to select a single cell becoming the tip of the sprout which migrate towards the pro-angiogenic stimulus (e.g. VEGF and Sphingosine-1-1phosphate, SP1) and probes the microenvironment via cytoplasmic protrusions called filopodia rich in VEGF Receptor 2 (VEGFR2, KDR) (De Smet et al., 2009, Lucke and Levkau, 2010). KDR is the major VEGF receptor transducing angiogenic stimuli in EC via its kinase activity. The growing (elongation) of the sprout is supported by proliferating EC called stalk cells that follow the trailing tip cell (Carmeliet and Jain, 2011).

4.1.1 Notch signalling in angiogenesis

The selection of a single tip cell versus the bulk of the stalk cells (lateral inhibition) is regulated by Notch signalling (Figure 4.1). Briefly, tip cells (driven by VEGF signalling) express the membrane bound Notch ligand DLL4 which upon binding with Notch induces Notch intracellular domain (NICD) mediated signalling leading to inhibition of tip and promotion of stalk phenotype in the target cell (Phng and Gerhardt, 2009). New vessel loop is formed when a tip cell contacts another vessel or another tip cell and the two branches are fused. This branch fusion process is also supported by accessory cells such as pro-angiogenic Tie2 Expressing Monocytes/Macrophages (TEM) (De Palma et al., 2007). Vascular accessory cells including pericytes, Monocytes/Macrophages (Mo/Mf) and Smooth Muscle Cells (SMC) provide vessel stability and regulate vessel perfusion during angiogenesis (Jain, 2003, De Palma and Naldini, 2009).

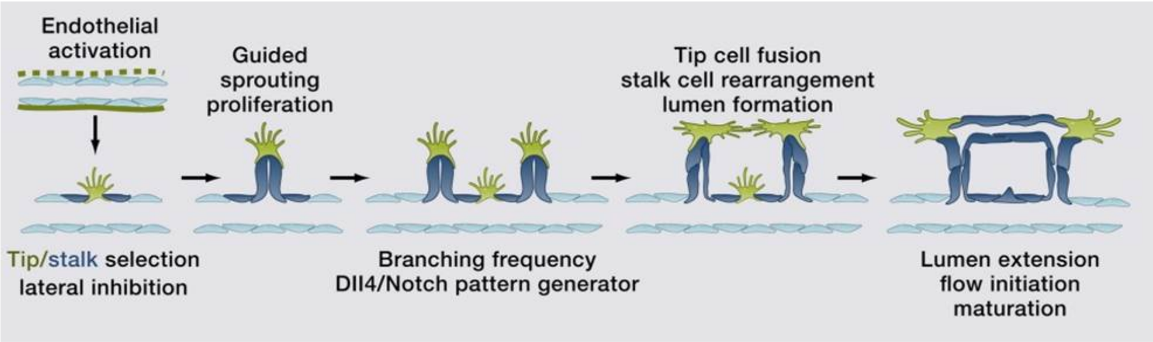

Figure 4.1 Diagram showing sprouting angiogenesis. Endothelial activation start with a tip cell (green) selection and stalk cells (blue) formation. Tip cell guides the sprouting process and stalk cells follow the tip cell trail. Tip cell fuses with another vessel or another tip cell to form a lumen (Adapted from Potente et al., 2011).

Angiogenesis is either activated by tissue derived stimuli such as parenchymal/stromal cells derived GFs (e.g. VEGF, SP1 and ANG2) or hypoxia which activates an evolutionary conserved hypoxia responsive pathway (Hypoxia Inducible Factor, HIF) in EC and in other cells inducing angiogenesis and/or the production of pro-angiogenic cytokines (Holmes et al., 2007). Overall, this angiogenic process drives EC to sprout in order to form new blood vessels and therefore support tissues' oxygen and nutrients demand.

4.1.2 Angiogenesis in endochondral bone ossification

VEGF signalling is crucial for angiogenesis as demonstrated by several evidences (Shweiki et al., 1992, Carmeliet, 2005, Lucitti et al., 2012). For this reason, therapies targeting VEGF or its receptors to block VEGF signalling have been developed and are used to limit angiogenesis in cancer and proliferative diabetic retinopathy (PDR) therapy with promising results but variable clinical outcomes (Titchenell and Antonetti, 2013) . On the other side, promoting angiogenesis is fundamental to improve success of tissue engineering (TE) strategies (e.g. therapeutic angiogenesis of ischemic tissues). Importantly, it has been recently demonstrated that blood vessels/EC derived (angiocrine) signalling to stem or parenchymal cells is important to drive their differentiation and functions (Rafii et al., 2016). At the same time, the cross-talk between EC, stromal and parenchymal cells induce EC specialisation into organ-specific EC.

Angiogenesis have been demonstrated to be crucial during endochondral bone development (Gerber et al., 1999, Maes et al., 2002). Inactivation of VEGF signalling through a soluble receptor chimeric protein (Flt-(1-3)-IgG), impaired endochondral ossification in juvenile mouse model (Gerber et al., 1999). In particular, specific ECs have been identified during endochondral ossification, these cells are distinguishable from other bone ECs by their differential expression of CD31 (PECAM) and Endomucin (Emcn) (Kusumbe et al., 2014). Furthermore, endothelial Notch activity has been demonstrated to differ in bone angiogenesis to other vascular beds (e.g. tumours) in which Notch inhibits sprouting angiogenesis (Ramasamy et al., 2014). Disruption of Notch signalling by inducible inactivation of the Rbpj gene encoding RBP-Jk, an essential mediator of Notch-induced gene transcription, resulted in compromised bone vessels and defective bone development (Ramasamy et al., 2014). This phenotype was rescued by the administration of recombinant Noggin which mediates the downstream effects of Notch signalling in EC during endochondral ossification.

Overall, it is clear that promoting adequate angiogenesis is fundamental to achieve success in all tissue engineering strategies. In the field of bone regeneration scaffolds are used to provide initial mechanical stability, to maintain space and to promote ossification. Therefore, inducing a functional vascular network within implanted scaffold is a major challenge that needs to be overcome to achieve success in bone regeneration. Strategies incorporating GFs within engineered scaffolds have been employed in animals with some success. Nonetheless, all the strategies developed so far employ supra-physiological concentrations of GF which are released erratically and might lead to systemic side effects Genetic over-expression of VEGF in mouse skeletal progenitors led to excessively ossified bones (Maes et al., 2010). Therefore, it is necessary to develop ways to provide adequate signalling delivered in spatiotemporal controlled manner to promote proper bone regeneration (Lee et al., 2011).

4.1.3 The role of inflammatory cells in bone engineering

Bone homeostasis is regulated by a dynamic balance between osteoblastic bone formation and osteoclastic bone resorption. Osteoclastogenesis is controlled by the ratio of receptor activator of NF-κB ligand (RANKL) relative to its decoy receptor, osteoprotegerin (OPG) a potent physiological inhibitor of osteoclastogenesis (Teitelbaum, 2000, Khosla, 2001). Historically, osteoblasts were considered the source of OPG however, it has been shown that B cells are the main source of bone marrow-derived OPG (Li et al., 2007, Pacifici, 2010). The importance of the immune system in inhibiting osteoclastogenesis in normal physiology, led to the shift towards the development of "smart" biomaterials able to modulate the immune response to improve bone regeneration (Chen et al., 2014b, Franz et al., 2011). These biomaterials activate specific immune response to develop a favourable osteogenic environment for bone cell recruitment and differentiation. Macrophages (Mf) are considered the most important immune cells which contribute to material-induced inflammatory reactions (Bartneck et al., 2012). Mf also have a significant impact on bone physiology and pathology as they are OC precursors which mediate bone remodelling (resorption) and promote biomaterial degradation (Alexander et al., 2011, Chang et al., 2008). In addition, Mf can affect bone formation by expressing and secreting osteogenic regulatory molecules such as BMP2 and transforming growth factor β (TGF-β) (Pettit et al., 2008, Honda et al., 2006, Wahl et al., 1990). Mf are also required for bone mineralization as their depletion was found to reduce OB capacity of forming bone (Chang et al., 2008). Furthmore, subsets of Mf have been demonstrated to promote angiogenesis by secreting pro-angiogenic growth factors, matrix-remodelling proteases and by interacting with endothelial cells sprouting and vascular network development (Fantin et al., 2010, Nucera et al., 2011). Hence, recruiting inflammatory cells to the bone healing site is a critical step during bone development and repair. Finally, tissue resident osteal Mf have been recently identified and have been shown to be necessary for bone repair (Alexander et al., 2011).

It has been shown that microenvironments developed by RAD16-II (the reverse sequence of DAR16-II described in the present study) promote vascular cell recruitment (Davis et al., 2005). This was demonstrated by injecting a solution of RAD16-II in mouse myocardium resulting in the assembly of a nanofiber hydrogel. This microenvironment promoted the recruitment of progenitor cells expressing endothelial markers (isolectin b4 and CD31) and smooth muscle cells promoting the formation of functional vascular structures. Therefore, since self-assembling peptides (SAPs) can create favourable microenvironments for endothelial cells recruitment, the objective of this study was to explore if the DAR16-II (described in chapter 2) could influence EC adhesion, phenotype, sprouting and morphogenesis as well as Mo/Mf attachment and polarisation.

Aims of the study:

1. Determine if DAR16-II can induce an angiogenic phenotype in HUVEC *in vitro*.

2. Evaluate the effect of DAR16-II on THP-1 cells attachment and gene expressions *in vitro*.

4.2 Materials and methods

4.2.1 Endothelial cell culturing

Primary isolated human umbilical vein ECs (HUVECs; Promocell, Heidelberg, Germany) were cultured up to passage 6. Cells were maintained in endothelial cell growth medium-1 (EGM-1) (Promocell, Heidelberg, Germany) at 37°C , 5% CO_2 and 95% humidity.

4.2.2 Endothelial cell proliferation (MTT assay)

The MTT assay is a colorimetric assay frequently used to assess cell metabolic activity; live cells exposed to MTT [3-(4,5-dimethylthiazol-2-yl)-2,5-diphenyltetrazolium bromide] catalyse the reduction of this salt by mitochondrial enzyme, succinate dehydrogenase to a formazan, with a deep purple colour, the amount of formed formazan is proportional to the number of cells and to their metabolic activity. Therefore, if the metabolic activity of cells is fixed, the MTT assay is used as an indirect method to assess cell number and then proliferation overtime. A standard curve was generated by HUVEC at 5,10,15,20,25,50x10^3 (in 96 well plates) in triplicates. The curve was established by charting cell numbers vs optical densities (OD) obtained by MTT treated wells. This provided an equation linking OD to cell number/well. To assess the effect of DAR16-II (previously described in chapter 2) on HUVECs proliferation, different coating concentrations of DAR16-II (in aqueous gelatine solution) were explored; 20, 25, 33, 50, 57 %, (n=12). HUVEC were seeded at a density of 5x10^3 cells per well in 96-well plates with 100µl of EGM-2 media (Promocell, Heidelberg, Germany) and incubated at 37 ^{0}C, 5% CO_2. After 24 hrs, media was replaced with 100µl/well of MTT solution (5% w/v MTT in PBS added 1:10 to ascorbate free media). The plates were incubated for 4 hrs (37°C, 5% CO_2), the solution was then removed and formazan crystals were solubilised with DMSO (Sigma-Aldrich, Dorset, U.K) 100µl per well under shaking for 5 min. Absorbance was measured on a DYNEX plate reader (Dynex Technologies, Chantilly, VA, USA) (test wavelength: 570 nm; reference wavelength: 630 nm).

4.2.3 Endothelial cell spreading

To investigate the effect of DAR16-II on HUVECs adhesion, 48-well plate was coated with DAR16-II: gelatine at 1:1 ratio (or gelatine as control). Cells were seeded at a density of $2x10^3$ cells per well in EGM-1 (Promocell, Heidelberg, Germany) for 30 min. After that, media was removed and wells were washed twice with PBS (Sigma-Aldrich, Dorset, U.K) fixed in 2% buffered PFA (FD Neurotechnologies, INC, MD, USA) for 15 minutes and blocked in 1% Foetal bovine serum (FBS) in PBS for 15 minutes at 37°C. Wells were rinsed with PBS then treated with PBS-buffer 0.1% Triton X-100 (Sigma-Aldrich, Dorset, U.K) for 2 min to permeabilise the cell membranes. Actinic cytoskeleton was stained with TRITC-conjugated Phalliodin (Molecular Probes, USA) was added to localise actin microfilaments of attached HUVECs in 1:1000 dilution in PBS for 45 min at room temperature (RT). The wells were washed three times with PBS before nuclear counterstaining using Höechst 33342 (ThermoFisher Scientific, Paisley, UK) at $1\mu g.mL^{-1}$ for 10 mins at RT. Finally wells were washed twice with PBS (Sigma-Aldrich, Dorset, U.K) and visualized with a wide field inverted microscope equipped with charged-coupled device (CCD) camera to capture photographic images using CellSens software (Olympus IX51, Biosystems, Munich, Germany). The surface area of attached cells were measured using ImageJ software (Schneider et al., 2012).

4.2.4 Endothelial cell morphology

Standard 22x22 mm square coverslips (VWR, PA, USA) were coated either with gelatine or gelatine:DAR16-II (1:1) in 6-well plates. Slides were micro-seeded with $3x10^4$ HUVECs per slide in 50 µl and left to attach for 30 min at 37°C in a 5% CO_2 atmosphere. Next, 1.5 ml of EGM-1 was added to each well and slides were maintained at 37°C/5%CO_2 atmosphere. After 48 hours, media was removed and slides were fixed and stained as previously described. Coverslips were mounted on standard histological slides in Mowiol® 4-88 (Sigma-Aldrich, Dorset, U.K) and visualized with an Olympus microscope to quantify the relative abundance of different cell phenotypes (determined by cell morphology) (Olympus Biosystems, Munich, Germany).

4.2.5 Angiogenic assay

Matrigel is an ECM extract derived from mouse Engelbreth-Holm-Swarm (EHS) mouse sarcoma cells and frequently used to assess the EC potential in forming tubular structures *in vitro*. Four different coating conditions were prepared in 96 well plates. The first group was coated with gelatine as a control while the second was coated with 1:1 gelatine:DAR16-II. The third was coated with 1:1 gelatine:BCP (15% HA and 85% TCP powders, Sigma, UK). The last was coated with 1:1 (gelatine:BCP):DAR16-II. Matrigel (Corning, Netherlands) was thawed on ice and mixed with EGM-2 in a 1:1 ratio. Then the Matrigel solution was mixed with each group in 1:1 ratio and 50µl of each solution was transferred into its designated well in 96-well plate and incubated at 37°C in a 5% CO_2 atmosphere for 30 min. EC suspension ($1x10^4$ HUVEC/well in EGM-2 pre warmed at 37°C) was added to each well. After 24 hours, results were visualised and imaged as previously described. Images were analysed to assess tubule-like structures length and connectivity with ImageJ (Schneider et al., 2012).

4.2.6 RT^2 Profiler PCR Arrays

RT^2 Profiler PCR Array is a low density qRT-PCR based array (PAHS-024Z, Qiagen, UK, profiles 84 genes key in EC biology and angiogenesis). $2x10^5$ HUVECs were seeded in T25 gelatine and 1:1 gelatine:DAR16-II coated flasks (Greiner Bio-one CELLSTAR®, Frickenhausen, Germany). Cells were maintained in EGM for 48 hours at 37°C in a 5% CO_2 atmosphere. Total RNA was isolated by using the method described in chapter 3. cDNA was prepared by retro transcribing 1 µg of total RNA using the RT^2 qPCR Array First Strand Kit in accordance with the supplier instructions (Qiagen, Crawley, UK). The template was mixed with RT^2 SYBR Green/Fluorescein PCR master mix (Qiagen, Crawley, UK). 10 µl were added to each well of the RT2 qPCR profiler plate containing SYBR green-optimized primer assays for 84 genes related to angiogenesis (see Appendix). Five housekeeping genes, controls for genomic DNA contamination, RNA quality and general PCR performance were included in the array. The thermal cycling conditions were 10 min at 95 °C followed by 40 cycles at 95 °C for 15 s and then 60 °C for 1 min. The data were collected using Bio-Rad CFX384 analytical thermal cycler (Bio-Rad Laboratories, USA). Control and positive PCR controls were within the accepted range. Threshold cycle values were analyzed using the ΔΔCt method using the PCR Array Data Analaysis Web portal at www.SABiosciences.com/pcrarraydataanalysis.php

4.2.7 THP-1 cell culture

THP-1 monocytes, human monocytic leukaemia cells (ATCC®, Teddington, UK) were cultured in a Roswell Park Memorial Institute-1640 medium (Gibco, Gaithersburg, Maryland, USA) supplemented with 10% FBS, 100µg/ml penicillin, 100µg/ml streptomycin and 2mM Lglutamine (all from Sigma-Aldrich, Dorset, U.K). Cells were maintained between $1x10^5$ and $1x10^6$ cells/ml and passaged every 2 to 5 days. Before passaging, cells were counted in a 1:1 dilution with filtered trypan blue (ThermoFisher Scientific, Paisley, UK) using an automated cell counter (TC10, Bio-Rad, Hemel Hempstead, UK). The tube was subject to centrifugation for 30 min at 2000rpm at RT with soft acceleration and deceleration settings activated. The cloudy interface of cells was removed by pipette, centrifuged and re-suspended.

4.2.8 THP-1 differentiation

To obtain macrophages, THP-1 monocytes can be differentiated into THP-1 derived Mf (M0 phenotype) using phorbol 12-myristate 13-acetate (PMA) (Park et al. (2007). PMA medium consisted of Dulbecco's Modified Eagle Medium (DMEM) (phenol red free), PMA at a concentration of 5 ng/ml, 10% FBS, 2mM L-glutamine, 100µg/ml penicillin and 100µg/ml streptomycin (all from Sigma-Aldrich, Dorset, U.K).

4.2.9 Macrophage and DAR16-II culture

6-well plates were coated with 1:1 gelatine:DAR16-II and gelatine (control) as before. THP-1 cells were seeded at a density of $5x10^5$ per well in PMA medium. Cells were maintained for 48 hrs at 37°C in a 5% CO_2 atmosphere. For RNA extraction, media was removed and attached cells were washed twice with PBS (Sigma-Aldrich, Dorset, U.K). 300 µl Tri-reagent was added directly to wells, RNA was extracted and then retro transcribed into cDNA as described in chapter 3. The Forward and Reverse Primers used were: Glut-1, VEGFA, MRC1 and a ribosomal proteins (RPL, housekeeping gene) control.

Target gene	Forward primer	Reverse primer
Glut1-1	AACTCTTCAGCCAGGGTCCAC	CACAGTGAAGATGATGAAGAC
VEGFA	AATGTGAATGCAGACCAAAG	GACTTATACCGGGATTTCTTG
MRC1	AAATTTGAGGGCAGTGAAAG	GGTTTGGAGTTTATCTGGTAG
RPL	CGCTCACAATGTTTCCTCCA	TGACTCTGATGGCCAGTTGG

Table 4-1 Primer pairs used for qRT-PCR.

4.2.10 Macrophage attachment

96-well plates were coated with 1:1 gelatine:DAR16-II and gelatine (control) overnight. Cells were seeded at a density of $1x10^3$ cells per well in 100 µl of EGM-1 media (Promocell, Heidelberg, Germany) for 30 min at 37°C/5%CO_2 atmosphere. Wells were washed three times with PBS (Sigma-Aldrich, Dorset, U.K) and fixed as previously described. The nuclei of attached cells were stained with Hoeschst 33342 (ThermoFisher Scientific, Paisley, UK) at 1µg.mL^{-1} concentration for 10 mins at RT. Next, wells were washed twice with PBS and visualized with an Olympus microscope and attached cells were counted (Olympus IX51, Biosystems, Munich, Germany).

4.2.11 Statistical analysis

Results are expressed as mean ± standard deviation (SD). Data were analysed as follows: 1.One-way ANOVA with post hoc Dunnett's multiple comparisons test to compare the means of the test groups to the mean of the control group (HUVECs proliferation and THP-1 qPCR studies) 2. Two-way ANOVA with post hoc Tukey's multiple comparisons test to compare means among groups (cell morphology and angiogenesis assay studies), 3. Two-tailed t-test with Wilcoxon-Mann-Whitney test (HUVECs spread and THP-1 adhesion studies). GraphPad Prism 6.0c software (GraphPad Software Inc., La Jolla, USA) was used as the statistical software. Statistical differences were designated as significant if p-values were less than 0.05 (* $p \leq 0.05$), and as highly significant if P-values were less than 0.01 (** $p \leq 0.01$) or less than 0.001 (*** $p \leq 0.001$).

4.3 Results

4.3.1 EC proliferation

In order to determine the effect of DAR16-II on EC proliferation, a 48 hrs proliferation assay was performed. 5x 10^3 HUVECs were seeded on 96 wells plate coated with gelatine or a mixture of gelatine and DAR 16-II at different ratios (20 to 75% DAR 16-II). Furthermore, on the day of the experiment, 5-10-20-40-80 X10^3 cells were seeded in separate gelatine coated plate to generate a standard curve. MTT assay was used as an indirect measure of cell number by relating absorbance measurements with cell number through the standard curve.

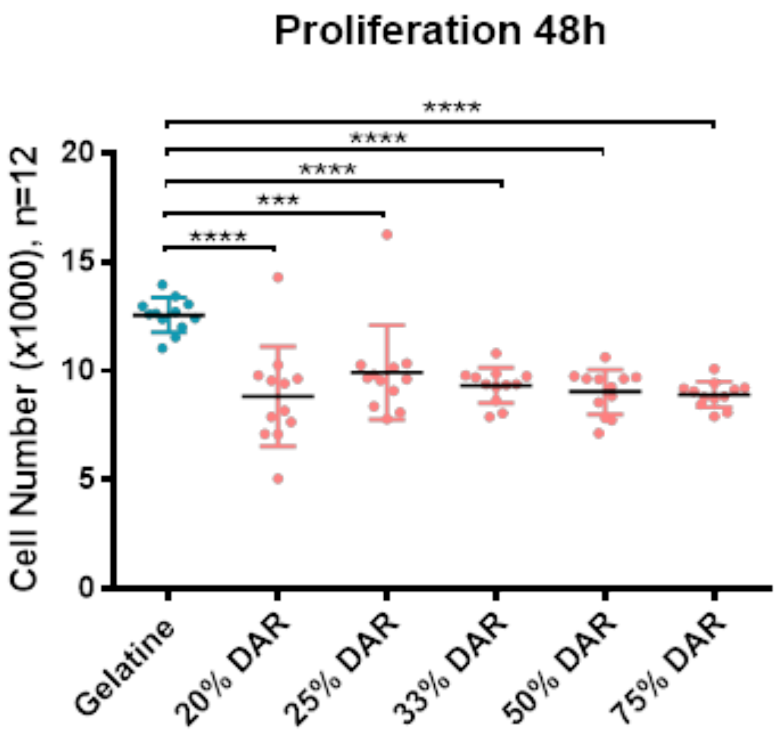

Figure 4.2 48 hrs HUVECs proliferation. Exposure of HUVEC to different DAR16-II concentrations inhibited proliferation ($p<0.0001$). Data represented as mean±SD, (n=12).

The results showed that, in comparison to gelatine, DAR16-II inhibits HUVECs proliferation at all concentrations. No dose/response correlation could be observed with increasing DAR16-II concentrations. Nonetheless, higher DAR16-II concentrations reduced inter-sample variability (Figure 4.2). Previous observations support the idea that DAR16-II forms agglomerates on tissue culture plastic leaving zones of uncoated plastic. This effect is reduced with higher peptide's concentrations. This could justify the proliferation results indicating that a more homogeneous coating can affect a larger percentage of cells and therefore produce more consistent results. Proliferation was reduced by about Δ66% with DAR16-II and this was compatible with either a migratory (tip) or a quiescent (phalanx) EC phenotype. Consequently, 50% DAR 16-II concentration was used for further experiments.

4.3.1 Endothelial cell adhesion and spreading

In order to determine if DAR16-II has an influence on early EC adhesion, HUVECs were seeded on 1:1 gelatine/DAR16-II coated wells for 30 min and compared to cells seeded on gelatine coated wells. The surface area of attached HUVECs was measured with ImageJ.

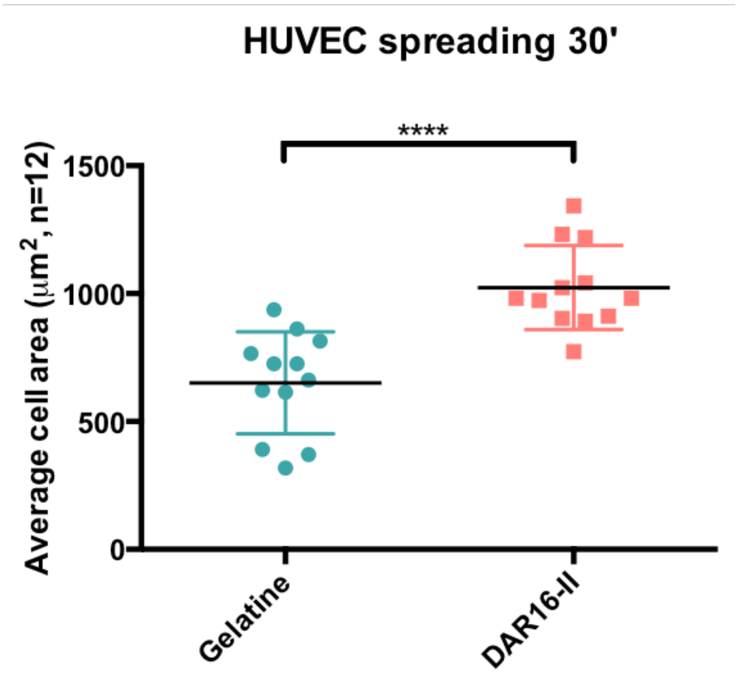

Figure 4.3 Cell attachment assay showing the effect of DAR16-II on HUVECs adhesion. It showed that the average cell area of attached HUVECs was significantly higher (about 160%) with DAR16-II after 30 min of incubation ($p < 0.0001$). Data represented as mean±SD, (n=12).

The average cell area of HUVECs that adhered at this early time point was comparable on both substrates but HUVECs spreading was markedly higher (about 160%) in the presence of DAR16-II ($p<0.0001$). This data suggests that DAR16-II may partially exert its functions by promoting faster EC adhesion.

4.3.3 Endothelial cell morphology

Morphology is indicative of EC functions in particular quiescent EC (resembling *in vivo* phalanx EC) are polygonal, mostly well juxtaposed to each other, slowly proliferating and devoid of lamellipodia or filopodia. (Potente et al., 2011). In contrast, activated, migratory EC (resembling *in vivo* tip EC) are elongated, often isolated, non-proliferating and presenting filopodia and lamellipodia. Finally proliferating stalk-like EC have a polygonal morphology and are smaller. From previous proliferation data (Figure 4.2) we inferred that DAR 16-II might promote a tip-like or a phalanx-like phenotype. To determine whether DAR16-II could indeed induce the morphological features typical of tip or phalanx cells we examined and quantified morphology of EC seeded on DAR 16-II in comparison to gelatine. HUVECs were cultured on slides coated with DAR16-II and gelatine and stained with TRITC-conjugated Phalloidin (staining actinic cytoskeleton) and Höechst (nuclei) (Figure 4.4). The relative abundance of tip and phalanx cells, defined as above, was quantified. The results demonstrated clear morphological differences in HUVECs cultured with DAR 16-II which on average, appear more elongated, isolated and produced more filopodia and lamellipodia indicating a more migratory phenotype in comparison to gelatine. The quantifications performed confirmed these findings showing a prevalence of quiescent/proliferating HUVECs (peripheral actin, contacting juxtaposed cells) on gelatine and a prevalence of migratory (tip) EC in presence of DAR16-II. These data in combination with those obtained with proliferation assay suggest that DAR16-II induced a migratory non-proliferating phenotype in HUVECs, this is fully compatible with a tip phenotype suggestive of angiogenic activation.

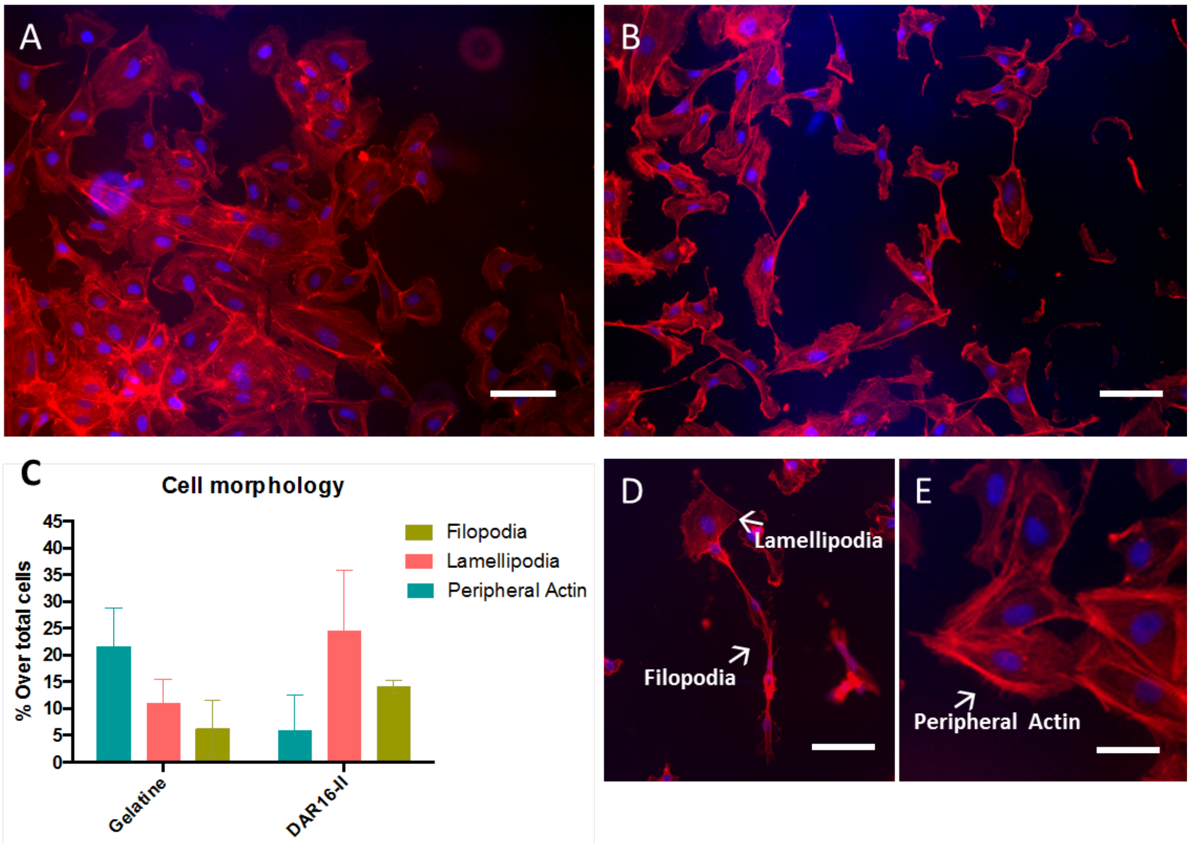

Figure 4.4 Cytoskeletal staining (Phalloidin (red) for actin and of Hoechst (blue) for nuclei) of HUVECS cultured on DAR16-II and gelatine coated slides for 48 hrs. A) and E) Show the cell morphology of HUVECs cultured on gelatine with quiescent phenotype with abundant peripheral actin cells. B) and D) show less peripheral actin in HUVECs cultured on DAR16-II with more lamellipodia and filopodia. C) Shows the quantification of the different cell phenotypes associated with DAR16-II and gelatine. HUVECs with more filopodia, lamellipodia and less peripheral actin were detected with DAR16-II compared to gelatine. (20x magnification, A.B,D scale bar=40µm and E scale bar=20µm).

4.3.3 Angiogenic assay

Considering previous data suggesting angiogenic EC activation, Matrigel morphogenesis assay was used to determine if DAR16-II has the potential to promote the formation of tubular-like structures. Moreover, BCP powder was added as a second variable to explore if the presence of BCP has influence on DAR16-II angiogenic effect.

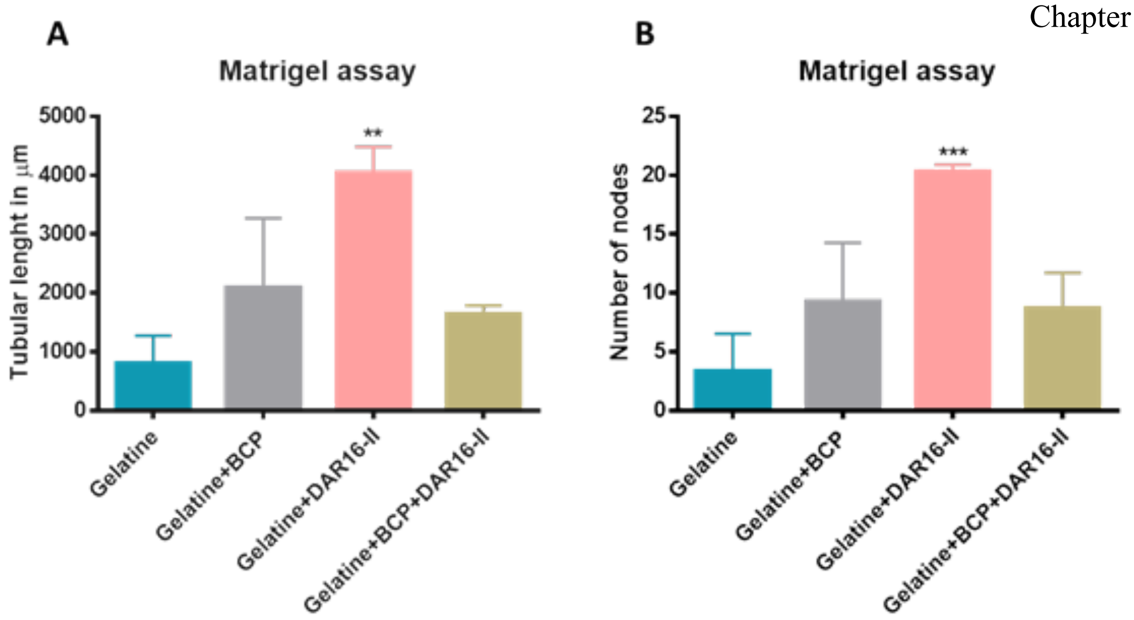

Figure 4.5 Matrigel assay comparing tubular-like structures developed with 1) Gelatine, 2) Gelatine+BCP, 3) Gelatine+DAR16-II and 4) Gelatine+BCP+DRA16-II. A) HUVECs cultured in Gelatine+DAR16-II resulted in significantly longer tubular-like structure formation compared to other conditions ($p<0.01$). B) HUVECS cultured in Gelatine+DAR16-II resulted in significant increase in number of nodes compared to other culturing conditions ($p<0.001$). Data represented as mean±SD, (n=3).

By comparing the length and number of nodes of tubular-like structures developed in Matrigel containing: 1) Gelatine, 2) Gelatine and BCP, 3) Gelatine and DAR16-II and 4) Gelatine, BCP and DAR16-II. It was found that the 1:1:2 combination of gelatine, DAR16-II and Matrigel produced the longest and more complex networks. Both tubular length and number of nodes were significantly higher ($p<0.001$) with gelatine+DAR16-II compared to structures developed with the other culturing conditions (400% in comparison to gelatine only control). The presence of BCP in Matrigel did not enhance tubular-like structures formation. These data are compatible with previous ones, indicating an overall EC activation toward an angiogenic phenotype in the presence of DAR 16-II.

4.3.4 RT² Profiler PCR Arrays

To identify the molecular effectors responsible for the observed phenotype a low density qRT-PCR based array was employed. The array included profiling of 84 genes involved (Figure 4.6).

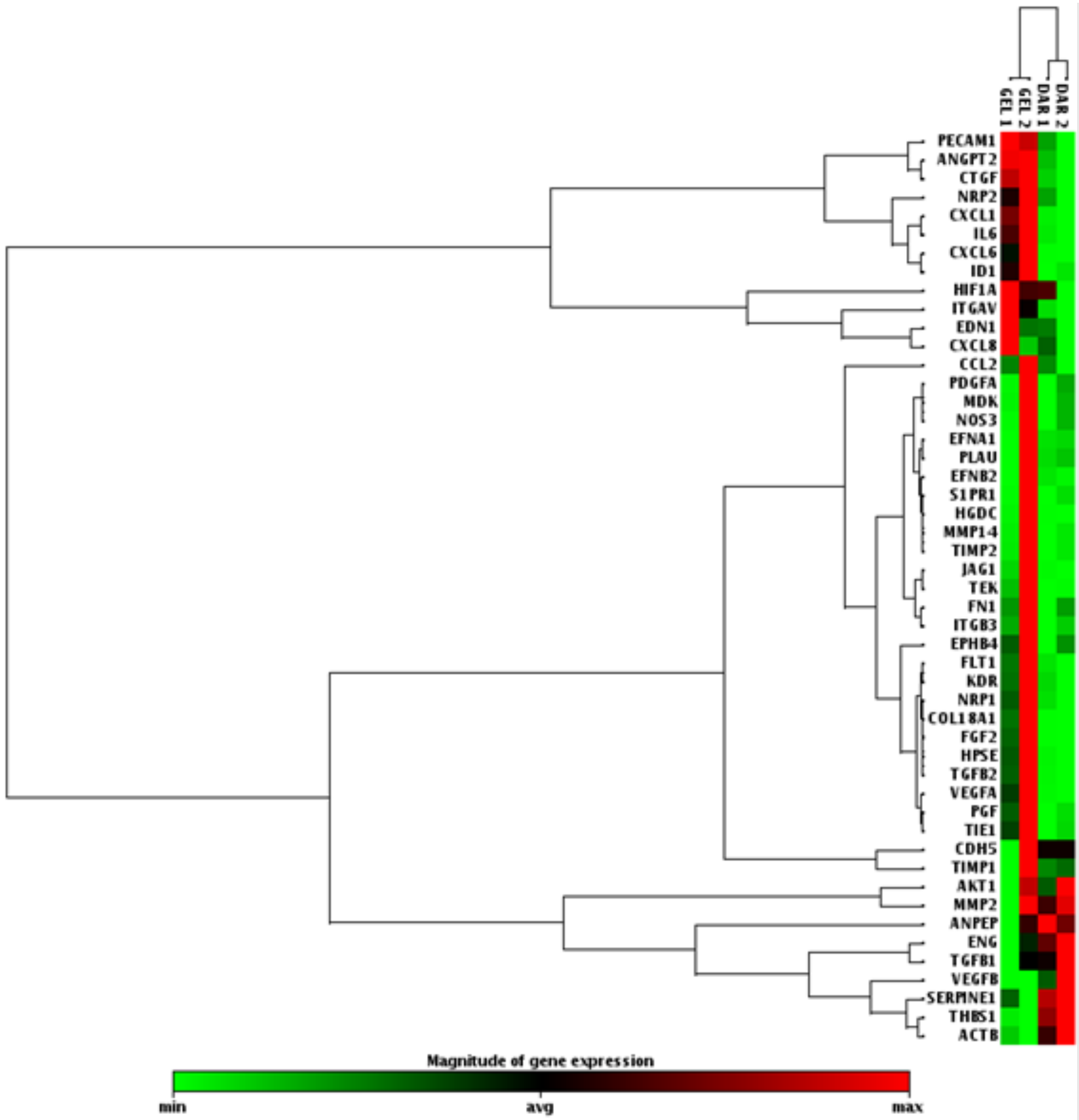

Figure 4.6 Clustergram RT² Profiler PCR Array of genes expressed by HUVECs cultured on DAR16-II and gelatine (control) coated flasks for 48 hrs. The graph demonstrates that DAR16-II consistently show different gene expressions compared to the control (gelatine), (n = 2).

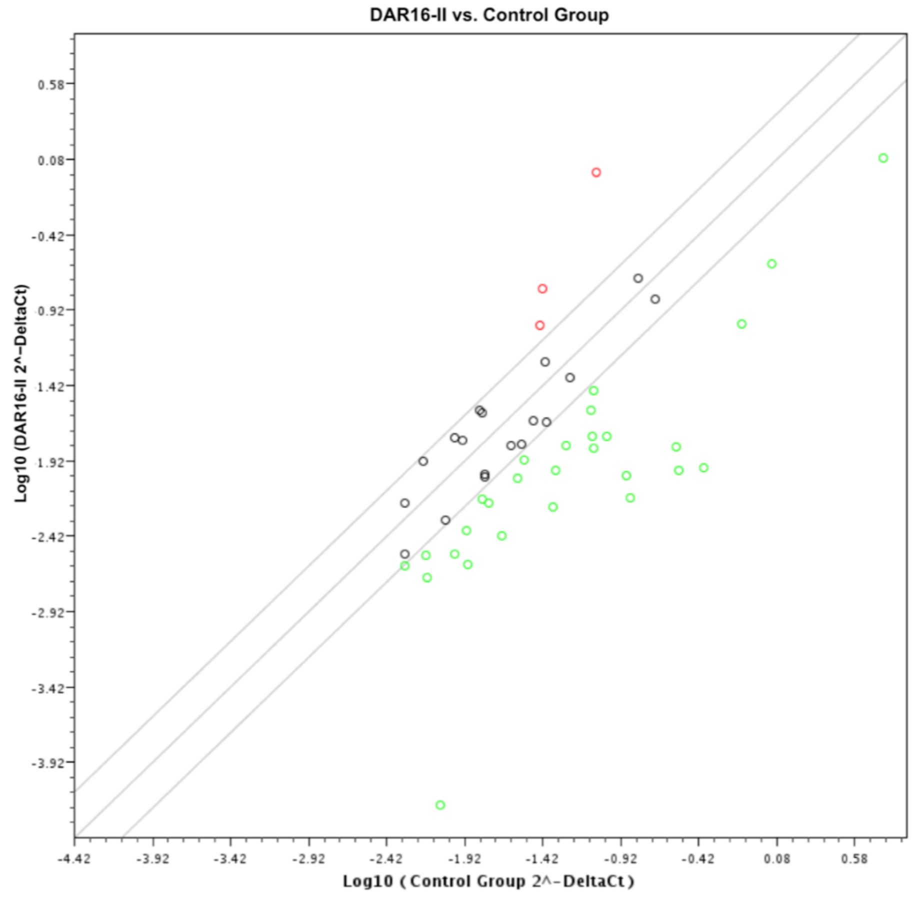

Genes overexpressed in	
Gene Symbol	Fold Regulation
ENG	2.6057
SERPINE1	4.3822
ACTB	11.6857
Genes Under-Expressed in	
Gene Symbol	Fold Regulation
ANGPT2	-5.3641
COL18A1	-5.0747
CTGF	-4.6859
CXCL1	-7.2518
CXCL6	-26.8776
EFNA1	-2.0539
EFNB2	-2.9554
FGF2	-37.7481
FLT1	-7.4299
HPSE	-20.2287
ID1	-4.5578
IL6	-17.9802
ITGAV	-2.8448
ITGB3	-3.5884
JAG1	-4.4485
MDK	-2.3674
MMP14	-3.3714
NRP1	-2.9349
NRP2	-2.6914
PECAM1	-5.6503
PGF	-4.5736
S1PR1	-2.3839
TEK	-3.5884
TGFB2	-5.5149
TIE1	-2.3349
TIMP2	-2.271
VEGFA	-13.4855

Figure 4.7 Scatterplot of RT^2 Profiler PCR Array of genes overexpressed (red) and under-expressed (green) by HUVECs following 48 hrs of culture on DAR16-II and gelatine (control) coated flasks, (n = 2).

The array clustergram showed that the genes expressed by each group (DAR16-II or gelatine) were consistently equivalent (Figure 4.6). In addition, it showed that the exposure of HUVECs to DAR16-II in un-stimulated culture conditions lead to different gene expression profile compared to gelatine (control). Although the more classical angiogenic pathways (e.g. VEGF) were not activated and corresponding genes were not overexpressed, Endoglin (ENG) was among the few overexpressed genes (2.6 fold change) in the presence of DAR16-II (Figure 4.7). ENG is essential for angiogenesis and it is involved in a pro-angiogenic endoglin/transforming growth factor-β (TGF-β) signalling pathway (Bergers and Hanahan, 2008). Moreover, a significant increase in clade E member of the serine protease inhibitor 1 (SERPIN1) was detected and

SERPINE1 expression promotes angiogenesis of cancer cells (Pavón et al., 2016). In addition, a significant increase in the production of ACTB is indicative of cytoskeleton remodelling and rearrangement which is compatible with a migratory phenotype of ECs subjected to DAR16-II (Bunnell et al., 2011). VEGF receptor I (Flt1, non-transducing decoy receptor) and VEGF receptor II (KDR, kinase receptor responsible for the majority of VEGF responses in HUVECs), were reduced. Nonetheless, Flt1 was reduced by 7 folds while KDR was barely down-regulated (-1.7 fold). This might suggest that HUVECs exposed to DAR16-II could be in a more active state prone to transduce VEGF signalling upon exposure

4.3.5 THP-1

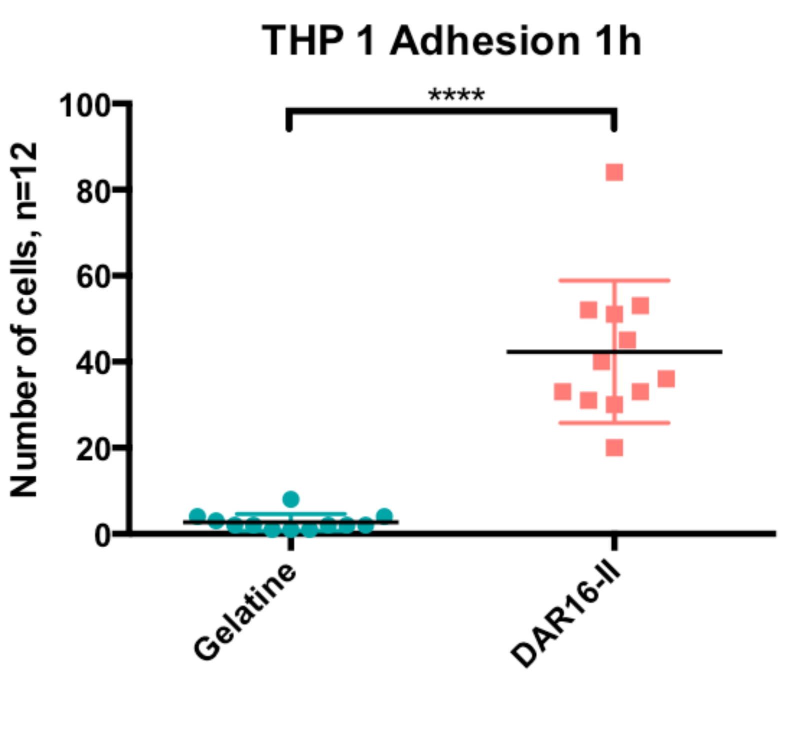

Figure 4.8 THP-1 adhesion assay showing the effect of DAR16-II on cell attachment compared to gelatine after 1hr of culture. The number of attached THP-1 too DAR16-II was significantly higher compared to gelatine (p<0.001). Data represented as mean±SD, (n=12).

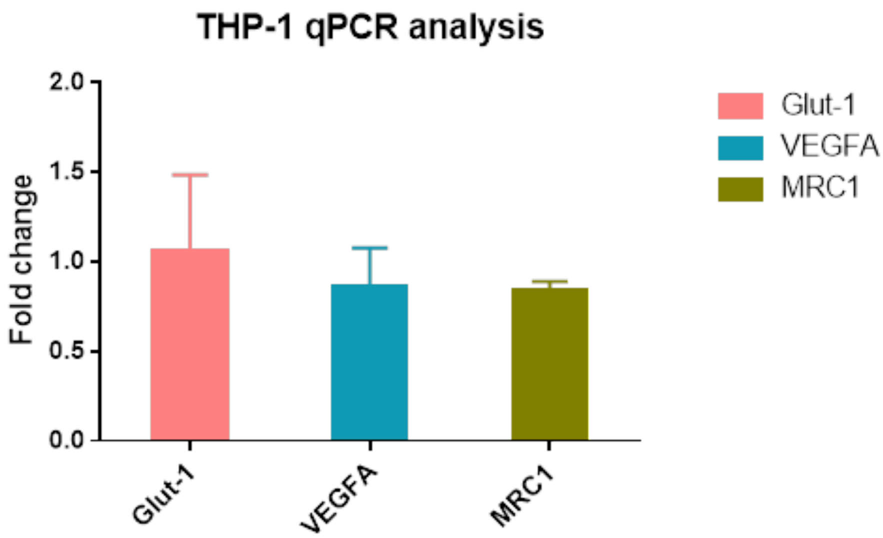

Figure 4.9 mRNA expression of GLUTI, VEGFA and MRC1 was analysed by quantitative-reverse transcription polymerase chain reaction (qRT-PCR). No variations in gene expression were detected in THP-1 cultured for 48 hrs with non-conditioned media. Data represented as mean±SD , (n=3).

Since, monocytes/macrophages are essential for initial tissue response upon injury and have been demonstrated to elicit a pro-angiogenic effect, experiments were performed to assess monocytes (THP1 model) responses to DAR16-II. Initially, results indicated that DAR 16-II promotes THP1 adhesion similarly to what happens with EC suggesting an ability of DAR 16-II to promote monocytes recruitment (Figure 4.8). Gene expression analysis to assess THP-1 polarisation revealed that THP-1 exposure to DAR16-II for 48 h did not induce neither osteogenic (Glut-1) nor angiogenic (VEGFA) activation (Figure 4.9). In addition, the M2 macrophages polarization marker (MRC1) was not affected by DAR16-II. Since these experiments were performed on monocytes only (naïve THP1 without previous differentiation into macrophages with PMA) gene expression analysis is not conclusive for what regards eventual Mf polarisation.

4.4 Discussion

Angiogenesis is induced when ECs are subjected to pro-angiogenic signals e.g. VEGF. Activated ECs project filopodia (enriched in KDR) and become motile tip cells which migrates toward the pro-angiogenic stimulus (Potente et al., 2011). Stalk cells follow the tip, proliferate to support sprout elongation and establish a lumen. During angiogenesis, cells shuffle between tip and stalk cell phenotypes in dynamic cycles of sprouting and tubulogenesis (Phng and Gerhardt, 2009, Eilken and Adams, 2010). This process is terminated when pro-angiogenic signal is ceased and quiescence is restored (Potente et al., 2011). The data presented in this study supports the idea that DAR16-II promotes a pro-angiogenic switch in ECs. The results presented in this study demonstrate that DAR16-II promote better EC adhesion (Figure 4.3) which is compatible with faster angiogenesis *in vivo*. Furthermore, our results showed that cell proliferation was significantly reduced upon exposure to DAR16-II and that proliferation rate was not affected by different concentrations (ranging from 20 to 75%) (Figure 4.2). These results indicate that the mere exposure to DAR16-II could induce a phenotype switch in EC. This was investigated by morphological analysis of HUVECs exposed to DAR16-II. Cytoskeletal staining showed a different phenotype associated with DAR16-II with more distinct lamellipodia and filopodia observed (Figure 4.4). Endothelial migratory processes are characterized by the filopodia and lamellipodia projections. Filopodia are thin membrane extensions that contain long parallel actin filaments and act as sensors to motility stimuli (Lamalice et al., 2007). Lamellipodia are cytoplasmic protrusions that act as a guiding point for spreading and migration (Small et al., 2002). These data suggest that indeed, exposure to DAR16-II promote a more migratory (tip-like) phenotype in EC. In order to explore the effect of DAR16-II on EC morphogenesis, HUVECs were seeded on Matrigel mixed with DAR16-II. DAR16-II was found to promote tubular-like structures formation (Figure 4.5). This result is comparable to previously reported study of Narmoneva et al. in which self-assembly peptides RAD16-II induced both capillary-like networks formation and ECs attachment (Narmoneva et al., 2004). DAR16-II in Matrigel significantly stimulated longer and more interconnected tubular network (Figure 4.5 A and B). Finally, in order to determine the molecular mechanism of the observed functions, a qRT-PCR based array was used to screen the genes involved in angiogenic pathways. Three genes were significantly up-regulated in DAR16-II treated EC in comparison to gelatine treated ones which were ENG also known as CD105, SERPIN1 and ACTB (Figure 4.7).

ENG is a homodimeric transmembrane glycoprotein highly expressed on angiogenic EC surface and acts as a co-receptor to TGF- β which regulates angiogenesis through balancing pro-proliferative and pro-differentiation pathways of EC (Dallas et al., 2008, Park et al., 2013). This is achieved through balancing signals of TGFb-receptor II (TGFbRII) and two TGFbRI (Activin-receptor like kinase-1 (ALK1) and ALK5) pathways (Lutty et al., 1993, Oh et al., 2000, Seki et al., 2003, Lu, 2008). ENG binds to TGF- β phosphorylate ALK1 and ALK5 which phosphorylate downstream Small mothers against decapentaplegic (Smad) proteins inducing an angiogenic phenotype (Pérez-Gómez et al., 2010). Decreased ENG expression leads to distorted angiogensis *in vitro* and results in defective vascular development *in vivo* (Arthur et al., 2000, Bourdeau et al., 2000). Mutations in ENG and ALK1 result in hereditary haemorrhagic telangiectasia (HHT) in human, an arteriovenous disease characterized by malformed vessel walls (Pardali et al., 2010). On the other hand, SERPINE1 expression promotes spreading, migration and angiogenesis of cancer cells (Pavón et al., 2016). As SERPINE1 expression enhances cell migration, it also reduces cell proliferation simultaneously (Czekay et al., 2011, Pavón et al., 2015). Both ENG and SERPINE1 expression are upregulated by hypoxia (Rosen et al., 2014, Sun et al., 2016). In addition, SERPINE1 expression is modulated by TGF-β1 and SMAD proteins (Pavón et al., 2016). The over-expression of ACTB is also an indicative of migratory phenotype of ECs (Figure 4.7) (Bunnell et al., 2011). Taken together, DAR16-II induction of migratory gene expressions after 48 hrs of culture proposes that DAR16-II acquires a proangiogenic potential. DAR16-II was also found to significantly induce THP-1 adhesion; a macrophage model (Figure 4.8). Macrophages support vessel development by facilitating fusion during angiogenesis (Potente et al., 2011). However, the lack of essential cytokines in the THP-1 culturing medium might explain the absence of differentiating gene expressions (Figure 4.9).

4.5 Conclusion

In previous studies the use of SAPs with the RADA motif were found to promote angiogenesis when used as a 3D scaffold, the exact mechanism was not determined (Genové et al., 2005, Narmoneva et al., 2005). In this study, DAR16-II (a reverse sequence) was found to induce an angiogenic effect. DAR16-II promoted EC spread, migration, tubular-like structure formation and THP-1 attachment. Results have shown that DAR16-II mediated effects on EC might be derived from activation of ENG, SEPINE1 and ACTB pathways. This data has to be confirmed with further studies. The presented data also suggests that DAR16-II affects Mo adhesion, which allows speculation regarding an immunomodulatory effect. Nonetheless, this has to be established with further experiments.

5. Chapter 5: General Discussion

The main aim of the present study was to develop a biologically active bone scaffold able to promote early vascularization of the construct and, inherently, of the angio-osteogenic coupling i.e. bone formation. The potential osteoconductive and osteoinductive effects of 3D printed scaffolds of different pore size and geometries whose surface was functionalised with a novel SAP (DAR16-II) was firstly investigated *in vivo* by CSD calvaria rabbit model. Although there is no unanimous agreement in the literature on the pore shape that could improve bone development within scaffolds, different studies have shown better outcome in both bone development and vessels ingrowth with circular surfaces (Zadpoor, 2015). However, our data revealed that there was no significant difference between round and square pores in inducing bone formation (Chapter 2, Figures 2.8 and 2.9). According to Rumpler et al. which compared different pore geometries in scaffolds for bone regeneration (Figure 5.1) all tissue 'fronts' would eventually become circular (Rumpler et al., 2008).

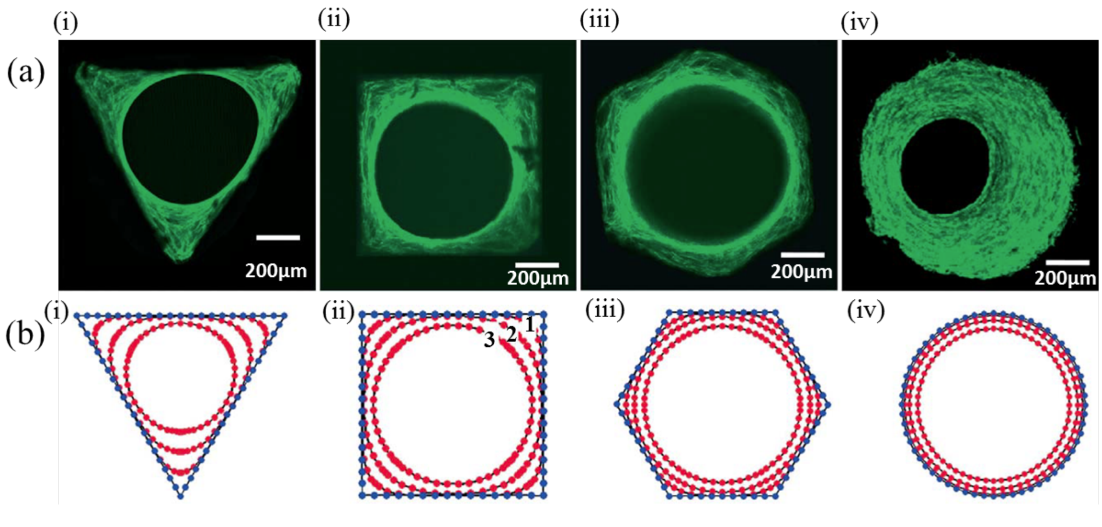

Figure 5.1 (a) Staining of actin stress fibres developed *in vitro* by MC3T3-E1 cells in different channel geometries of HA plates with phalloidin-FITC; (i) triangular, (ii) square, (iii) hexagonal and (iv) round shape channels, the tissue regeneration process based on a linear curvature-dependent theoretical mode was depicted in subfigure (b). The lines (early time point 1, ongoing times 2 and 3 of 21 and 30 days) mark the simulated development of tissue formation over the experiment time (Adapted from Rumpler et al. 2008).

The same finding was supported by a study from Van Bael *et al.* in which human periosteum-derived cells (hPDC) after 14 days of culture *in vitro* resulted in circular filling of different pore geometries including triangular, hexagonal and rectangular titanium scaffolds (Van Bael et al., 2012). Hence, our result agrees with their conclusion in that bridging behaviour of cells is geometry independent. However, Van Bael *et al.* claimed that the pore size was key in bone regeneration with more neo-formed bone associated with 1000 µm pore size compared to 500 µm but more ALP activity with 500 µm pore size (Van Bael et al., 2012). They suggested that the effect mediated by smaller pore (ALP activity) could be justified by enhanced cell adhesion. Our findings contradict this assumption by showing no significant difference between total neo-formed bone and the bone formed in direct contact with the biomaterial in 400 and 800 µm pore size scaffolds (Chapter 2, Figures 2.8 and 2.9). However, the model employed (*in vivo*) differs significantly from the one used by Van Bael and colleagues (*in vitro*) and this may explain the different outcomes. Interestingly, DAR16-II coating showed curious results of enhancing both the total bone formation and more evidently the bone in direct contact with the biomaterial. To our best knowledge, this is the first study to examine the use of SAPs as a surface coating for BCP functionalization. Our findings suggest that by coating BCP scaffolds with DAR16-II it is possible to promote better bone formation than utilising 3D printed BCP scaffolds alone.

The aim of the following studies was to investigate how this proactive factor induced a biological response and resulted in more bone formation. By testing the effect of DAR16-II on MSC differentiation *in vitro*, there was no upregulation of either osteogenic or angiogenic genes expression (Chapter 3, Figure 3.5). Also, the lack of osteoinductive property was demonstrated by alizarin red staining showing no calcium deposits with DAR16-II after 9 days of culture (Chapter 3, Figure 3.6). In addition, *in vitro* culture of

MSCs on BCP scaffolds coated with DAR16-II did not induce osteogenic differentiation (Chapter 3, Figures 3.3 and 3.4). However, DAR16-II significantly maintained cell viability compared to non-coated scaffolds (Chapter 3, Figure 3.2). These results suggest that the DAR16-II coating of BCP enhances the cell behaviour. The RADA-and RARADADA- based SAPs are supposed to mimic the RGD peptides sequence and provides a nanoscale environment similar to ECM that promote cell adhesion and proliferation (Gelain et al., 2007). This was demonstrated by Bokhari *et al*. as they used RAD16-1 (*PuraMatrix*^{TM}, self-assembly peptide with a reverse single RADA- motif sequence) to coat PolyHIPE polymer (PHP) (Bokhari et al., 2005). OBts cultured on RAD16-1 coated scaffolds showed a significant increase in cell proliferation during the 35 days of *in vitro* culture. Also, it was confirmed by Gelain *et al*. by studying the relation of neural precursor cells to RAD16-I scaffolds and found that cells were fully embedded in the peptides nanofibers in an analogous microenvironment to ECM structure (Gelain et al., 2006).

As the DAR16-II shares the basic peptide compartments of RAD16-II in a reverse sequence, we assumed that they might share the same biological properties in promoting angiogenesis (Narmoneva et al., 2004, Narmoneva et al., 2005). Our *in vitro* data demonstrated this assumption. Indeed, culturing HUVECs with DAR16-II significantly reduced cell proliferation suggesting more cells were undergoing activation and differentiation (Chapter 4, Figure 4.2). This was confirmed by significantly promoting tubular-like structure formation and cell adhesion (Chapter 4, Figures 4.3and 4.5). In addition, DAR16-II induced the formation of filopodia and lamellipodia thus demonstrating the activation of EC by inducing migratory phenotype (Chapter 4, figure 4.4). These results were broadly consistent with Narmoneva *et al*. study as they showed that RAD16-II provides an angiogenic environment (Narmoneva et al., 2005). RAD16-II promoted long-term cell survival and capillary-like network formation in 3D cultures of human microvascular endothelial cells isolated from fat tissue *in vitro*. They showed that RAD16-II enhanced VEGF gene expression; however the mechanism in which the SAP was inducing angiogenesis was not investigated. In our study, angiogenesis PCR array showed that three angiogenic genes were significantly upregulated by DAR16-II including; ENG, SERPIN-1 and ACTB while the VEGF decoy receptor Flt1 was down-regulated (Chapter 4, Figure 4.7). This down-regulation suggested that EC could be in a more active state ready to transduce VEGF signalling upon exposure. This also might agree with Narmoneva *et al*. finding although VEGF was not up-regulated in our study. Our results confirm that SAPs nanostructure influence cell adhesion and EC activation observed by other groups. Nonetheless, our results on EC indicated an inhibition rather than induction of proliferation thus highlighting that the different sequences are exerting different effects. On the basis of our RNA array data, we propose that the specific effects of DAR16-II might be mediated by ENG and SERPINE1 and TGF-β pathway (Figure 5.1).

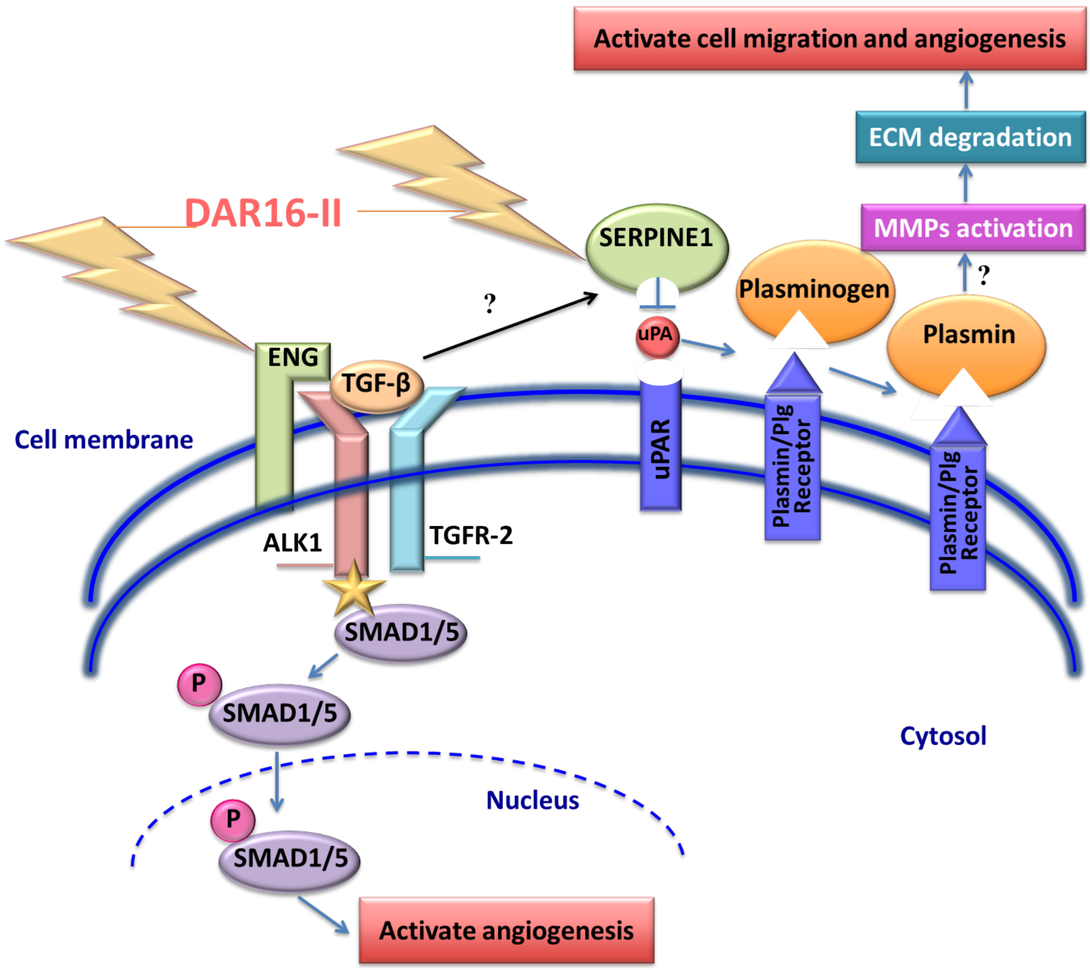

Figure 5.2 The proposed mechanism of DAR16-II in inducing endothelial cell migration. DAR16-II activates ENG expression which is a co-receptor to TGF-β. This phosphorylates a SMAD downstream through ALK1 activation which induces angiogenesis in endothelial cells. SERPINE1 overexpression upon exposure to DAR16-II is thought to activate the SERPINE1 pathway in inducing endothelial migration through MMP activation. In addition, as SERPINE1 is activated by TGF-β during angiogenesis, the DAR16-II activation of SERPINE1 might be regulated by expressing TGF-β through ENG.

RNA array data also demonstrates an up-regulation of ACTB expression which is compatible with the observed migratory phenotype of ECs (Bunnell et al., 2011). These results suggest that DAR16-II can induce angiogenesis via both ENG mediated signalling and by preparing EC for higher responsiveness to VEGF signalling. In addition, DAR16-II significantly enhanced THP-1 adhesion, which suggests that DAR16-II might have an effect on monocytes recruitment *in vitro* (Chapter 4, Figure 4.8). We can speculate that this might also reflect into an immuno-modulatory effect on macrophages but to demonstrate these further investigations are warranted. Indeed, DAR16-II did not induce

THP-1 differentiation into macrophages in the limited model (without cytokines added) used in this study (Chapter 4, Figure 4.9).

Overall our experiments have demonstrated for the first time that SAP and DAR16-II in particular is a viable substrate to functionalize the surface of scaffolds for bone engineering. The DAR16-II coating was able to provide a functioning matrix which promoted better osteogenesis *in vivo*. Furthermore, this work demonstrated that the observed *in vivo* effects might be mediated by better cell (inflammatory, mesenchymal and endothelial cells) recruitment from the neighbouring healthy tissue. Additionally, the *in vitro* data demonstrated a clear angiogenic effect on EC, due to osteo-angiogenic coupling, which can justify the observed increase in bone regeneration. The histo-morphometric analysis performed in this study highlights an increase in bone formation in DAR16-II functionalized scaffolds. Comparing the data of overall bone formation vs the bone in contact with biomaterial only, it is possible to infer that the observed effects were mainly mediated by the direct contact with DAR16-II adsorbed on the BCP surface rather than a diffusion of DAR16-II within the pores. Thus it was hypothesized and partially demonstrated that DAR16-II provides a supporting environment for cell attachment and interaction leading to enhancing the bone regeneration process around BCP scaffolds.

The work in this thesis has demonstrated that DAR16-II is able to provide a functioning matrix as a coating material. It induced the osteogenic capability of BCP scaffolds *in vivo* as well as maintaining cell viability on coated BCP scaffolds *in vitro*. It has a direct angiogenic effect on endothelial cell activation and on inflammatory cell attachment. Thus it provides a supporting environment for cell attachment and interaction in order to enhance the bone regeneration process. The long-term effect of DAR16-II in coating BCP scaffolds confirmed its stability and biological effectiveness in inducing bone formation. However, the mechanism of action requires more studies to confirm the proposed hypothesis to identify the molecular mode of action. In addition, identifying the integrins involved in enhancing cell adhesion is a prerequisite to understand these vital phenomena.

6. Chapter 6: Conclusions and Future Work

6.1 Conclusions

The BCP scaffolds used in this study were 3D printed using the robocasting (DW) methodology. Coating of 3D printed scaffolds was obtained by simple immersion into a 0.15% solution of DAR16-II, this strategy alone (without chemical crosslinking of the SAP to BCP surface) was able to exert the observed effects. Therefore, this study shows promising results for developing commercial off- the shelf functionalized scaffolds with very limited costs translating these discoveries into the clinical arena. A further asset of this proposed strategy is that the scaffolds can be 3D printed to any shape. This coupled with high resolution imaging of bone defects can pave the way to the realisation of personalised patient specific scaffolds.

A limitation of this study was that the cell/molecular mechanism of action of DAR16-II was only partially addressed. Therefore, further studies are warranted to confirm the proposed hypothesis, to identify the molecular mechanisms driving enhanced osteogenesis and finally to tailor even more effective strategies using the same basic components, 3D printed BCP and DAR16-II to functionalise BCP surface.

The main conclusions drawn regarding each aim were as follows:

1. To investigate the effect of pore size and geometry in functionalizing 3D printed BCP scaffolds:

   BCP scaffolds printed with two different pore sizes and geometries; round (800μm) and square (400μm) had no effect on bone regeneration in a rabbit calvaria model. There was no significant difference in the total bone developed as well as the bone in contact formation. There was no adverse reaction development thus confirming the biocompatibility of 3D printed BCP scaffolds.

2. To determine if DAR16-II can be used as a proactive coating matrix for BCP scaffolds:

Coating the BCP scaffolds with DAR16-II enhanced the total bone formation *in vivo*. Bone in contact was significantly increased with DAR16-II coating ($p<0.05$). The experiment was terminated after 8 weeks of implantation and this reflects the long-term effect of adding the coating factor the BCP scaffolds.

3. To investigate the biological effect of DAR16-II *in vitro* at the cell level on osteogenesis and angiogenesis:
   a) BCP scaffolds coated with DAR16-II significantly preserved MSCs viability up to day 42 compared to non-coated scaffolds ($p<0.05$). .
   b) DAR16-II did not induce neither osteogenic nor angiogenetic differentiation in MSCs. In addition, no mineralization effect of DAR16-II was detected when MSCs mesenspheres were used as a more pure stem cell MSC model.

   Therefore, DAR16-II can be used to augment the BCP effect in enhancing cell attachment and viability at the implanted site. The enhanced proliferation during the experiment reflected the preferable cellular environment provided by DAR16-II. The DAR16-II coating provides an ECM-like matrix that promotes cell survival and proliferation within its supportive microenvironment.

c) DAR16-II induced angiogenetic effects and cell attachment:

i. Culturing HUVECs with DAR16-II significantly promoted EC spreading ($p<0.0001$). In addition, DAR16-II significantly increased the tubular length ($p<0.01$) and the number of developed nodes ($p<0.001$) in Matrigel assay. Moreover, DAR16-II induced migratory phenotype in HUVEC as indicated by its more pronounced cell projections. The DAR16-II angiogenic effect is most likely activated through the expression of ENG, SEPINE1 and ACTB and the downregulation of VEGF receptors KDR and Flt1.

ii. DAR16-II significantly induced THP-1 cell attachment ($p<0.001$). However DAR16-II did not induce molecular changes after 48 h of exposure. This negative result is assumed to be related to the culturing conditions used in this study. Thus the required cytokines for THP-1 polarizations were not added to culture.

Using DAR16-II coating can induce vascularization at the implanted site by activating endothelial cell migration. This activation might be mediated by ENG and SERPINE1 and TGF-β pathway. Also, DAR16-II induced inflammatory cell attachment which suggests that it provides a supporting environment for cell attachment and interaction which can enhance vascularization and bone regeneration.

Finally:

- The method of using DAR16-II as a coating matrix is convenient for clinical application regarding the handling and the time required.
- The fact that a specific motif can be designed and incorporated within the peptide sequence can expand the range of clinical application to induce a specific biological response.
- Further studies are required to optimise the culturing of inflammatory cells, macrophages in particular in order to investigate if DAR16-II has an immunomodulatory effect.

6.2 Future Work

The results of this study give rise to further questions that require investigations both *in vivo* and *in vitro*:

- Proteomic analysis of protein changes in HUVECs in response to DAR16-II (the experiment was conducted and cell pellets are awaiting analysis).
- The angiogenic effects of DAR16-II require a specific model to study the effect of the peptides on angiogenesis *in vivo*.
- qRT-PCR validation of the genes of interest being expressed by DAR126-II in order to confirm the array results.
- A microscopical study of the DAR16-II coating using electron microscopy (SEM) and RAMAN spectroscopy to assess the coating topography and surface chemistry.
- Examination of the effectiveness of the DAR16-II matrix bonding with the ceramic surface by X-ray photoelectron spectroscopy.
- Investigation of the effect of DAR16-II on polarization and angiogenic differentiation markers by qRT-PCR using a more appropriate and physiological model of monocytes and macrophages.
- Assessing the molecular mechanism driving DAR16-II mediated cell adhesion.

7. Appendix

The gene list

Gene name	Abbreviation
Angiogenin	ANG
Angiopoietin 1	ANGPT1
Angiopoietin 2	ANGPT2
Alanyl aminopeptidase	ANPEP
Thymidine phosphorylase	TYMP
Fibroblast growth factor 1	FGF1
Fibroblast growth factor 2	FGF2 (BFGF)
Vascular endothelial growth factor D	VEGFD
Fms related tyrosine kinase 1	FLT1 (VEGFR1)
Jagged 1	JAG1
Kinase insert domain receptor	KDR (VEGFR3)
Neuropilin 1	NRP1
Neuropilin 2	NRP2
Placental growth factor	PGF
Vascular endothelial growth factor A	VEGFA
Vascular endothelial growth factor B	VEGFB
Vascular endothelial growth factor C	VEGFC
connective tissue growth factor	CTGF
Ephrin A1	EFNA1
Ephrin B2	EFNB2
Epidermal growth factor	EGF
EPH receptor B4	EPHB4
Fibroblast growth factor receptor 3	FGFR3
Hepatocyte growth factor	HGF
Insulin like growth factor 1	IGF1
Integrin subunit beta 3	ITGB3
Platelet derived growth factor subunit A	PDGFA
Sphingosine-1-phosphate receptor 1	S1PR1
TEK receptor tyrosine kinase	TEK (TIE2)
Transforming growth factor alpha	TGFA
Transforming growth factor beta 1	TGFB1
Transforming growth factor beta 2	TGFB2
Transforming growth factor beta receptor 1	TGFBR1 (ALK5)
Adhesion G protein-coupled receptor B1	ADGRB1
Collagen type IV alpha 3 chain	COL4A3
C-X-C motif chemokine ligand 8	CXCL8
Neuropilin 1	NRP1
Neuropilin 2	NRP2
C-C motif chemokine ligand 11	CCL11
C-C motif chemokine ligand 2	CCL2
Cadherin 5	CDH5
Collagen type XVIII alpha 1 chain	COL18A1
Connective tissue growth factor	CTGF
Endoglin	ENG
Erb-b2 receptor tyrosine kinase 2	ERBB2
Fibronectin 1	FN1
Integrin subunit alpha V	ITGAV
Integrin subunit beta 3	ITGB3
Sphingosine-1-phosphate receptor 1	S1PR1

Thrombospondin 1	THBS1
Thrombospondin 2	THBS2
Angiopoietin like 4	ANGPTL4
Coagulation factor III	F3
Platelet and endothelial cell adhesion molecule 1	PECAM1
Platelet factor 4	PF4
Prokineticin 2	PROK2
Serpin family E member 1	SERPINE1 (PAI-1)
Serpin family F member 1	SERPINF1
Leukocyte cell derived chemotaxin 1	LECT1
Leptin	LEP
Matrix metallopeptidase 14	MMP14
Matrix metallopeptidase 2	MMP2
Matrix metallopeptidase 9	MMP9
Plasminogen activator, urokinase	PLAU
Plasminogen	PLG
TIMP metallopeptidase inhibitor 1	TIMP1
TIMP metallopeptidase inhibitor 2	TIMP2
TIMP metallopeptidase inhibitor 3	TIMP3
C-X-C motif chemokine ligand 1	CXCL1
C-X-C motif chemokine ligand 10	CXCL10
C-X-C motif chemokine ligand 5	CXCL5
C-X-C motif chemokine ligand 6	CXCL6
C-X-C motif chemokine ligand 9	CXCL9
Endothelin 1	EDN1
Interferon alpha 1	IFNA1
Interferon gamma	IFNG
Interleukin 1 beta	IL1B
Interleukin 6	IL6
Midkine (neurite growth-promoting factor 2)	MDK
Tumor necrosis factor	TNF
Hypoxia inducible factor 1 alpha subunit	HIF1A
Nitric oxide synthase 3	NOS3
Sphingosine kinase 1	SPHK1
AKT serine/threonine kinase 1	AKT1
Heparanase	HPSE
Inhibitor of DNA binding 1, HLH protein	ID1
Notch 4	NOTCH4
Prostaglandin-endoperoxide synthase 1	PTGS1
Tyrosine kinase with immunoglobulin like and EGF like domains 1	TIE1

8. References

ALENEZI, A., NAITO, Y., ANDERSSON, M., CHRCANOVIC, B. R., WENNERBERG, A. & JIMBO, R. 2013. Characteristics of 2 different commercially available implants with or without nanotopography. *International journal of dentistry,* 2013.

ALEXANDER, K. A., CHANG, M. K., MAYLIN, E. R., KOHLER, T., MÜLLER, R., WU, A. C., VAN ROOIJEN, N., SWEET, M. J., HUME, D. A. & RAGGATT, L. J. 2011. Osteal macrophages promote in vivo intramembranous bone healing in a mouse tibial injury model. *Journal of Bone and Mineral Research,* 26**,** 1517-1532.

ALMEIDA, C. R., SERRA, T., OLIVEIRA, M. I., PLANELL, J. A., BARBOSA, M. A. & NAVARRO, M. 2014. Impact of 3-D printed PLA-and chitosan-based scaffolds on human monocyte/macrophage responses: unraveling the effect of 3-D structures on inflammation. *Acta biomaterialia,* 10**,** 613-622.

ALSBERG, E., ANDERSON, K., ALBEIRUTI, A., FRANCESCHI, R. & MOONEY, D. 2001. Cell-interactive alginate hydrogels for bone tissue engineering. *Journal of dental research,* 80**,** 2025-2029.

ANDERSON, H. C. 2003. Matrix vesicles and calcification. *Current rheumatology reports,* 5**,** 222-226.

ARANA-CHAVEZ, V., SOARES, A. & KATCHBURIAN, E. 1995. Junctions between early developing osteoblasts of rat calvaria as revealed by freeze-fracture and ultrathin section electron microscopy. *Archives of histology and cytology,* 58**,** 285-292.

ARINZEH, T. L., TRAN, T., MCALARY, J. & DACULSI, G. 2005. A comparative study of biphasic calcium phosphate ceramics for human mesenchymal stem-cell-induced bone formation. *Biomaterials,* 26**,** 3631-3638.

ARTHUR, H. M., URE, J., SMITH, A. J., RENFORTH, G., WILSON, D. I., TORSNEY, E., CHARLTON, R., PARUMS, D. V., JOWETT, T. & MARCHUK, D. A. 2000. Endoglin, an ancillary TGFβ receptor, is required for extraembryonic angiogenesis and plays a key role in heart development. *Developmental biology,* 217**,** 42-53.

BAI, F., WANG, Z., LU, J., LIU, J., CHEN, G., LV, R., WANG, J., LIN, K., ZHANG, J. & HUANG, X. 2010. The correlation between the internal structure and vascularization of controllable porous bioceramic materials in vivo: a quantitative study. *Tissue Engineering Part A,* 16**,** 3791-3803.

BAILEY, J., CRITSER, P., WHITTINGTON, C., KUSKE, J., YODER, M. & VOYTIK‐HARBIN, S. 2011. Collagen oligomers modulate physical and biological properties of three‐dimensional self‐assembled matrices. *Biopolymers,* 95**,** 77-93.

BANSAL, S., CHAUHAN, V., SHARMA, S., MAHESHWARI, R., JUYAL, A. & RAGHUVANSHI, S. 2009. Evaluation of hydroxyapatite and beta-tricalcium phosphate mixed with bone marrow aspirate as a bone graft substitute for posterolateral spinal fusion. *Indian journal of orthopaedics,* 43**,** 234.

BARRADAS, A. M., FERNANDES, H. A., GROEN, N., CHAI, Y. C., SCHROOTEN, J., VAN DE PEPPEL, J., VAN LEEUWEN, J. P., VAN BLITTERSWIJK, C. A. & DE BOER, J. 2012. A calcium-induced signaling cascade leading to osteogenic differentiation of human bone marrow-derived mesenchymal stromal cells. *Biomaterials,* 33**,** 3205-3215.

BARTNECK, M., HEFFELS, K.-H., PAN, Y., BOVI, M., ZWADLO-KLARWASSER, G. & GROLL, J. 2012. Inducing healing-like human primary macrophage phenotypes by 3D hydrogel coated nanofibres. *Biomaterials,* 33**,** 4136-4146.

BATTISTELLA, E., MELE, S., FOLTRAN, I., LESCI, I. G., ROVERI, N., SABATINO, P. & RIMONDINI, L. 2012. Cuttlefish bone scaffold for tissue engineering: a novel hydrothermal transformation, chemical-physical, and biological characterization. *J Appl Biomater Funct Mater,* 1**,** 2.

BECK, G. R. & KNECHT, N. 2003. Osteopontin regulation by inorganic phosphate is ERK1/2-, protein kinase C-, and proteasome-dependent. *Journal of Biological Chemistry,* 278**,** 41921-41929.

BEN-DAVID, D., KIZHNER, T. A., KOHLER, T., MÜLLER, R., LIVNE, E. & SROUJI, S. 2011. Cell-scaffold transplant of hydrogel seeded with rat bone marrow progenitors for bone regeneration. *Journal of Cranio-Maxillofacial Surgery,* 39**,** 364-371.

BERGERS, G. & HANAHAN, D. 2008. Modes of resistance to anti-angiogenic therapy. *Nature Reviews Cancer,* 8**,** 592-603.

BERGMANN, C. J., ODEKERKEN, J. C., WELTING, T. J., JUNGWIRTH, F., DEVINE, D., BOURÉ, L., ZEITER, S., VAN RHIJN, L. W., TELLE, R. & FISCHER, H. 2014. Calcium phosphate based three-dimensional cold plotted bone scaffolds for critical size bone defects. *BioMed Research International,* 2014.

BIANCHI, M., EDREIRA, E. R. U., WOLKE, J. G., BIRGANI, Z. T., HABIBOVIC, P., JANSEN, J. A., TAMPIERI, A., MARCACCI, M., LEEUWENBURGH, S. C. & VAN DEN BEUCKEN, J. J. 2014. Substrate geometry directs the in vitro mineralization of calcium phosphate ceramics. *Acta biomaterialia,* 10**,** 661-669.

BIANCO, P., RIMINUCCI, M., GRONTHOS, S. & ROBEY, P. G. 2001. Bone marrow stromal stem cells: nature, biology, and potential applications. *Stem cells,* 19**,** 180-192.

BIDAN, C. M., KOMMAREDDY, K. P., RUMPLER, M., KOLLMANNSBERGER, P., BRÉCHET, Y. J., FRATZL, P. & DUNLOP, J. W. 2012. How linear tension converts to curvature: geometric control of bone tissue growth. *PloS one,* 7**,** e36336.

BIDAN, C. M., KOMMAREDDY, K. P., RUMPLER, M., KOLLMANNSBERGER, P., FRATZL, P. & DUNLOP, J. W. 2013. Geometry as a factor for tissue growth: towards shape optimization of tissue engineering scaffolds. *Advanced healthcare materials,* 2**,** 186-194.

BILEZIKIAN, J. P., RAISZ, L. G. & MARTIN, T. J. 2008. *Principles of Bone Biology: Two-Volume Set*, Academic Press.

BOERCKEL, J. D., KOLAMBKAR, Y. M., DUPONT, K. M., UHRIG, B. A., PHELPS, E. A., STEVENS, H. Y., GARCÍA, A. J. & GULDBERG, R. E. 2011. Effects of protein dose and delivery system on BMP-mediated bone regeneration. *Biomaterials,* 32**,** 5241-5251.

BOIVIN, G., BALA, Y., DOUBLIER, A., FARLAY, D., STE-MARIE, L., MEUNIER, P. & DELMAS, P. 2008. The role of mineralization and organic matrix in the microhardness of bone tissue from controls and osteoporotic patients. *Bone,* 43**,** 532-538.

BOKHARI, M. A., AKAY, G., ZHANG, S. & BIRCH, M. A. 2005. The enhancement of osteoblast growth and differentiation in vitro on a peptide hydrogel—polyHIPE polymer hybrid material. *Biomaterials,* 26**,** 5198-5208.

BOSE, S. & TARAFDER, S. 2012. Calcium phosphate ceramic systems in growth factor and drug delivery for bone tissue engineering: a review. *Acta biomaterialia,* 8**,** 1401-1421.

BOURDEAU, A., FAUGHNAN, M. E. & LETARTE, M. 2000. Endoglin-deficient mice, a unique model to study hereditary hemorrhagic telangiectasia. *Trends in cardiovascular medicine,* 10**,** 279-285.

BOYLE, W. J., SIMONET, W. S. & LACEY, D. L. 2003. Osteoclast differentiation and activation. *Nature,* 423**,** 337-342.

BRIGHTON, C. T., SHAMAN, P., HEPPENSTALL, R. B., ESTERHAI, J. L., JR., POLLACK, S. R. & FRIEDENBERG, Z. B. 1995. Tibial nonunion treated with direct current, capacitive coupling, or bone graft. *Clin Orthop Relat Res***,** 223-34.

BROOKS, P. C., CLARK, R. & CHERESH, D. A. 1994. Requirement of vascular integrin alpha v beta 3 for angiogenesis. *Science,* 264**,** 569-571.

BROWN, B. N., RATNER, B. D., GOODMAN, S. B., AMAR, S. & BADYLAK, S. F. 2012. Macrophage polarization: an opportunity for improved outcomes in biomaterials and regenerative medicine. *Biomaterials,* 33**,** 3792-3802.

BUCKWALTER, J., GLIMCHER, M., COOPER, R. & RECKER, R. 1995. Bone biology. *J Bone Joint Surg Am,* 77**,** 1256-1275.

BUNNELL, T. M., BURBACH, B. J., SHIMIZU, Y. & ERVASTI, J. M. 2011. β-Actin specifically controls cell growth, migration, and the G-actin pool. *Molecular biology of the cell,* 22**,** 4047-4058.

BURR, D. B. 2002. The contribution of the organic matrix to bone's material properties. *Bone,* 31**,** 8-11.

CAMBRA‐MOO, O., NACARINO MENESES, C., RODRÍGUEZ BARBERO, M. Á., GARCÍA GIL, O., RASCÓN PÉREZ, J., RELLO‐VARONA, S., D'ANGELO, M., CAMPO MARTÍN, M. & GONZÁLEZ MARTÍN, A. 2014. An approach to the histomorphological and histochemical variations of the humerus cortical bone through human ontogeny. *Journal of anatomy,* 224**,** 634-646.

CAMENISCH, G., PISABARRO, M. T., SHERMAN, D., KOWALSKI, J., NAGEL, M., HASS, P., XIE, M.-H., GURNEY, A., BODARY, S. & LIANG, X. H. 2002. ANGPTL3 stimulates endothelial cell adhesion and migration via integrin αvβ3 and induces blood vessel formation in vivo. *Journal of Biological Chemistry,* 277**,** 17281-17290.

CAPULLI, M., PAONE, R. & RUCCI, N. 2014. Osteoblast and osteocyte: Games without frontiers. *Archives of biochemistry and biophysics,* 561**,** 3-12.

CARANO, R. A. & FILVAROFF, E. H. 2003. Angiogenesis and bone repair. *Drug discovery today,* 8**,** 980-989.

CARDOSO, G. B., MANIGLIO, D., VOLPATO, F. Z., TONDON, A., MIGLIARESI, C., KAUNAS, R. R. & ZAVAGLIA, C. A. 2015. Oleic acid surfactant in polycaprolactone/hydroxyapatite‐composites for bone tissue engineering. *Journal of Biomedical Materials Research Part B: Applied Biomaterials*.

CARMELIET, P. 2005. Angiogenesis in life, disease and medicine. *Nature,* 438**,** 932-936.

CARMELIET, P. & JAIN, R. K. 2000. Angiogenesis in cancer and other diseases. *Nature,* 407**,** 249-257.

CARMELIET, P. & JAIN, R. K. 2011. Molecular mechanisms and clinical applications of angiogenesis. *Nature,* 473**,** 298-307.

CASPI, O., LESMAN, A., BASEVITCH, Y., GEPSTEIN, A., ARBEL, G., HABIB, I. H. M., GEPSTEIN, L. & LEVENBERG, S. 2007. Tissue engineering of vascularized cardiac muscle from human embryonic stem cells. *Circulation research,* 100**,** 263-272.

CASTANEDA, S., LARGO, R., CALVO, E., RODRIGUEZ-SALVANES, F., MARCOS, M., DIAZ-CURIEL, M. & HERRERO-BEAUMONT, G. 2006. Bone mineral measurements of subchondral and trabecular bone in healthy and osteoporotic rabbits. *Skeletal radiology,* 35**,** 34-41.

CHANG, C. & CHIANG, H. 2003. Three-dimensional image reconstructions of complex objects by an abrasive computed tomography apparatus. *The International Journal of Advanced Manufacturing Technology,* 22**,** 708-712.

CHANG, M. K., RAGGATT, L.-J., ALEXANDER, K. A., KULIWABA, J. S., FAZZALARI, N. L., SCHRODER, K., MAYLIN, E. R., RIPOLL, V. M., HUME, D. A. & PETTIT, A. R. 2008. Osteal tissue macrophages are intercalated throughout human and mouse bone lining tissues and regulate osteoblast function in vitro and in vivo. *The Journal of Immunology,* 181**,** 1232-1244.

CHARULATHA, V. & RAJARAM, A. 2003. Influence of different crosslinking treatments on the physical properties of collagen membranes. *Biomaterials,* 24**,** 759-767.

CHEN, D. C., LAI, Y. L., LEE, S. Y., HUNG, S. L. & CHEN, H. L. 2007. Osteoblastic response to collagen scaffolds varied in freezing temperature and glutaraldehyde crosslinking. *Journal of biomedical materials research Part A,* 80**,** 399-409.

CHEN, S., JIAN, Z., HUANG, L., XU, W., LIU, S., SONG, D., WAN, Z., VAUGHN, A., ZHAN, R. & ZHANG, C. 2015a. Mesoporous bioactive glass surface modified poly (lactic-co-glycolic acid) electrospun fibrous scaffold for bone regeneration. *International journal of nanomedicine,* 10**,** 3815.

CHEN, W., THEIN-HAN, W., WEIR, M. D., CHEN, Q. & XU, H. H. 2014a. Prevascularization of biofunctional calcium phosphate cement for dental and craniofacial repairs. *Dental Materials,* 30**,** 535-544.

CHEN, X., ZHAO, Y., GENG, S., MIRON, R. J., ZHANG, Q., WU, C. & ZHANG, Y. 2015b. In vivo experimental study on bone regeneration in critical bone defects using PIB nanogels/boron-containing mesoporous bioactive glass composite scaffold. *International journal of nanomedicine,* 10**,** 839.

CHEN, Z., WU, C., GU, W., KLEIN, T., CRAWFORD, R. & XIAO, Y. 2014b. Osteogenic differentiation of bone marrow MSCs by β-tricalcium phosphate stimulating macrophages via BMP2 signalling pathway. *Biomaterials,* 35**,** 1507-1518.

CHILDS, S. G. 2005. Osteonecrosis: death of bone cells. *Orthopaedic Nursing,* 24**,** 295-301.

CHOI, K. D., YU, J., SMUGA‐OTTO, K., SALVAGIOTTO, G., REHRAUER, W., VODYANIK, M., THOMSON, J. & SLUKVIN, I. 2009. Hematopoietic and endothelial differentiation of human induced pluripotent stem cells. *Stem cells,* 27**,** 559-567.

CHOONG, C. S., HUTMACHER, D. W. & TRIFFITT, J. T. 2006. Co-culture of bone marrow fibroblasts and endothelial cells on modified polycaprolactone substrates for enhanced potentials in bone tissue engineering. *Tissue engineering,* 12**,** 2521-2531.

CHUNG, H. J. & PARK, T. G. 2007. Surface engineered and drug releasing pre-fabricated scaffolds for tissue engineering. *Advanced drug delivery reviews,* 59**,** 249-262.

CIPITRIA, A., REICHERT, J. C., EPARI, D. R., SAIFZADEH, S., BERNER, A., SCHELL, H., MEHTA, M., SCHUETZ, M. A., DUDA, G. N. & HUTMACHER, D. W. 2013. Polycaprolactone scaffold and reduced rhBMP-7 dose for the regeneration of critical-sized defects in sheep tibiae. *Biomaterials,* 34**,** 9960-9968.

CLAVERO, J. & LUNDGREN, S. 2003. Ramus or chin grafts for maxillary sinus inlay and local onlay augmentation: comparison of donor site morbidity and complications. *Clin Implant Dent Relat Res,* 5**,** 154-60.

COCHRAN, D. L. & WOZNEY, J. M. 1999. Biological mediators for periodontal regeneration. *Periodontology 2000,* 19**,** 40-58.

COELHO, M., CABRAL, A. T. & FERNANDES, M. 2000. Human bone cell cultures in biocompatibility testing. Part I: osteoblastic differentiation of serially passaged human bone marrow cells cultured in α-MEM and in DMEM. *Biomaterials,* 21**,** 1087-1094.

COELHO, M. & FERNANDES, M. 2000. Human bone cell cultures in biocompatibility testing. Part II: effect of ascorbic acid, β-glycerophosphate and dexamethasone on osteoblastic differentiation. *Biomaterials,* 21**,** 1095-1102.

COLNOT, C. 2009. Skeletal cell fate decisions within periosteum and bone marrow during bone regeneration. *Journal of Bone and Mineral Research,* 24**,** 274-282.

CRISAN, M., YAP, S., CASTEILLA, L., CHEN, C.-W., CORSELLI, M., PARK, T. S., ANDRIOLO, G., SUN, B., ZHENG, B. & ZHANG, L. 2008. A perivascular origin for mesenchymal stem cells in multiple human organs. *Cell stem cell,* 3**,** 301-313.

CURRY, A. S., PENSA, N. W., BARLOW, A. M. & BELLIS, S. L. 2016. Taking cues from the extracellular matrix to design bone-mimetic regenerative scaffolds. *Matrix Biology,* 52**,** 397-412.

CZEKAY, R.-P., WILKINS-PORT, C. E., HIGGINS, S. P., FREYTAG, J., OVERSTREET, J. M., KLEIN, R. M., HIGGINS, C. E., SAMARAKOON, R. & HIGGINS, P. J. 2011. PAI-1: an integrator of cell signaling and migration. *International journal of cell biology,* 2011.

DALLAS, N. A., SAMUEL, S., XIA, L., FAN, F., GRAY, M. J., LIM, S. J. & ELLIS, L. M. 2008. Endoglin (CD105): a marker of tumor vasculature and potential target for therapy. *Clinical Cancer Research,* 14**,** 1931-1937.

DAS, A., SEGAR, C. E., HUGHLEY, B. B., BOWERS, D. T. & BOTCHWEY, E. A. 2013. The promotion of mandibular defect healing by the targeting of S1P receptors and the recruitment of alternatively activated macrophages. *Biomaterials,* 34**,** 9853-9862.

DAVIS, M. E., MOTION, J. M., NARMONEVA, D. A., TAKAHASHI, T., HAKUNO, D., KAMM, R. D., ZHANG, S. & LEE, R. T. 2005. Injectable self-assembling peptide nanofibers create intramyocardial microenvironments for endothelial cells. *Circulation,* 111**,** 442-450.

DE LONG, W. G., EINHORN, T. A., KOVAL, K., MCKEE, M., SMITH, W., SANDERS, R. & WATSON, T. 2007. Bone grafts and bone graft substitutes in orthopaedic trauma surgery: a critical analysis. *Journal of bone and joint surgery. American volume,* 89**,** 649-658.

DE PALMA, M., MURDOCH, C., VENNERI, M. A., NALDINI, L. & LEWIS, C. E. 2007. Tie2-expressing monocytes: regulation of tumor angiogenesis and therapeutic implications. *Trends in immunology,* 28**,** 519-524.

DE PALMA, M. & NALDINI, L. 2009. Tie2-expressing monocytes (TEMs): novel targets and vehicles of anticancer therapy? *Biochimica et Biophysica Acta (BBA)-Reviews on Cancer,* 1796**,** 5-10.

DE SMET, F., SEGURA, I., DE BOCK, K., HOHENSINNER, P. J. & CARMELIET, P. 2009. Mechanisms of vessel branching filopodia on endothelial tip cells lead the way. *Arteriosclerosis, thrombosis, and vascular biology,* 29**,** 639-649.

DECLERCQ, H. A., DESMET, T., BERNEEL, E. E., DUBRUEL, P. & CORNELISSEN, M. J. 2013. Synergistic effect of surface modification and scaffold design of bioplotted 3-D poly-ε-caprolactone scaffolds in osteogenic tissue engineering. *Acta biomaterialia,* 9**,** 7699-7708.

DI MARTINO, A., SITTINGER, M. & RISBUD, M. V. 2005. Chitosan: a versatile biopolymer for orthopaedic tissue-engineering. *Biomaterials,* 26**,** 5983-5990.

DIMITRIOU, R., JONES, E., MCGONAGLE, D. & GIANNOUDIS, P. V. 2011. Bone regeneration: current concepts and future directions. *BMC medicine,* 9**,** 66.

DOHLE, E., FUCHS, S., KOLBE, M., HOFMANN, A., SCHMIDT, H. & KIRKPATRICK, C. J. 2010. Sonic hedgehog promotes angiogenesis and osteogenesis in a coculture system consisting of primary osteoblasts and outgrowth endothelial cells. *Tissue Engineering Part A,* 16**,** 1235-1237.

DOHLE, E., FUCHS, S., KOLBE, M., HOFMANN, A., SCHMIDT, H. & KIRKPATRICK, C. J. 2011. Comparative study assessing effects of sonic hedgehog and VEGF in a human co-culture model for bone vascularisation strategies. *Eur Cell Mater,* 21**,** e56.

EHRBAR, M., DJONOV, V. G., SCHNELL, C., TSCHANZ, S. A., MARTINY-BARON, G., SCHENK, U., WOOD, J., BURRI, P. H., HUBBELL, J. A. & ZISCH, A. H. 2004. Cell-demanded liberation of VEGF121 from fibrin implants induces local and controlled blood vessel growth. *Circ Res,* 94**,** 1124-1132.

EILKEN, H. M. & ADAMS, R. H. 2010. Dynamics of endothelial cell behavior in sprouting angiogenesis. *Current opinion in cell biology,* 22**,** 617-625.

EKAPUTRA, A. K., PRESTWICH, G. D., COOL, S. M. & HUTMACHER, D. W. 2011. The three-dimensional vascularization of growth factor-releasing hybrid scaffold of poly (ε-caprolactone)/collagen fibers and hyaluronic acid hydrogel. *Biomaterials,* 32**,** 8108-8117.

ELICEIRI, B. P. & CHERESH, D. A. 1999. The role of αv integrins during angiogenesis: insights into potential mechanisms of action and clinical development. *The Journal of clinical investigation,* 103**,** 1227-1230.

ELICEIRI, B. P. & CHERESH, D. A. 2001. Adhesion events in angiogenesis. *Current opinion in cell biology,* 13**,** 563-568.

ELLIS-BEHNKE, R. G., LIANG, Y.-X., TAY, D. K., KAU, P. W., SCHNEIDER, G. E., ZHANG, S., WU, W. & SO, K.-F. 2006. Nano hemostat solution: immediate hemostasis at the nanoscale. *Nanomedicine: Nanotechnology, Biology and Medicine,* 2**,** 207-215.

FANTIN, A., VIEIRA, J. M., GESTRI, G., DENTI, L., SCHWARZ, Q., PRYKHOZHIJ, S., PERI, F., WILSON, S. W. & RUHRBERG, C. 2010. Tissue macrophages act as cellular chaperones for vascular anastomosis downstream of VEGF-mediated endothelial tip cell induction. *Blood,* 116**,** 829-840.

FARRELL, E., O'BRIEN, F. J., DOYLE, P., FISCHER, J., YANNAS, I., HARLEY, B. A., O'CONNELL, B., PRENDERGAST, P. J. & CAMPBELL, V. A. 2006. A collagen-glycosaminoglycan scaffold supports adult rat mesenchymal stem cell differentiation along osteogenic and chondrogenic routes. *Tissue Eng,* 12**,** 459-468.

FELLAH, B. H., GAUTHIER, O., WEISS, P., CHAPPARD, D. & LAYROLLE, P. 2008. Osteogenicity of biphasic calcium phosphate ceramics and bone autograft in a goat model. *Biomaterials,* 29**,** 1177-1188.

FERRARA, N., GERBER, H.-P. & LECOUTER, J. 2003. The biology of VEGF and its receptors. *Nat Med,* 9**,** 669-676.

FIELDING, G. A., BANDYOPADHYAY, A. & BOSE, S. 2012. Effects of silica and zinc oxide doping on mechanical and biological properties of 3D printed tricalcium phosphate tissue engineering scaffolds. *Dental Materials,* 28**,** 113-122.

FINKEMEIER, C. G. 2002. Bone-grafting and bone-graft substitutes. *J Bone Joint Surg Am,* 84-A**,** 454-64.

FIRTH, A., AGGELI, A., BURKE, J. L., YANG, X. & KIRKHAM, J. 2006. Biomimetic self-assembling peptides as injectable scaffolds for hard tissue engineering.

FLORENCIO-SILVA, R., SASSO, G. R. D. S., SASSO-CERRI, E., SIMÕES, M. J. & CERRI, P. S. 2015. Biology of Bone Tissue: Structure, Function, and Factors That Influence Bone Cells. *BioMed Research International,* 2015.

FRANZ, S., RAMMELT, S., SCHARNWEBER, D. & SIMON, J. C. 2011. Immune responses to implants–a review of the implications for the design of immunomodulatory biomaterials. *Biomaterials,* 32**,** 6692-6709.

FREEMAN, I. & COHEN, S. 2009. The influence of the sequential delivery of angiogenic factors from affinity-binding alginate scaffolds on vascularization. *Biomaterials,* 30**,** 2122-2131.

FU, W.-L., XIANG, Z., HUANG, F.-G., GU, Z.-P., YU, X.-X., CEN, S.-Q., ZHONG, G., DUAN, X. & LIU, M. 2014. Coculture of peripheral blood-derived mesenchymal stem cells and endothelial progenitor cells on strontium-doped calcium polyphosphate scaffolds to generate vascularized engineered bone. *Tissue Engineering Part A,* 21**,** 948-959.

FUCHS, S., DOHLE, E., KOLBE, M. & KIRKPATRICK, C. J. 2010a. Outgrowth endothelial cells: sources, characteristics and potential applications in tissue engineering and regenerative medicine. *Bioreactor Systems for Tissue Engineering II.* Springer.

FUCHS, S., GHANAATI, S., ORTH, C., BARBECK, M., KOLBE, M., HOFMANN, A., EBLENKAMP, M., GOMES, M., REIS, R. L. & KIRKPATRICK, C. J. 2009. Contribution of outgrowth endothelial cells from human peripheral blood on in vivo vascularization of bone tissue engineered constructs based on starch polycaprolactone scaffolds. *Biomaterials,* 30**,** 526-34.

FUCHS, S., HOFMANN, A. & KIRKPATRICK, C. 2007. Microvessel-like structures from outgrowth endothelial cells from human peripheral blood in 2-dimensional and 3-dimensional co-cultures with osteoblastic lineage cells. *Tissue Eng,* 13**,** 2577-88.

FUCHS, S., JIANG, X., GOTMAN, I., MAKAROV, C., SCHMIDT, H., GUTMANAS, E. & KIRKPATRICK, C. 2010b. Influence of polymer content in Ca-deficient hydroxyapatite–polycaprolactone nanocomposites on the formation of microvessel-like structures. *Acta biomaterialia,* 6**,** 3169-3177.

GAMSJÄGER, E., BIDAN, C., FISCHER, F., FRATZL, P. & DUNLOP, J. 2013. Modelling the role of surface stress on the kinetics of tissue growth in confined geometries. *Acta biomaterialia,* 9**,** 5531-5543.

GAO, C., DENG, Y., FENG, P., MAO, Z., LI, P., YANG, B., DENG, J., CAO, Y., SHUAI, C. & PENG, S. 2014. Current progress in bioactive ceramic scaffolds for bone repair and regeneration. *International journal of molecular sciences,* 15**,** 4714-4732.

GASTON, M. S. & SIMPSON, A. H. 2007. Inhibition of fracture healing. *J Bone Joint Surg Br,* 89**,** 1553-60.

GELAIN, F., BOTTAI, D., VESCOVI, A. & ZHANG, S. 2006. Designer self-assembling peptide nanofiber scaffolds for adult mouse neural stem cell 3-dimensional cultures. *PLoS One,* 1**,** e119.

GELAIN, F., HORII, A. & ZHANG, S. 2007. Designer Self‐Assembling Peptide Scaffolds for 3‐D Tissue Cell Cultures and Regenerative Medicine. *Macromolecular bioscience,* 7**,** 544-551.

GELAIN, F., UNSWORTH, L. D. & ZHANG, S. 2010. Slow and sustained release of active cytokines from self-assembling peptide scaffolds. *J Control Release,* 145**,** 231-9.

GENOVÉ, E., SHEN, C., ZHANG, S. & SEMINO, C. E. 2005. The effect of functionalized self-assembling peptide scaffolds on human aortic endothelial cell function. *Biomaterials,* 26**,** 3341-3351.

GERBER, H.-P. & FERRARA, N. 2000. Angiogenesis and bone growth. *Trends Cardiovasc Med,* 10**,** 223-228.

GERBER, H.-P., VU, T. H., RYAN, A. M., KOWALSKI, J., WERB, Z. & FERRARA, N. 1999. VEGF couples hypertrophic cartilage remodeling, ossification and angiogenesis during endochondral bone formation. *Nat Med,* 5**,** 623-628.

GHANAATI, S., FUCHS, S., WEBBER, M. J., ORTH, C., BARBECK, M., GOMES, M. E., REIS, R. L. & JAMES KIRKPATRICK, C. 2011. Rapid vascularization of starch–poly (caprolactone) in vivo by outgrowth endothelial cells in co‐culture with primary osteoblasts. *J Tissue Eng Regen Med,* 5**,** e136-e143.

GLIMCHER, M. 1998. The nature of the mineral phase in bone: biological and clinical implications. *Metabolic bone disease and clinically related disorders,* 2**,** 23-50.

GLOWACKI, J. & MIZUNO, S. 2008. Collagen scaffolds for tissue engineering. *Biopolymers,* 89**,** 338-344.

GOLDSTEIN, S. A. 2002. Tissue Engineering. *Annals of the New York Academy of Sciences,* 961**,** 183-192.

GREENWALD, A. S., BODEN, S. D., GOLDBERG, V. M., KHAN, Y., LAURENCIN, C. T. & ROSIER, R. N. 2001. Bone-graft substitutes: facts, fictions, and applications. *The Journal of Bone & Joint Surgery,* 83**,** S98-103.

GRELLIER, M., FERREIRA‐TOJAIS, N., BOURGET, C., BAREILLE, R., GUILLEMOT, F. & AMÉDÉE, J. 2009. Role of vascular endothelial growth factor in the communication between human osteoprogenitors and endothelial cells. *Journal of cellular biochemistry,* 106**,** 390-398.

GUILLOTIN, B., BAREILLE, R., BOURGET, C., BORDENAVE, L. & AMEDEE, J. 2008. Interaction between human umbilical vein endothelial cells and human osteoprogenitors triggers pleiotropic effect that may support osteoblastic function. *Bone,* 42**,** 1080-1091.

HARLEY, B. A. & GIBSON, L. J. 2008. In vivo and in vitro applications of collagen-GAG scaffolds. *Chemical Engineering Journal,* 137**,** 102-121.

HARTGERINK, J. D., BENIASH, E. & STUPP, S. I. 2001. Self-assembly and mineralization of peptide-amphiphile nanofibers. *Science,* 294**,** 1684-1688.

HASEGAWA, K., TURNER, C. & BURR, D. 1994. Contribution of collagen and mineral to the elastic anisotropy of bone. *Calcified Tissue International,* 55**,** 381-386.

HAUGH, M. G., JAASMA, M. J. & O'BRIEN, F. J. 2009. The effect of dehydrothermal treatment on the mechanical and structural properties of collagen‐GAG scaffolds. *Journal of biomedical materials research Part A,* 89**,** 363-369.

HAUGH, M. G., MURPHY, C. M., MCKIERNAN, R. C., ALTENBUCHNER, C. & O'BRIEN, F. J. 2011. Crosslinking and mechanical properties significantly influence cell attachment, proliferation, and migration within collagen glycosaminoglycan scaffolds. *Tissue Engineering Part A,* 17**,** 1201-1208.

HAUSER, C. A. & ZHANG, S. 2010. Designer self-assembling peptide nanofiber biological materials. *Chemical Society Reviews,* 39**,** 2780-2790.

HAYFLICK, L. & MOORHEAD, P. S. 1961. The serial cultivation of human diploid cell strains. *Experimental cell research,* 25**,** 585-621.

HAYNESWORTH, S. E., GOSHIMA, J., GOLDBERG, V. M. & CAPLAN, A. I. 1992. Characterization of cells with osteogenic potential from human marrow. *Bone,* 13**,** 81-88.

HE, X., DZIAK, R., MAO, K., GENCO, R., SWIHART, M., LI, C. & YANG, S. 2012. Integration of a novel injectable nano calcium sulfate/alginate scaffold and BMP2 gene-modified mesenchymal stem cells for bone regeneration. *Tissue Engineering Part A,* 19**,** 508-518.

HENCH, L. L. & POLAK, J. M. 2002. Third-generation biomedical materials. *Science,* 295**,** 1014-1017.

HERZOG, D. P. E., DOHLE, E., BISCHOFF, I. & KIRKPATRICK, C. J. 2014. Cell communication in a coculture system consisting of outgrowth endothelial cells and primary osteoblasts. *BioMed Research International,* 2014.

HIRANO, S., SHOJI, K., KOJIMA, H. & OMORI, K. 1997. Use of hydroxyapatite for reconstruction after surgical removal of intraosseous hemangioma in the zygomatic bone. *Plastic and reconstructive surgery,* 100**,** 86-90.

HOLLISTER, S. J. 2005. Porous scaffold design for tissue engineering. *Nature materials,* 4**,** 518-524.

HOLMES, K., ROBERTS, O. L., THOMAS, A. M. & CROSS, M. J. 2007. Vascular endothelial growth factor receptor-2: structure, function, intracellular signalling and therapeutic inhibition. *Cellular signalling,* 19**,** 2003-2012.

HOLMES, T. C., DE LACALLE, S., SU, X., LIU, G., RICH, A. & ZHANG, S. 2000. Extensive neurite outgrowth and active synapse formation on self-assembling peptide scaffolds. *Proceedings of the National Academy of Sciences,* 97**,** 6728-6733.

HONDA, Y., ANADA, T., KAMAKURA, S., NAKAMURA, M., SUGAWARA, S. & SUZUKI, O. 2006. Elevated extracellular calcium stimulates secretion of bone morphogenetic protein 2 by a macrophage cell line. *Biochem Biophys Res Commun,* 345**,** 1155-1160.

HORII, A., WANG, X., GELAIN, F. & ZHANG, S. 2007. Biological designer self-assembling peptide nanofiber scaffolds significantly enhance osteoblast proliferation, differentiation and 3-D migration. *PloS one,* 2**,** e190.

HULBERT, S., YOUNG, F., MATHEWS, R., KLAWITTER, J., TALBERT, C. & STELLING, F. 1970. Potential of ceramic materials as permanently implantable skeletal prostheses. *Journal of biomedical materials research,* 4**,** 433-456.

HUTTON, D. L. & GRAYSON, W. L. 2014. Stem cell-based approaches to engineering vascularized bone. *Current Opinion in Chemical Engineering,* 3**,** 75-82.

ISERN, J., MARTÍN-ANTONIO, B., GHAZANFARI, R., MARTÍN, A. M., LÓPEZ, J. A., DEL TORO, R., SÁNCHEZ-AGUILERA, A., ARRANZ, L., MARTÍN-PÉREZ, D. & SUÁREZ-LLEDÓ, M. 2013. Self-renewing human bone marrow mesenspheres promote hematopoietic stem cell expansion. *Cell reports,* 3**,** 1714-1724.

ITÄLÄ, A. I., YLÄNEN, H. O., EKHOLM, C., KARLSSON, K. H. & ARO, H. T. 2001. Pore diameter of more than 100 μm is not requisite for bone ingrowth in rabbits. *Journal of biomedical materials research,* 58**,** 679-683.

IVANKOVIC, H., TKALCEC, E., ORLIC, S., FERRER, G. G. & SCHAUPERL, Z. 2010. Hydroxyapatite formation from cuttlefish bones: kinetics. *Journal of Materials Science: Materials in Medicine,* 21**,** 2711-2722.

IVKOVIC, S., YOON, B. S., POPOFF, S. N., SAFADI, F. F., LIBUDA, D. E., STEPHENSON, R. C., DALUISKI, A. & LYONS, K. M. 2003. Connective tissue growth factor coordinates chondrogenesis and angiogenesis during skeletal development. *Development,* 130**,** 2779-2791.

JACOBS, T., DECLERCQ, H., DE GEYTER, N., CORNELISSEN, R., DUBRUEL, P., LEYS, C. & MORENT, R. 2013. Improved cell adhesion to flat and porous plasma-treated poly-ε-caprolactone samples. *Surface and Coatings Technology,* 232**,** 447-455.

JAFFE, E. A., NACHMAN, R. L., BECKER, C. G. & MINICK, C. R. 1973. Culture of human endothelial cells derived from umbilical veins. Identification by morphologic and immunologic criteria. *Journal of Clinical Investigation,* 52**,** 2745.

JAIN, R. K. 2003. Molecular regulation of vessel maturation. *Nat Med,* 9**,** 685-693.

JAIN, R. K. 2005. Normalization of tumor vasculature: an emerging concept in antiangiogenic therapy. *Science,* 307**,** 58-62.

JELL, G. & STEVENS, M. M. 2006. Gene activation by bioactive glasses. *Journal of Materials Science: Materials in Medicine,* 17**,** 997-1002.

JEPSEN, K. J. 2009. Systems analysis of bone. *Wiley Interdisciplinary Reviews: Systems Biology and Medicine,* 1**,** 73-88.

JIN, G.-Z., HAN, C.-M. & KIM, H.-W. 2015. In vitro co-culture strategies to prevascularization for bone regeneration: A brief update. *Tissue Engineering and Regenerative Medicine,* 12**,** 69-79.

JONES, G. & CARTMELL, S. 2005. Optimization of cell seeding efficiencies on a three-dimensional gelatin scaffold for bone tissue engineering. *Journal of applied biomaterials & biomechanics: JABB,* 4**,** 172-180.

JONES, J. R. & HENCH, L. L. 2004. Factors affecting the structure and properties of bioactive foam scaffolds for tissue engineering. *Journal of Biomedical Materials Research Part B: Applied Biomaterials,* 68**,** 36-44.

JUNG, G.-Y., PARK, Y.-J. & HAN, J.-S. 2010. Effects of HA released calcium ion on osteoblast differentiation. *Journal of Materials Science: Materials in Medicine,* 21**,** 1649-1654.

KAIGLER, D., KREBSBACH, P. H., POLVERINI, P. J. & MOONEY, D. J. 2003. Role of vascular endothelial growth factor in bone marrow stromal cell modulation of endothelial cells. *Tissue Eng,* 9**,** 95-103.

KANCZLER, J. & OREFFO, R. 2008. Osteogenesis and angiogenesis: the potential for engineering bone. *Eur Cell Mater,* 15**,** 100-114.

KANG, Y., KIM, S., FAHRENHOLTZ, M., KHADEMHOSSEINI, A. & YANG, Y. 2013. Osteogenic and angiogenic potentials of monocultured and co-cultured human-bone-marrow-derived mesenchymal stem cells and human-umbilical-vein endothelial cells on three-dimensional porous beta-tricalcium phosphate scaffold. *Acta biomaterialia,* 9**,** 4906-4915.

KANG, Y., REN, L. & YANG, Y. 2014. Engineering vascularized bone grafts by integrating a biomimetic periosteum and β-TCP scaffold. *ACS applied materials & interfaces,* 6**,** 9622-9633.

KARSENTY, G. & WAGNER, E. F. 2002. Reaching a genetic and molecular understanding of skeletal development. *Developmental cell,* 2**,** 389-406.

KASSEM, M., ANKERSEN, L., ERIKSEN, E. F., CLARK, B. F. & RATTAN, S. I. 1997. Demonstration of cellular aging and senescence in serially passaged long-term cultures of human trabecular osteoblasts. *Osteoporosis International,* 7**,** 514-524.

KASTEN, P., BEYEN, I., NIEMEYER, P., LUGINBÜHL, R., BOHNER, M. & RICHTER, W. 2008. Porosity and pore size of β-tricalcium phosphate scaffold can influence protein production and osteogenic differentiation of human mesenchymal stem cells: an in vitro and in vivo study. *Acta biomaterialia,* 4**,** 1904-1915.

KEENEY, M., VAN DEN BEUCKEN, J. J., VAN DER KRAAN, P. M., JANSEN, J. A. & PANDIT, A. 2010. The ability of a collagen/calcium phosphate scaffold to act as its own vector for gene delivery and to promote bone formation via transfection with VEGF 165. *Biomaterials,* 31**,** 2893-2902.

KEMPEN, D. H., LU, L., HEIJINK, A., HEFFERAN, T. E., CREEMERS, L. B., MARAN, A., YASZEMSKI, M. J. & DHERT, W. J. 2009. Effect of local sequential VEGF and BMP-2 delivery on ectopic and orthotopic bone regeneration. *Biomaterials,* 30**,** 2816-2825.

KEOGH, M. B., O'BRIEN, F. J. & DALY, J. S. 2010. A novel collagen scaffold supports human osteogenesis—applications for bone tissue engineering. *Cell and tissue research,* 340**,** 169-177.

KHOSHNIAT, S., BOURGINE, A., JULIEN, M., PETIT, M., PILET, P., ROUILLON, T., MASSON, M., GATIUS, M., WEISS, P. & GUICHEUX, J. 2011. Phosphate-dependent stimulation of MGP and OPN expression in osteoblasts via the ERK1/2 pathway is modulated by calcium. *Bone,* 48**,** 894-902.

KHOSLA, S. 2001. Minireview: The opg/rankl/rank system. *Endocrinology,* 142**,** 5050-5055.

KIM, B.-S., KANG, H. J., YANG, S.-S. & LEE, J. 2014a. Comparison of in vitro and in vivo bioactivity: cuttlefish-bone-derived hydroxyapatite and synthetic hydroxyapatite granules as a bone graft substitute. *Biomedical Materials,* 9**,** 025004.

KIM, K.-I., PARK, S. & IM, G.-I. 2014b. Osteogenic differentiation and angiogenesis with cocultured adipose-derived stromal cells and bone marrow stromal cells. *Biomaterials,* 35**,** 4792-4804.

KIM, K., YEATTS, A., DEAN, D. & FISHER, J. P. 2010. Stereolithographic bone scaffold design parameters: osteogenic differentiation and signal expression. *Tissue Engineering Part B: Reviews,* 16**,** 523-539.

KIMELMAN-BLEICH, N., PELLED, G., ZILBERMAN, Y., KALLAI, I., MIZRAHI, O., TAWACKOLI, W., GAZIT, Z. & GAZIT, D. 2011. Targeted gene-and-host progenitor cell therapy for nonunion bone fracture repair. *Molecular Therapy,* 19**,** 53-59.

KIRKHAM, J., FIRTH, A., VERNALS, D., BODEN, N., ROBINSON, C., SHORE, R., BROOKES, S. & AGGELI, A. 2007. Self-assembling peptide scaffolds promote enamel remineralization. *Journal of dental research,* 86**,** 426-430.

KNESER, U., POLYKANDRIOTIS, E., OHNOLZ, J., HEIDNER, K., GRABINGER, L., EULER, S., AMANN, K. U., HESS, A., BRUNE, K., GREIL, P., STURZL, M. & HORCH, R. E. 2006. Engineering of vascularized transplantable bone tissues: induction of axial vascularization in an osteoconductive matrix using an arteriovenous loop. *Tissue Eng,* 12**,** 1721-31.

KOLBE, M., XIANG, Z., DOHLE, E., TONAK, M., KIRKPATRICK, C. J. & FUCHS, S. 2011. Paracrine effects influenced by cell culture medium and consequences on microvessel-like structures in cocultures of mesenchymal stem cells and outgrowth endothelial cells. *Tissue Engineering Part A,* 17**,** 2199-2212.

KOUTSOPOULOS, S., UNSWORTH, L. D., NAGAI, Y. & ZHANG, S. 2009. Controlled release of functional proteins through designer self-assembling peptide nanofiber hydrogel scaffold. *Proceedings of the National Academy of Sciences,* 106**,** 4623-4628.

KREBSBACH, P. H., GU, K., FRANCESCHI, R. T. & RUTHERFORD, R. B. 2000. Gene therapy-directed osteogenesis: BMP-7-transduced human fibroblasts form bone in vivo. *Human gene therapy,* 11**,** 1201-1210.

KREČIČ STRES, H., KRKOVIČ, M., KODER, J., MALIČEV, E., MAROLT, D., DROBNIC, M. & KREGAR-VELIKONJA, N. Mesenchymal Stem Cells: a Modern Approach to Treat Long Bones Defects. 11th Mediterranean Conference on Medical and Biomedical Engineering and Computing 2007, 2007. Springer, 253-256.

KRONENBERG, H. M. 2003. Developmental regulation of the growth plate. *Nature,* 423**,** 332-336.

KRUYT, M., DE BRUIJN, J., WILSON, C., ONER, F., VAN BLITTERSWIJK, C., VERBOUT, A. & DHERT, W. 2003. Viable osteogenic cells are obligatory for tissue-engineered ectopic bone formation in goats. *Tissue Eng,* 9**,** 327-336.

KUBOKI, Y., JIN, Q. & TAKITA, H. 2001. Geometry of carriers controlling phenotypic expression in BMP-induced osteogenesis and chondrogenesis. *J Bone Joint Surg Am,* 83**,** S105-S115.

KUBOKI, Y., TAKITA, H., KOBAYASHI, D., TSURUGA, E., INOUE, M., MURATA, M., NAGAI, N., DOHI, Y. & OHGUSHI, H. 1998. BMP‐induced osteogenesis

on the surface of hydroxyapatite with geometrically feasible and nonfeasible structures: topology of osteogenesis. *Journal of biomedical materials research,* 39**,** 190-199.
KUMADA, Y., HAMMOND, N. A. & ZHANG, S. 2010. Functionalized scaffolds of shorter self-assembling peptides containing MMP-2 cleavable motif promote fibroblast proliferation and significantly accelerate 3-D cell migration independent of scaffold stiffness. *Soft Matter,* 6**,** 5073-5079.
KUMADA, Y. & ZHANG, S. 2010. Significant type I and type III collagen production from human periodontal ligament fibroblasts in 3D peptide scaffolds without extra growth factors. *PLoS One,* 5**,** e10305.
KURODA, R., MATSUMOTO, T., KAWAKAMI, Y., FUKUI, T., MIFUNE, Y. & KUROSAKA, M. 2014. Clinical impact of circulating CD34-positive cells on bone regeneration and healing. *Tissue Engineering Part B: Reviews,* 20**,** 190-199.
KUSUMBE, A. P., RAMASAMY, S. K. & ADAMS, R. H. 2014. Coupling of angiogenesis and osteogenesis by a specific vessel subtype in bone. *Nature,* 507**,** 323-328.
KYRIAKIDOU, K., LUCARINI, G., ZIZZI, A., SALVOLINI, E., BELMONTE, M. M., MOLLICA, F., GLORIA, A. & AMBROSIO, L. 2008. Dynamic co-seeding of osteoblast and endothelial cells on 3D polycaprolactone scaffolds for enhanced bone tissue engineering. *Journal of bioactive and compatible polymers,* 23**,** 227-243.
LAFAGE-PROUST, M.-H., ROCHE, B., LANGER, M., CLERET, D., BOSSCHE, A. V., OLIVIER, T. & VICO, L. 2015. Assessment of bone vascularization and its role in bone remodeling. *BoneKEy reports,* 4.
LEBRIN, F., DECKERS, M., BERTOLINO, P. & TEN DIJKE, P. 2005. TGF-β receptor function in the endothelium. *Cardiovascular research,* 65**,** 599-608.
LEE, J. W., AHN, G., KIM, J. Y. & CHO, D.-W. 2010. Evaluating cell proliferation based on internal pore size and 3D scaffold architecture fabricated using solid freeform fabrication technology. *Journal of Materials Science: Materials in Medicine,* 21**,** 3195-3205.
LEE, K., SILVA, E. A. & MOONEY, D. J. 2011. Growth factor delivery-based tissue engineering: general approaches and a review of recent developments. *Journal of The Royal Society Interface,* 8**,** 153-170.
LEGEROS, R. Z. 2002. Properties of osteoconductive biomaterials: calcium phosphates. *Clin Orthop Relat Res,* 395**,** 81-98.
LEGEROS, R. Z. 2008. Calcium phosphate-based osteoinductive materials. *Chemical reviews,* 108**,** 4742-4753.
LENG, H., REYES, M. J., DONG, X. N. & WANG, X. 2013. Effect of age on mechanical properties of the collagen phase in different orientations of human cortical bone. *Bone,* 55**,** 288-291.
LEVENBERG, S., ROUWKEMA, J., MACDONALD, M., GARFEIN, E. S., KOHANE, D. S., DARLAND, D. C., MARINI, R., VAN BLITTERSWIJK, C. A., MULLIGAN, R. C. & D'AMORE, P. A. 2005. Engineering vascularized skeletal muscle tissue. *Nature biotechnology,* 23**,** 879-884.
LEWIS, J. A., SMAY, J. E., STUECKER, J. & CESARANO, J. 2006. Direct ink writing of three‐dimensional ceramic structures. *Journal of the American Ceramic Society,* 89**,** 3599-3609.
LI, D. Y., SORENSEN, L. K., BROOKE, B. S., URNESS, L. D., DAVIS, E. C., TAYLOR, D. G., BOAK, B. B. & WENDEL, D. P. 1999. Defective angiogenesis in mice lacking endoglin. *Science,* 284**,** 1534-1537.
LI, H., DACULSI, R., BAREILLE, R., BOURGET, C. & AMEDEE, J. 2013a. uPA and MMP‐2 were involved in self‐assembled network formation in a two

dimensional co‐culture model of bone marrow stromal cells and endothelial cells. *Journal of cellular biochemistry,* 114, 650-657.
LI, H., DACULSI, R., GRELLIER, M., BAREILLE, R., BOURGET, C., REMY, M. & AMEDEE, J. 2011. The role of vascular actors in two dimensional dialogue of human bone marrow stromal cell and endothelial cell for inducing self-assembled network. *PLoS One,* 6, e16767.
LI, H., GHAZANFARI, R., ZACHARAKI, D., DITZEL, N., ISERN, J., EKBLOM, M., MÉNDEZ-FERRER, S., KASSEM, M. & SCHEDING, S. 2014. Low/negative expression of PDGFR-α identifies the candidate primary mesenchymal stromal cells in adult human bone marrow. *Stem Cell Reports,* 3, 965-974.
LI, M., FUCHS, S., BÖSE, T., SCHMIDT, H., HOFMANN, A., TONAK, M., UNGER, R. & KIRKPATRICK, C. J. 2013b. Mild heat stress enhances angiogenesis in a co-culture system consisting of primary human osteoblasts and outgrowth endothelial cells. *Tissue Engineering Part C: Methods,* 20, 328-339.
LI, Y., CHEN, S.-K., LI, L., QIN, L., WANG, X.-L. & LAI, Y.-X. 2015. Bone defect animal models for testing efficacy of bone substitute biomaterials. *Journal of Orthopaedic Translation,* 3, 95-104.
LI, Y., TORALDO, G., LI, A., YANG, X., ZHANG, H., QIAN, W.-P. & WEITZMANN, M. N. 2007. B cells and T cells are critical for the preservation of bone homeostasis and attainment of peak bone mass in vivo. *Blood,* 109, 3839-3848.
LI, Z., RAMAY, H. R., HAUCH, K. D., XIAO, D. & ZHANG, M. 2005. Chitosan–alginate hybrid scaffolds for bone tissue engineering. *Biomaterials,* 26, 3919-3928.
LIU, Y., TEOH, S. H., CHONG, M. S., LEE, E. S., MATTAR, C. N., RANDHAWA, N. S. K., ZHANG, Z. Y., MEDINA, R. J., KAMM, R. D. & FISK, N. M. 2012. Vasculogenic and Osteogenesis‐Enhancing Potential of Human Umbilical Cord Blood Endothelial Colony‐Forming Cells. *Stem cells,* 30, 1911-1924.
LOKMIC, Z. & MITCHELL, G. M. 2008. Engineering the microcirculation. *Tissue Engineering Part B: Reviews,* 14, 87-103.
LOO, Y., ZHANG, S. & HAUSER, C. A. 2012. From short peptides to nanofibers to macromolecular assemblies in biomedicine. *Biotechnology advances,* 30, 593-603.
LU, J., DESCAMPS, M., DEJOU, J., KOUBI, G., HARDOUIN, P., LEMAITRE, J. & PROUST, J. P. 2002. The biodegradation mechanism of calcium phosphate biomaterials in bone. *Journal of biomedical materials research,* 63, 408-412.
LU, Q. 2008. Transforming growth factor-β1 protects against pulmonary artery endothelial cell apoptosis via ALK5. *American Journal of Physiology-Lung Cellular and Molecular Physiology,* 295, L123-L133.
LUCITTI, J. L., MACKEY, J. K., MORRISON, J. C., HAIGH, J. J., ADAMS, R. H. & FABER, J. E. 2012. Formation of the collateral circulation is regulated by vascular endothelial growth factor-A and a disintegrin and metalloprotease family members 10 and 17. *Circ Res,* 111, 1539-1550.
LUCKE, S. & LEVKAU, B. 2010. Endothelial functions of sphingosine-1-phosphate. *Cellular Physiology and Biochemistry,* 26, 87-96.
LUO, Z., WANG, S. & ZHANG, S. 2011. Fabrication of self-assembling D-form peptide nanofiber scaffold d-EAK16 for rapid hemostasis. *Biomaterials,* 32, 2013-2020.
LUTTY, G. A., MERGES, C., THRELKELD, A. B., CRONE, S. & MCLEOD, D. S. 1993. Heterogeneity in localization of isoforms of TGF-beta in human retina, vitreous, and choroid. *Investigative ophthalmology & visual science,* 34, 477-487.
MA, J., YANG, F., BOTH, S. K., PRINS, H.-J., HELDER, M. N., PAN, J., CUI, F.-Z., JANSEN, J. A. & VAN DEN BEUCKEN, J. J. 2014. In vitro and in vivo

angiogenic capacity of BM-MSCs/HUVECs and AT-MSCs/HUVECs cocultures. *Biofabrication,* 6**,** 015005.

MAES, C., CARMELIET, P., MOERMANS, K., STOCKMANS, I., SMETS, N., COLLEN, D., BOUILLON, R. & CARMELIET, G. 2002. Impaired angiogenesis and endochondral bone formation in mice lacking the vascular endothelial growth factor isoforms VEGF 164 and VEGF 188. *Mech Dev,* 111**,** 61-73.

MAES, C., GOOSSENS, S., BARTUNKOVA, S., DROGAT, B., COENEGRACHTS, L., STOCKMANS, I., MOERMANS, K., NYABI, O., HAIGH, K. & NAESSENS, M. 2010. Increased skeletal VEGF enhances β‐catenin activity and results in excessively ossified bones. *The EMBO journal,* 29**,** 424-441.

MANJUBALA, I., WOESZ, A., PILZ, C., RUMPLER, M., FRATZL-ZELMAN, N., ROSCHGER, P., STAMPFL, J. & FRATZL, P. 2005. Biomimetic mineral-organic composite scaffolds with controlled internal architecture. *Journal of Materials Science: Materials in Medicine,* 16**,** 1111-1119.

MANKANI, M. H., KUZNETSOV, S. A., SHANNON, B., NALLA, R. K., RITCHIE, R. O., QIN, Y. & ROBEY, P. G. 2006a. Canine cranial reconstruction using autologous bone marrow stromal cells. *The American journal of pathology,* 168**,** 542-550.

MANKANI, M. H., KUZNETSOV, S. A., WOLFE, R. M., MARSHALL, G. W. & ROBEY, P. G. 2006b. In vivo bone formation by human bone marrow stromal cells: reconstruction of the mouse calvarium and mandible. *Stem cells,* 24**,** 2140-2149.

MANNSFELD, S. C., TEE, B. C., STOLTENBERG, R. M., CHEN, C. V. H., BARMAN, S., MUIR, B. V., SOKOLOV, A. N., REESE, C. & BAO, Z. 2010. Highly sensitive flexible pressure sensors with microstructured rubber dielectric layers. *Nature materials,* 9**,** 859-864.

MARIE, P. J. 2008. Transcription factors controlling osteoblastogenesis. *Archives of biochemistry and biophysics,* 473**,** 98-105.

MARUYAMA, T., JEONG, J., SHEU, T.-J. & HSU, W. 2016. Stem cells of the suture mesenchyme in craniofacial bone development, repair and regeneration. *Nature communications,* 7.

MCFADDEN, T., DUFFY, G., ALLEN, A., STEVENS, H., SCHWARZMAIER, S., PLESNILA, N., MURPHY, J., BARRY, F., GULDBERG, R. & O'BRIEN, F. 2013. The delayed addition of human mesenchymal stem cells to pre-formed endothelial cell networks results in functional vascularization of a collagen–glycosaminoglycan scaffold in vivo. *Acta biomaterialia,* 9**,** 9303-9316.

MELLON, S. & TANNER, K. 2012. Bone and its adaptation to mechanical loading: a review. *International Materials Reviews,* 57**,** 235-255.

MÉNDEZ‐FERRER, S., SCADDEN, D. T. & SÁNCHEZ‐AGUILERA, A. 2015. Bone marrow stem cells: current and emerging concepts. *Annals of the New York Academy of Sciences,* 1335**,** 32-44.

MERCIER, P., BELLAVANCE, F., CHOLEWA, J. & DJOKOVIC, S. 1996. Long-term stability of atrophic ridges reconstructed with hydroxylapatite: a prospective study. *Journal of oral and maxillofacial surgery,* 54**,** 960-968.

MESIMÄKI, K., LINDROOS, B., TÖRNWALL, J., MAUNO, J., LINDQVIST, C., KONTIO, R., MIETTINEN, S. & SUURONEN, R. 2009. Novel maxillary reconstruction with ectopic bone formation by GMP adipose stem cells. *International journal of oral and maxillofacial surgery,* 38**,** 201-209.

MICHNA, S., WU, W. & LEWIS, J. A. 2005. Concentrated hydroxyapatite inks for direct-write assembly of 3-D periodic scaffolds. *Biomaterials,* 26**,** 5632-5639.

MIKOS, A. G., SARAKINOS, G., LYMAN, M. D., INGBER, D. E., VACANTI, J. P. & LANGER, R. 1993. Prevascularization of porous biodegradable polymers. *Biotechnology and Bioengineering,* 42**,** 716-723.

MILLER, R. E., GRODZINSKY, A. J., VANDERPLOEG, E. J., LEE, C., FERRIS, D. J., BARRETT, M. F., KISIDAY, J. D. & FRISBIE, D. D. 2010. Effect of self-assembling peptide, chondrogenic factors, and bone marrow-derived stromal cells on osteochondral repair. *Osteoarthritis Cartilage,* 18**,** 1608-19.

MINUTH, W. W., DENK, L. & GLASHAUSER, A. 2010. A modular culture system for the generation of multiple specialized tissues. *Biomaterials,* 31**,** 2945-2954.

MIRANDA, P., SAIZ, E., GRYN, K. & TOMSIA, A. P. 2006. Sintering and robocasting of β-tricalcium phosphate scaffolds for orthopaedic applications. *Acta biomaterialia,* 2**,** 457-466.

MISAWA, H., KOBAYASHI, N., SOTO-GUTIERREZ, A., CHEN, Y., YOSHIDA, A., RIVAS-CARRILLO, J. D., NAVARRO-ALVAREZ, N., TANAKA, K., MIKI, A., TAKEI, J., UEDA, T., TANAKA, M., ENDO, H., TANAKA, N. & OZAKI, T. 2006. PuraMatrix facilitates bone regeneration in bone defects of calvaria in mice. *Cell Transplant,* 15**,** 903-10.

MITSAK, A. G., KEMPPAINEN, J. M., HARRIS, M. T. & HOLLISTER, S. J. 2011. Effect of polycaprolactone scaffold permeability on bone regeneration in vivo. *Tissue Engineering Part A,* 17**,** 1831-1839.

MOUNTZIARIS, P. M., SPICER, P. P., KASPER, F. K. & MIKOS, A. G. 2011. Harnessing and modulating inflammation in strategies for bone regeneration. *Tissue Engineering Part B: Reviews,* 17**,** 393-402.

MULLEN, C., HAUGH, M., SCHAFFLER, M., MAJESKA, R. & MCNAMARA, L. 2013. Osteocyte differentiation is regulated by extracellular matrix stiffness and intercellular separation. *Journal of the mechanical behavior of biomedical materials,* 28**,** 183-194.

NAKASHIMA, K., ZHOU, X., KUNKEL, G., ZHANG, Z., DENG, J. M., BEHRINGER, R. R. & DE CROMBRUGGHE, B. 2002. The novel zinc finger-containing transcription factor osterix is required for osteoblast differentiation and bone formation. *Cell,* 108**,** 17-29.

NARMONEVA, D. A., ONI, O., SIEMINSKI, A. L., ZHANG, S., GERTLER, J. P., KAMM, R. D. & LEE, R. T. 2005. Self-assembling short oligopeptides and the promotion of angiogenesis. *Biomaterials,* 26**,** 4837-4846.

NARMONEVA, D. A., VUKMIROVIC, R., DAVIS, M. E., KAMM, R. D. & LEE, R. T. 2004. Endothelial cells promote cardiac myocyte survival and spatial reorganization implications for cardiac regeneration. *Circulation,* 110**,** 962-968.

NEYT, J., BUCKWALTER, J. A. & CARROLL, N. 1998. Use of animal models in musculoskeletal research. *The Iowa orthopaedic journal,* 18**,** 118.

NOMI, M., ATALA, A., DE COPPI, P. & SOKER, S. 2002. Principals of neovascularization for tissue engineering. *Molecular aspects of medicine,* 23**,** 463-483.

NUCERA, S., BIZIATO, D. & DE PALMA, M. 2011. The interplay between macrophages and angiogenesis in development, tissue injury and regeneration. *The International journal of developmental biology,* 55**,** 495-503.

NYMAN, J. S., ROY, A., SHEN, X., ACUNA, R. L., TYLER, J. H. & WANG, X. 2006. The influence of water removal on the strength and toughness of cortical bone. *J Biomech,* 39**,** 931-8.

O'BRIEN, F. J. 2011. Biomaterials & scaffolds for tissue engineering. *Materials Today,* 14**,** 88-95.

OH, S. P., SEKI, T., GOSS, K. A., IMAMURA, T., YI, Y., DONAHOE, P. K., LI, L., MIYAZONO, K., TEN DIJKE, P. & KIM, S. 2000. Activin receptor-like kinase 1 modulates transforming growth factor-β1 signaling in the regulation of angiogenesis. *Proceedings of the National Academy of Sciences,* 97**,** 2626-2631.

OKII, N., NISHIMURA, S., KURISU, K., TAKESHIMA, Y. & UOZUMI, T. 2001. In Vivo Histological Changes Occurring in Hydroxyapatite Cranial Reconstruction. Case Report. *Neurologia medico-chirurgica,* 41**,** 100-104.

OSWALD, J., BOXBERGER, S., JØRGENSEN, B., FELDMANN, S., EHNINGER, G., BORNHÄUSER, M. & WERNER, C. 2004. Mesenchymal stem cells can be differentiated into endothelial cells in vitro. *Stem cells,* 22**,** 377-384.

OZAKI, A., TSUNODA, M., KINOSHITA, S. & SAURA, R. 2000. Role of fracture hematoma and periosteum during fracture healing in rats: interaction of fracture hematoma and the periosteum in the initial step of the healing process. *Journal of orthopaedic science,* 5**,** 64-70.

PACIFICI, R. 2010. The immune system and bone. *Archives of biochemistry and biophysics,* 503**,** 41-53.

PANDA, N. N., PRAMANIK, K. & SUKLA, L. B. 2014. Extraction and characterization of biocompatible hydroxyapatite from fresh water fish scales for tissue engineering scaffold. *Bioprocess and biosystems engineering,* 37**,** 433-440.

PARDALI, E., GOUMANS, M.-J. & TEN DIJKE, P. 2010. Signaling by members of the TGF-β family in vascular morphogenesis and disease. *Trends in cell biology,* 20**,** 556-567.

PARFITT, A. M. 2001. The bone remodeling compartment: a circulatory function for bone lining cells. *J Bone Miner Res,* 16**,** 1583-5.

PARK, S., DIMAIO, T. A., LIU, W., WANG, S., SORENSON, C. M. & SHEIBANI, N. 2013. Endoglin regulates the activation and quiescence of endothelium by participating in canonical and non-canonical TGF-β signaling pathways. *J Cell Sci,* 126**,** 1392-1405.

PATEL, Z. S., YOUNG, S., TABATA, Y., JANSEN, J. A., WONG, M. E. & MIKOS, A. G. 2008. Dual delivery of an angiogenic and an osteogenic growth factor for bone regeneration in a critical size defect model. *Bone,* 43**,** 931-940.

PAVÓN, M., ARROYO-SOLERA, I., CÉSPEDES, M., CASANOVA, I., LEÓN, X. & MANGUES, R. 2016. uPA/uPAR and SERPINE1 in head and neck cancer: role in tumor resistance, metastasis, prognosis and therapy. *Oncotarget*.

PAVÓN, M. A., ARROYO-SOLERA, I., TÉLLEZ-GABRIEL, M., LEÓN, X., VIRÓS, D., LÓPEZ, M., GALLARDO, A., CÉSPEDES, M. V., CASANOVA, I. & LÓPEZ-POUSA, A. 2015. Enhanced cell migration and apoptosis resistance may underlie the association between high SERPINE1 expression and poor outcome in head and neck carcinoma patients. *Oncotarget,* 6**,** 29016.

PEDERSEN, T. O., BLOIS, A. L., XUE, Y., XING, Z., COTTLER-FOX, M., FRISTAD, I., LEKNES, K. N., LORENS, J. B. & MUSTAFA, K. 2012. Osteogenic stimulatory conditions enhance growth and maturation of endothelial cell microvascular networks in culture with mesenchymal stem cells. *Journal of tissue engineering***,** 2041731412443236.

PÉREZ-GÓMEZ, E., DEL CASTILLO, G., SANTIBÁÑEZ, J. F., LÊPEZ-NOVOA, J. M., BERNABÉU, C. & QUINTANILLA, M. 2010. The role of the TGF-β coreceptor endoglin in cancer. *The Scientific World Journal,* 10**,** 2367-2384.

PETERS, K., SCHMIDT, H., UNGER, R. E., OTTO, M., KAMP, G. & KIRKPATRICK, C. J. 2002. Software-supported image quantification of angiogenesis in an in vitro culture system: application to studies of biocompatibility. *Biomaterials,* 23**,** 3413-3419.

PETTIT, A. R., CHANG, M. K., HUME, D. A. & RAGGATT, L.-J. 2008. Osteal macrophages: a new twist on coupling during bone dynamics. *Bone,* 43**,** 976-982.

PHILLIPS, J., FORREST, C. & GRUSS, J. S. 1992. Current concepts in the use of bone grafts in facial fractures. *Clinics in plastic surgery,* 19**,** 41-58.

PHNG, L.-K. & GERHARDT, H. 2009. Angiogenesis: a team effort coordinated by notch. *Developmental cell,* 16**,** 196-208.

PITTENGER, M. F., MACKAY, A. M., BECK, S. C., JAISWAL, R. K., DOUGLAS, R., MOSCA, J. D., MOORMAN, M. A., SIMONETTI, D. W., CRAIG, S. & MARSHAK, D. R. 1999. Multilineage potential of adult human mesenchymal stem cells. *Science,* 284**,** 143-147.

PLANELL, J. A., BEST, S., LACROIX, D. & MEROLLI, A. 2009. *Bone repair biomaterials*, Elsevier.

POTENTE, M., GERHARDT, H. & CARMELIET, P. 2011. Basic and therapeutic aspects of angiogenesis. *Cell,* 146**,** 873-887.

PRATT, A. B., WEBER, F. E., SCHMOEKEL, H. G., MÜLLER, R. & HUBBELL, J. A. 2004. Synthetic extracellular matrices for in situ tissue engineering. *Biotechnology and bioengineering,* 86**,** 27-36.

QUARTO, R., MASTROGIACOMO, M., CANCEDDA, R., KUTEPOV, S. M., MUKHACHEV, V., LAVROUKOV, A., KON, E. & MARCACCI, M. 2001. Repair of large bone defects with the use of autologous bone marrow stromal cells. *New England Journal of Medicine,* 344**,** 385-386.

QUINLAN, E., LÓPEZ ‐ NORIEGA, A., THOMPSON, E. M., HIBBITTS, A., CRYAN, S. A. & O'BRIEN, F. J. 2015. Controlled release of vascular endothelial growth factor from spray ‐ dried alginate microparticles in collagen–hydroxyapatite scaffolds for promoting vascularization and bone repair. *J Tissue Eng Regen Med*.

RAFII, S., BUTLER, J. M. & DING, B.-S. 2016. Angiocrine functions of organ-specific endothelial cells. *Nature,* 529**,** 316-325.

RAGGATT, L. J., WULLSCHLEGER, M. E., ALEXANDER, K. A., WU, A. C., MILLARD, S. M., KAUR, S., MAUGHAM, M. L., GREGORY, L. S., STECK, R. & PETTIT, A. R. 2014. Fracture healing via periosteal callus formation requires macrophages for both initiation and progression of early endochondral ossification. *The American journal of pathology,* 184**,** 3192-3204.

RAMASAMY, S. K., KUSUMBE, A. P., WANG, L. & ADAMS, R. H. 2014. Endothelial Notch activity promotes angiogenesis and osteogenesis in bone. *Nature,* 507**,** 376-380.

REYNOLDS, A. R., HART, I. R., WATSON, A. R., WELTI, J. C., SILVA, R. G., ROBINSON, S. D., DA VIOLANTE, G., GOURLAOUEN, M., SALIH, M. & JONES, M. C. 2009. Stimulation of tumor growth and angiogenesis by low concentrations of RGD-mimetic integrin inhibitors. *Nat Med,* 15**,** 392-400.

RICCI, J. L., CLARK, E. A., MURRIKY, A. & SMAY, J. E. 2012. Three-Dimensional Printing of Bone Repair and Replacement Materials: Impact on Craniofacial Surgery. *Journal of Craniofacial Surgery,* 23**,** 304-308.

RICH, H., ODLYHA, M., CHEEMA, U., MUDERA, V. & BOZEC, L. 2014. Effects of photochemical riboflavin-mediated crosslinks on the physical properties of collagen constructs and fibrils. *Journal of Materials Science: Materials in Medicine,* 25**,** 11-21.

RIPAMONTI, U., RODEN, L. C. & RENTON, L. F. 2012. Osteoinductive hydroxyapatite-coated titanium implants. *Biomaterials,* 33**,** 3813-3823.

RIVRON, N. C., RAISS, C. C., LIU, J., NANDAKUMAR, A., STICHT, C., GRETZ, N., TRUCKENMÜLLER, R., ROUWKEMA, J. & VAN BLITTERSWIJK, C. A. 2012. Sonic Hedgehog-activated engineered blood vessels enhance bone tissue formation. *Proceedings of the National Academy of Sciences,* 109**,** 4413-4418.

RIZZI, S. C., EHRBAR, M., HALSTENBERG, S., RAEBER, G. P., SCHMOEKEL, H. G., HAGENMÜLLER, H., MÜLLER, R., WEBER, F. E. & HUBBELL, J. A.

2006. Recombinant protein-co-PEG networks as cell-adhesive and proteolytically degradable hydrogel matrixes. Part II: biofunctional characteristics. *Biomacromolecules,* 7**,** 3019-3029.

ROSEN, L. S., GORDON, M. S., ROBERT, F. & MATEI, D. E. 2014. Endoglin for targeted cancer treatment. *Current oncology reports,* 16**,** 1-9.

ROUWKEMA, J., BOER, J. D. & BLITTERSWIJK, C. A. V. 2006. Endothelial cells assemble into a 3-dimensional prevascular network in a bone tissue engineering construct. *Tissue engineering,* 12**,** 2685-2693.

ROUWKEMA, J., RIVRON, N. C. & VAN BLITTERSWIJK, C. A. 2008. Vascularization in tissue engineering. *Trends Biotechnol,* 26**,** 434-41.

ROY, T. D., SIMON, J. L., RICCI, J. L., REKOW, E. D., THOMPSON, V. P. & PARSONS, J. R. 2003. Performance of degradable composite bone repair products made via three‐dimensional fabrication techniques. *Journal of biomedical materials research Part A,* 66**,** 283-291.

RUMPLER, M., WOESZ, A., DUNLOP, J. W., VAN DONGEN, J. T. & FRATZL, P. 2008. The effect of geometry on three-dimensional tissue growth. *Journal of the Royal Society Interface,* 5**,** 1173-1180.

SAFADI, F. F., BARBE, M. F., ABDELMAGID, S. M., RICO, M. C., ASWAD, R. A., LITVIN, J. & POPOFF, S. N. 2009. Bone structure, development and bone biology. *Bone pathology.* Springer.

SANTOS, M. I., UNGER, R. E., SOUSA, R. A., REIS, R. L. & KIRKPATRICK, C. J. 2009. Crosstalk between osteoblasts and endothelial cells co-cultured on a polycaprolactone-starch scaffold and the in vitro development of vascularization. *Biomaterials,* 30**,** 4407-15.

SCARANO, A., PERROTTI, V., ARTESE, L., DEGIDI, M., DEGIDI, D., PIATTELLI, A. & IEZZI, G. 2014. Blood vessels are concentrated within the implant surface concavities: a histologic study in rabbit tibia. *Odontology,* 102**,** 259-266.

SCHEUFLER, O., SCHAEFER, D. J., JAQUIERY, C., BRACCINI, A., WENDT, D. J., GASSER, J. A., GALLI, R., PIERER, G., HEBERER, M. & MARTIN, I. 2008. Spatial and temporal patterns of bone formation in ectopically pre‐fabricated, autologous cell‐based engineered bone flaps in rabbits. *Journal of cellular and molecular medicine,* 12**,** 1238-1249.

SCHNEIDER, C. A., RASBAND, W. S. & ELICEIRI, K. W. 2012. NIH Image to ImageJ: 25 years of image analysis. *Nat methods,* 9**,** 671-675.

SEKI, T., YUN, J. & OH, S. P. 2003. Arterial endothelium-specific activin receptor-like kinase 1 expression suggests its role in arterialization and vascular remodeling. *Circulation research,* 93**,** 682-689.

SHAH, A. R., CORNEJO, A., GUDA, T., SAHAR, D. E., STEPHENSON, S. M., CHANG, S., KRISHNEGOWDA, N. K., SHARMA, R. & WANG, H. T. 2014. Differentiated adipose-derived stem cell cocultures for bone regeneration in polymer scaffolds in vivo. *Journal of Craniofacial Surgery,* 25**,** 1504-1509.

SHASTRI, V. P. 2009. In vivo engineering of tissues: Biological considerations, challenges, strategies, and future directions. *Advanced Materials,* 21**,** 3246-3254.

SHAYESTEH, Y. S., KHOJASTEH, A., SOLEIMANI, M., ALIKHASI, M., KHOSHZABAN, A. & AHMADBEIGI, N. 2008. Sinus augmentation using human mesenchymal stem cells loaded into a β-tricalcium phosphate/hydroxyapatite scaffold. *Oral Surgery, Oral Medicine, Oral Pathology, Oral Radiology, and Endodontology,* 106**,** 203-209.

SHEKARAN, A., GARCÍA, J. R., CLARK, A. Y., KAVANAUGH, T. E., LIN, A. S., GULDBERG, R. E. & GARCÍA, A. J. 2014. Bone regeneration using an alpha 2 beta 1 integrin-specific hydrogel as a BMP-2 delivery vehicle. *Biomaterials,* 35**,** 5453-5461.

SHEPHERD, B. R., ENIS, D. R., WANG, F., SUAREZ, Y., POBER, J. S. & SCHECHNER, J. S. 2006. Vascularization and engraftment of a human skin substitute using circulating progenitor cell-derived endothelial cells. *The FASEB journal,* 20**,** 1739-1741.

SHI, Y., KRAMER, G., SCHRÖDER, A., KIRKPATRICK, C. J., SEEKAMP, A., SCHMIDT, H. & FUCHS, S. 2014. Early endothelial progenitor cells as a source of myeloid cells to improve the pre-vascularisation of bone constructs. *Eur. Cell. Mater.,* 27**,** 64-79.

SHRIVATS, A. R., MCDERMOTT, M. C. & HOLLINGER, J. O. 2014. Bone tissue engineering: state of the union. *Drug discovery today,* 19**,** 781-786.

SHWEIKI, D., ITIN, A., SOFFER, D. & KESHET, E. 1992. Vascular endothelial growth factor induced by hypoxia may mediate hypoxia-initiated angiogenesis. *Nature,* 359**,** 843-845.

SMAY, J. E., CESARANO, J. & LEWIS, J. A. 2002. Colloidal inks for directed assembly of 3-D periodic structures. *Langmuir,* 18**,** 5429-5437.

SMITH, D. M., COOPER, G. M., MOONEY, M. P., MARRA, K. G. & LOSEE, J. E. 2008. Bone morphogenetic protein 2 therapy for craniofacial surgery. *Journal of Craniofacial Surgery,* 19**,** 1244-1259.

SOMMERFELDT, D. & RUBIN, C. 2001. Biology of bone and how it orchestrates the form and function of the skeleton. *European Spine Journal,* 10**,** S86-S95.

SOO, S. & YU, K. 2003. Rapid prototyping for self-similarity design. *Journal of materials processing technology,* 139**,** 219-225.

STAHL, A., WENGER, A., WEBER, H., STARK, G. B., AUGUSTIN, H. G. & FINKENZELLER, G. 2004. Bi-directional cell contact-dependent regulation of gene expression between endothelial cells and osteoblasts in a three-dimensional spheroidal coculture model. *Biochem Biophys Res Commun,* 322**,** 684-692.

STAMATI, K., PRIESTLEY, J. V., MUDERA, V. & CHEEMA, U. 2014. Laminin promotes vascular network formation in 3D in vitro collagen scaffolds by regulating VEGF uptake. *Experimental cell research,* 327**,** 68-77.

SUN, J. & TAN, H. 2013. Alginate-based biomaterials for regenerative medicine applications. *Materials,* 6**,** 1285-1309.

SUN, L., PARKER, S. T., SYOJI, D., WANG, X., LEWIS, J. A. & KAPLAN, D. L. 2012. Direct‐Write Assembly of 3D Silk/Hydroxyapatite Scaffolds for Bone Co‐Cultures. *Advanced healthcare materials,* 1**,** 729-735.

SUN, Z.-J., YU, G.-T., HUANG, C.-F., BU, L.-L., LIU, J.-F., MA, S.-R., ZHANG, W.-F., LIU, B. & ZHANG, L. 2016. Hypoxia induces TFE3 expression in head and neck squamous cell carcinoma. *Oncotarget,* 7**,** 11651-11663.

TAKAHASHI, Y. & TABATA, Y. 2004. Effect of the fiber diameter and porosity of non-woven PET fabrics on the osteogenic differentiation of mesenchymal stem cells. *Journal of Biomaterials Science, Polymer Edition,* 15**,** 41-57.

TANIGUCHI, N., FUJIBAYASHI, S., TAKEMOTO, M., SASAKI, K., OTSUKI, B., NAKAMURA, T., MATSUSHITA, T., KOKUBO, T. & MATSUDA, S. 2016. Effect of pore size on bone ingrowth into porous titanium implants fabricated by additive manufacturing: an in vivo experiment. *Materials Science and Engineering: C,* 59**,** 690-701.

TAO, J., SUN, Y., WANG, Q.-G. & LIU, C.-W. 2009. Induced endothelial cells enhance osteogenesis and vascularization of mesenchymal stem cells. *Cells Tissues Organs,* 190**,** 185-193.

TAYLOR, M., DANIELS, A., ANDRIANO, K. & HELLER, J. 1994. Six bioabsorbable polymers: in vitro acute toxicity of accumulated degradation products. *Journal of applied biomaterials,* 5**,** 151-157.

TEITELBAUM, S. L. 2000. Bone resorption by osteoclasts. *Science,* 289**,** 1504-1508.

THÉBAUD, N., SIADOUS, R., BAREILLE, R., REMY, M., DACULSI, R., AMÉDÉE, J. & BORDENAVE, L. 2012. Whatever their differentiation status, human progenitor derived–or mature–endothelial cells induce osteoblastic differentiation of bone marrow stromal cells. *J Tissue Eng Regen Med,* 6**,** e51-e60.

THEIN-HAN, W. & XU, H. H. 2013. Prevascularization of a gas-foaming macroporous calcium phosphate cement scaffold via coculture of human umbilical vein endothelial cells and osteoblasts. *Tissue Engineering Part A,* 19**,** 1675-1685.

TIERNEY, C. M., HAUGH, M. G., LIEDL, J., MULCAHY, F., HAYES, B. & O'BRIEN, F. J. 2009. The effects of collagen concentration and crosslink density on the biological, structural and mechanical properties of collagen-GAG scaffolds for bone tissue engineering. *Journal of the mechanical behavior of biomedical materials,* 2**,** 202-209.

TITCHENELL, P. M. & ANTONETTI, D. A. 2013. Using the past to inform the future: anti-VEGF therapy as a road map to develop novel therapies for diabetic retinopathy. *Diabetes,* 62**,** 1808-1815.

TURCO, G., MARSICH, E., BELLOMO, F., SEMERARO, S., DONATI, I., BRUN, F., GRANDOLFO, M., ACCARDO, A. & PAOLETTI, S. 2009. Alginate/hydroxyapatite biocomposite for bone ingrowth: a trabecular structure with high and isotropic connectivity. *Biomacromolecules,* 10**,** 1575-1583.

UEBERSAX, L., HAGENMÜLLER, H., HOFMANN, S., GRUENBLATT, E., MÜLLER, R., VUNJAKNOVAKOVIC, G., KAPLAN, D. L., MERKLE, H. & MEINEL, L. 2006. Effect of scaffold design on bone morphology in vitro. *Tissue Eng,* 12**,** 3417-3429.

UNGER, R. E., GHANAATI, S., ORTH, C., SARTORIS, A., BARBECK, M., HALSTENBERG, S., MOTTA, A., MIGLIARESI, C. & KIRKPATRICK, C. J. 2010. The rapid anastomosis between prevascularized networks on silk fibroin scaffolds generated in vitro with cocultures of human microvascular endothelial and osteoblast cells and the host vasculature. *Biomaterials,* 31**,** 6959-6967.

UNGER, R. E., SARTORIS, A., PETERS, K., MOTTA, A., MIGLIARESI, C., KUNKEL, M., BULNHEIM, U., RYCHLY, J. & KIRKPATRICK, C. J. 2007. Tissue-like self-assembly in cocultures of endothelial cells and osteoblasts and the formation of microcapillary-like structures on three-dimensional porous biomaterials. *Biomaterials,* 28**,** 3965-76.

URBICH, C. & DIMMELER, S. 2004. Endothelial progenitor cells characterization and role in vascular biology. *Circ Res,* 95**,** 343-353.

VAN BAEL, S., CHAI, Y. C., TRUSCELLO, S., MOESEN, M., KERCKHOFS, G., VAN OOSTERWYCK, H., KRUTH, J.-P. & SCHROOTEN, J. 2012. The effect of pore geometry on the in vitro biological behavior of human periosteum-derived cells seeded on selective laser-melted Ti6Al4V bone scaffolds. *Acta biomaterialia,* 8**,** 2824-2834.

VENKATESAN, J. & KIM, S.-K. 2010. Chitosan composites for bone tissue engineering—An overview. *Marine drugs,* 8**,** 2252-2266.

VERRON, E., KHAIROUN, I., GUICHEUX, J. & BOULER, J.-M. 2010. Calcium phosphate biomaterials as bone drug delivery systems: a review. *Drug discovery today,* 15**,** 547-552.

VITTET, D., PRANDINI, M.-H., BERTHIER, R., SCHWEITZER, A., MARTIN-SISTERON, H., UZAN, G. & DEJANA, E. 1996. Embryonic stem cells differentiate in vitro to endothelial cells through successive maturation steps. *Blood,* 88**,** 3424-3431.

VUOLA, J., BÖHLING, T., KINNUNEN, J., HIRVENSALO, E. & ASKO–SELJAVAARA, S. 2000. Natural coral as bone ‐ defect ‐ filling material. *Journal of biomedical materials research,* 51**,** 117-122.

WAHL, S., MCCARTNEY‐FRANCIS, N., ALLEN, J., DOUGHERTY, E. & DOUGHERTY, S. 1990. Macrophage production of TGF‐β and regulation by TGF‐β. *Annals of the New York Academy of Sciences,* 593**,** 188-196.

WALSER, R., METZGER, W., GÖRG, A., POHLEMANN, T., MENGER, M. & LASCHKE, M. 2013. Generation of co-culture spheroids as vascularisation units for bone tissue engineering. *Eur Cell Mater,* 26**,** 222-33.

WANG, J. & SHAW, L. L. 2009. Nanocrystalline hydroxyapatite with simultaneous enhancements in hardness and toughness. *Biomaterials,* 30**,** 6565-6572.

WANG, X., HORII, A. & ZHANG, S. 2008. Designer functionalized self-assembling peptide nanofiber scaffolds for growth, migration, and tubulogenesis of human umbilical vein endothelial cells. *Soft Matter,* 4**,** 2388-2395.

WANG, X., MABREY, J. D. & AGRAWAL, C. M. 1998. An interspecies comparison of bone fracture properties. *Biomedical Materials and Engineering,* 8**,** 1-10.

WEI, J., SHIMAZU, J., MAKINISTOGLU, M. P., MAURIZI, A., KAJIMURA, D., ZONG, H., TAKARADA, T., IEZAKI, T., PESSIN, J. E. & HINOI, E. 2015. Glucose uptake and Runx2 synergize to orchestrate osteoblast differentiation and bone formation. *Cell,* 161**,** 1576-1591.

WERNIKE, E., MONTJOVENT, M., LIU, Y., WISMEIJER, D., HUNZIKER, E., SIEBENROCK, K., HOFSTETTER, W. & KLENKE, F. 2010. VEGF incorporated into calcium phosphate ceramics promotes vascularisation and bone formation in vivo. *Eur Cell Mater,* 19.

WHEELER, D. L. & ENNEKING, W. F. 2005. Allograft bone decreases in strength in vivo over time. *Clin Orthop Relat Res***,** 36-42.

WITEK, L., SMAY, J., SILVA, N. R., GUDA, T., ONG, J. L. & COELHO, P. G. 2013. Sintering effects on chemical and physical properties of bioactive ceramics. *Journal of Advanced Ceramics,* 2**,** 274-284.

XING, Z., XUE, Y., FINNE‐WISTRAND, A., YANG, Z. Q. & MUSTAFA, K. 2013. Copolymer cell/scaffold constructs for bone tissue engineering: Co‐culture of low ratios of human endothelial and osteoblast‐like cells in a dynamic culture system. *Journal of biomedical materials research Part A,* 101**,** 1113-1120.

XU, M., ZHAI, D., CHANG, J. & WU, C. 2014. In vitro assessment of three-dimensionally plotted nagelschmidtite bioceramic scaffolds with varied macropore morphologies. *Acta biomaterialia,* 10**,** 463-476.

YANG, H., FUNG, S. Y., PRITZKER, M. & CHEN, P. 2007. Modification of hydrophilic and hydrophobic surfaces using an ionic-complementary peptide. *PLoS One,* 2**,** e1325.

YANG, S., LEONG, K.-F., DU, Z. & CHUA, C.-K. 2001. The design of scaffolds for use in tissue engineering. Part I. Traditional factors. *Tissue engineering,* 7**,** 679-689.

YANG, S., LEONG, K.-F., DU, Z. & CHUA, C.-K. 2002. The design of scaffolds for use in tissue engineering. Part II. Rapid prototyping techniques. *Tissue Eng,* 8**,** 1-11.

YEONG, W.-Y., CHUA, C.-K., LEONG, K.-F. & CHANDRASEKARAN, M. 2004. Rapid prototyping in tissue engineering: challenges and potential. *Trends Biotechnol,* 22**,** 643-652.

YOKOI, H., KINOSHITA, T. & ZHANG, S. 2005. Dynamic reassembly of peptide RADA16 nanofiber scaffold. *Proc Natl Acad Sci U S A,* 102**,** 8414-8419.

YOUNG, S., PATEL, Z. S., KRETLOW, J. D., MURPHY, M. B., MOUNTZIARIS, P. M., BAGGETT, L. S., UEDA, H., TABATA, Y., JANSEN, J. A. & WONG, M. 2009. Dose effect of dual delivery of vascular endothelial growth factor and bone morphogenetic protein-2 on bone regeneration in a rat critical-size defect model. *Tissue Engineering Part A,* 15**,** 2347-2362.

ZADPOOR, A. A. 2015. Bone tissue regeneration: the role of scaffold geometry. *Biomaterials science,* 3**,** 231-245.

ZAYZAFOON, M., FULZELE, K. & MCDONALD, J. M. 2005. Calmodulin and calmodulin-dependent kinase IIα regulate osteoblast differentiation by controlling c-fos expression. *Journal of Biological Chemistry,* 280**,** 7049-7059.

ZHANG, S. 2003. Fabrication of novel biomaterials through molecular self-assembly. *Nature biotechnology,* 21**,** 1171-1178.

ZHANG, S., GELAIN, F. & ZHAO, X. Designer self-assembling peptide nanofiber scaffolds for 3D tissue cell cultures. Seminars in cancer biology, 2005. Elsevier, 413-420.

ZHANG, S., HOLMES, T., LOCKSHIN, C. & RICH, A. 1993. Spontaneous assembly of a self-complementary oligopeptide to form a stable macroscopic membrane. *Proceedings of the National Academy of Sciences,* 90**,** 3334-3338.

ZHANG, S., HOLMES, T. C., DIPERSIO, C. M., HYNES, R. O., SU, X. & RICH, A. 1995. Self-complementary oligopeptide matrices support mammalian cell attachment. *Biomaterials,* 16**,** 1385-1393.

ZHANG, S., LOCKSHIN, C., COOK, R. & RICH, A. 1994. Unusually stable β‐sheet formation in an ionic self‐complementary oligopeptide. *Biopolymers,* 34**,** 663-672.

ZHANG, S., LOCKSHIN, C., HERBERT, A., WINTER, E. & RICH, A. 1992. Zuotin, a putative Z-DNA binding protein in Saccharomyces cerevisiae. *The EMBO journal,* 11**,** 3787.

ZHAO, H., FENG, J., HO, T.-V., GRIMES, W., URATA, M. & CHAI, Y. 2015. The suture provides a niche for mesenchymal stem cells of craniofacial bones. *Nature cell biology*.